SOLAR ENERGY
JOURNAL OF SOLAR ENERGY SCIENCE AND ENGINEERING

VOLUME II | JULY-OCTOBER, 1958 | NUMBER 3-4

Table of Contents

Cover photo of the sun by Stuart Weiner, Phoenix.

PERFORMANCE OF EXPERIMENTAL SOLAR WATER HEATERS IN AUSTRALIA

By J. T. CZARNECKI

Engineering Section, Commonwealth Scientific and Industrial Research Organization, Melbourne, Australia

Seven experimental solar water heaters were installed at C.S.I.R.O. laboratories throughout Australia in order to gain field experience and performance data for various localities. Each heater included an insulated 70-gal hot water storage tank with a built-in electric booster and two solar absorbers of total active area of 45 sq ft.

Each morning approximately 45 gal of water at a temperature of about 135°F were discharged from the tank. Average monthly values for a 12-month period are given for the daily electric power consumption and the solar contribution. Mean yearly contribution of the solar energy under these conditions was from 60 to 80 per cent of the total energy required, depending on the district in which the heaters were located. In order to determine the extent to which the results are typical, a comparison is given, for some of the districts, of the sunshine hours recorded during the test period, with the nominal 30-year average.

INTRODUCTION

Heating of water for domestic purposes is a simple and effective way of utilizing solar energy, which can already compete on an economic basis with other types of fuel.

In Australia, a program of development and testing of solar water heaters has been undertaken by C.S.I.R.O. Engineering Section, and the work performed was summarized by Morse.[1]

Performance data of a flat-plate absorber were first collected for Melbourne, and the design of a solar water heater suitable for domestic application followed. A detailed description of such a heater was given by Morse.[2]

To provide information on suitability of the heaters in other parts of Australia and also to obtain field experience under local conditions, seven similar units were built and installed at C.S.I.R.O. laboratories in Adelaide, Brisbane, Canberra, Deniliquin, Geelong, Melbourne, and Sydney.

The purpose of this paper is to report the results of one year's operation of these heaters.

EXPERIMENTAL ARRANGEMENT

(a) Equipment

A typical experimental solar water heater is shown diagrammatically in Fig. 1, and in Fig. 2 the electrical circuit is given. It comprises two absorbers of total absorbing area of 45 sq ft with angle of inclination equal to latitude plus 2½°, a 70-gal outdoor copper tank insulated with 4 in. of mineral wool, auxiliary electric heater of 2-kw rating, controlled by a thermostat and a time switch, flow and return connections of 1-in. diameter copper

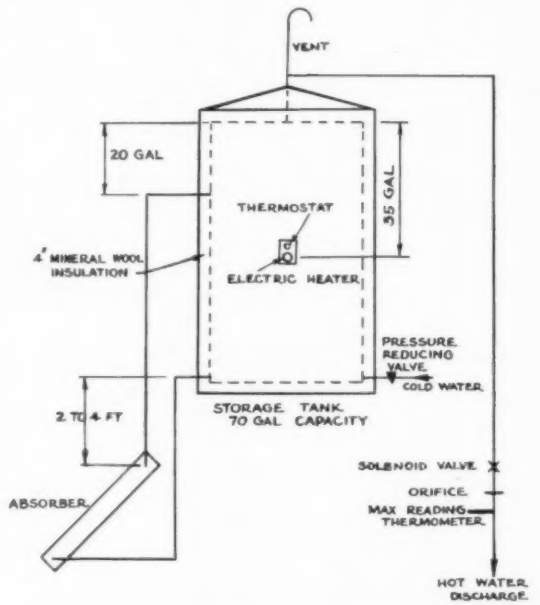

FIG. 1 — Schematic diagram of an experimental solar water heater.

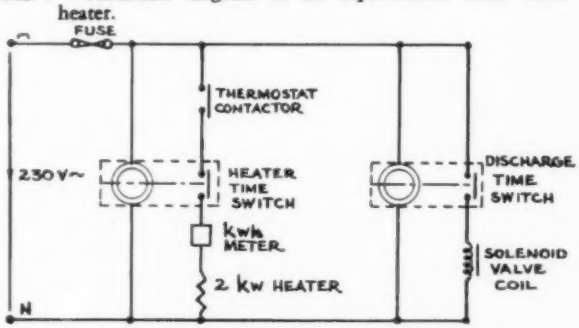

FIG. 2 — Electrical circuit of an experimental solar water heater.

tubes insulated with 1-in.-thick polythene-covered "Onazote", and a solenoid valve which is energized by a second time switch for a fixed time in order to discharge 45 gal of hot water through an orifice each day commencing at 6 a.m.

A maximum reading thermometer located at the hot water outlet records the temperature of the water discharged.

In the Brisbane installation, where hail storms are known to be exceptionally severe, a hail-protection screen was suspended above the absorbers, consisting of ½-in. mesh of 22 S.W.G. galvanized wire netting. This hail protection reduces the absorbers' active area by 12 per cent.

(b) Operation

Solar radiation reaching the absorbers heats the water, decreasing its density and causing thermosyphon circulation. When equilibrium is reached, the incident radiant energy must be equal to the heat energy removed by the water, plus the heat loss from the absorber to the environment.

When the temperature of the water in the storage tank does not, during the day, reach the temperature set on the thermostat, the electric heater takes over the heating at night. The associated time switch is set to switch on the electric heater only between 8 p.m. and 5 a.m., so that under the control of the thermostat the water discharged in the morning is approximately 135°F. On days when insolation is high, the temperature will exceed 135°F, due to solar radiation alone.

(c) Measurements

Regular measurements of the following quantities were made for each solar water heater for twelve consecutive months:

(i) amount of hot water discharged daily,
(ii) electrical energy consumed daily,
(iii) temperature of the mains water,
(iv) temperature of the hot water discharged.

These values were read daily at Deniliquin and every working day at all other localities. In addition, data on bright sunshine hours were obtained for Adelaide, Brisbane, Canberra, and Melbourne for the test period.

TEST RESULTS

Daily means of the measured and derived values for the experimental solar water heaters over the period of twelve consecutive months are shown in Table I.

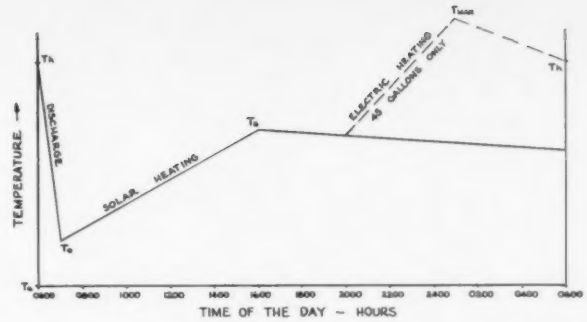

FIG. 3 — Distribution of temperature in the storage tank during 24 hours: T_c is cold water temperature; T_h is mean water temperature before discharge; T_s is mean temperature of of water after solar heating; T_{max} is maximum temperature of water heated electrically; T_o is mean water temperature after discharge.

The mean daily heat loss from the storage tank was computed under assumptions that all tanks had a heat-transfer coefficient $k = 6$ Btu per hr per °F, i.e., the same as at the Melbourne installation, and that the mean ambient temperature over the year was equal to the mean mains water temperature at the corresponding locality. The heat loss was then evaluated using the formula

$$Q_L = kt\,(T_m - T_a) \qquad [1]$$

where:

Q_L = heat loss from the storage tank (Btu per day)
k = heat-transfer coefficient of the storage tank,
T_m = mean daily water temperature in the 70 gal storage tank (°F),
T_a = mean ambient temperature (°F),
t = time = 24 hours.

The mean daily water temperature in the storage tank T_m was evaluated, taking into consideration temperature distribution of water in the storage tank, as shown in Fig. 3.

The energy required to heat water in Table I is the difference between the heat energy contained in the hot water discharged and the heat energy in cold water replacing it. The value of this expressed in kwh is given by

$$Q_R = 10^{-3} \times 2.93(T_H - T_c)W \qquad [2]$$

where:

T_H = mean temperature of the hot water discharged (°F),
T_c = mean temperature of the mains water (°F),
W = mean daily hot water discharge (gal).

TABLE I
DAILY MEANS FOR TWELVE CONSECUTIVE MONTHS OF OPERATION OF SOLAR WATER HEATERS AT VARIOUS LOCALITIES

Location	Adelaide	Brisbane*	Canberra	Deniliquin	Geelong	Melbourne	Sydney
Hot water discharge (gal)	45.2	45.5	42.8	42.4	42.0	45.5	44.9
Electrical energy consumed (kwh)	3.5	2.5	3.4	2.5	3.8	4.6	4.4
Cold water temperature (°F)	63.8	70.8	54.8	62.3	60.7	60.9	61.8
Hot water temperature (°F)	138.0	133.5	137.2	140.5	137.6	135.3	135.8
Energy required to heat water (kwh)	9.8	8.4	10.3	9.7	9.5	9.9	9.8
Heat loss from storage tank (kwh)	2.2	1.9	2.5	2.5	2.2	1.9	1.9
Total energy consumed (kwh)	12.0	10.3	12.8	12.2	11.7	11.8	11.7
Solar energy contributed (kwh)	8.5	7.8	9.4	9.7	7.9	7.2	7.3
Solar energy contributed (%)	71	76	73	81	67	61	62

*Hail protection suspended above the absorbers. No correction made for reduction of absorbing area.

TABLE II

SOLAR WATER HEATER, ADELAIDE — TEST RESULTS

Mo. ('56)	Mean daily hot water discharge (gal)	Daily electrical energy consumption (kwh)			Mean cold water temp. (°F)	Mean hot water temp. (°F)	Mean solar contribution (%)
		Mean	Max.	Min.			
Jan.	43.0	0.7	3.3	0.0	70.6	140.5	94
Feb.	46.0	0.1	2.5	0.0	77.7	152.5	99
Mar.	47.2	1.2	6.1	0.0	74.0	142.0	90
April	49.4	5.2	8.7	1.5	67.0	142.0	60
May	49.8	6.2	10.1	0.4	62.1	139.9	54
June	44.2	6.5	9.6	1.8	55.8	137.0	49
July	44.7	7.1	9.8	3.0	53.8	136.9	47
Aug.	45.0	6.1	9.6	2.2	53.4	136.4	53
Sept.	44.9	3.7	8.1	0.0	56.0	132.4	70
Oct.	44.5	2.5	6.3	0.0	60.5	131.2	78
Nov.	41.5	1.4	6.4	0.0	67.6	134.5	86
Dec.	42.1	0.9	4.6	0.0	68.6	130.7	91

TABLE III

SOLAR WATER HEATER, BRISBANE — TEST RESULTS

Mo. ('56)	Mean daily hot water discharge (gal)	Daily electrical energy consumption (kwh)			Mean cold water temp. (°F)	Mean hot water temp. (°F)	Mean solar contribution (%)
		Mean	Max.	Min.			
Jan.	37.2	0.5	3.5	0.0	81.3	138.0	94
Feb.	42.0	1.3	6.2	0.0	79.2	132.8	85
Mar.	44.0	2.0	5.1	0.0	77.1	127.9	76
April	41.0	1.0	4.1	0.0	74.0	131.4	89
May	57.7	2.8	8.0	0.7	66.6	128.3	77
June	44.7	4.6	7.8	1.7	60.8	128.7	57
July	49.2	5.5	8.6	0.0	57.9	136.4	58
Aug.	46.3	3.4	6.0	0.0	60.0	136.8	72
Sept.	46.8	2.8	6.0	0.2	65.7	135.3	75
Oct.	47.0	2.2	7.1	0.0	71.1	135.6	80
Nov.	47.0	1.7	6.4	0.0	76.0	135.2	83
Dec.	47.2	2.3	4.9	0.0	80.4	137.0	76

TABLE IV

SOLAR WATER HEATER, CANBERRA — TEST RESULTS

Mo. ('56)	Mean daily hot water discharge (gal)	Daily electrical energy consumption (kwh)			Mean cold water temp. (°F)	Mean hot water temp. (°F)	Mean solar contribution (%)
		Mean	Max.	Min.			
Jan.*	36.5	0.3	1.8	0.0	70.2	146.7	97
Feb.	43.2	1.3	6.0	0.0	70.0	135.5	88
Mar.	46.7	3.3	7.8	0.0	65.3	134.5	72
April	47.0	3.9	5.7	0.0	57.0	135.2	71
May	46.7	6.5	11.0	3.2	49.0	134.0	54
June	45.6	6.8	11.6	5.1	43.7	133.5	53
July	40.2	7.6	13.1	4.0	42.0	134.0	43
Aug.	40.7	4.3	12.1	1.1	40.8	134.0	68
Sept.	42.2	2.2	5.9	0.0	47.7	137.0	84
Oct.	42.2	2.7	8.4	0.0	53.0	136.8	79
Nov.	42.0	1.3	4.1	0.0	56.1	141.9	90
Dec.	40.8	0.3	5.3	0.0	63.1	145.6	98

*Readings started on January 9.

Total energy consumed

$$Q_t = Q_R + Q_L \qquad [3]$$

and solar energy contributed

$$Q_s = Q_t - Q_E \qquad [4]$$

where Q_E is the electrical energy consumed.

In Tables II to VIII the daily means of the measured quantities are shown for each month. The minimum and maximum electrical energy consumption in the corresponding month is also included. The mean solar contribution was evaluated assuming that the heat loss from the storage tank was constant throughout the year and equal to the loss shown in Table I. This assumption can be made without introducing a great error, as the mean water temperature in the tank was higher during warmer months of the year because of higher insolation, compensating largely for the increased ambient temperature during this period.

TABLE V

SOLAR WATER HEATER, DENILIQUIN — TEST RESULTS

Mo. ('56)	Mean daily hot water discharge (gal)	Daily electrical energy consumption (kwh)			Mean cold water temp. (°F)	Mean hot water temp. (°F)	Mean solar contribution (%)
		Mean	Max.	Min.			
Jan.	43.1	0.7	8.6	0.0	74.3	145.0	94
Feb.	40.5	0.0	0.0	0.0	79.7	155.5	100
Mar.	46.0	1.2	5.9	0.0	74.7	144.0	90
April	48.8	4.2	8.6	0.0	63.5	140.8	69
May	41.5	3.3	8.3	0.0	56.7	131.5	72
June	45.2	5.9	10.5	0.4	51.5	138.5	58
July	46.4	6.2	9.9	0.9	50.9	139.3	57
Aug.	38.5	3.3	7.0	0.0	50.4	136.1	73
Sept.	40.5	1.6	6.3	0.0	53.6	136.5	87
Oct.	38.7	2.2	8.3	0.0	58.4	137.0	81
Nov.	39.1	0.9	4.0	0.0	63.7	137.1	92
Dec.	40.3	0.1	0.8	0.0	71.3	145.5	99

TABLE VI

SOLAR WATER HEATER, GEELONG — TEST RESULTS

Mo. ('56)	Mean daily hot water discharge (gal)	Daily electrical energy consumption (kwh)			Mean cold water temp. (°F)	Mean hot water temp. (°F)	Mean solar contribution (%)
		Mean	Max.	Min.			
Jan.	45.3	2.0	7.8	0.0	68.5	139.2	83
Feb.	42.2	0.9	5.2	0.0	71.0	140.5	92
Mar.	43.7	2.3	5.7	0.0	68.7	141.0	80
April	44.0	4.4	8.7	0.0	67.4	140.8	62
May	42.7	6.5	12.7	2.5	60.0	140.3	47
June	40.9	7.2	11.0	4.5	53.2	144.0	45
July	40.0	5.2	8.9	2.4	47.0	133.2	58
Aug.	38.1	4.4	7.5	3.1	50.0	131.3	61
Sept.	35.8	2.5	6.2	0.0	55.7	129.0	75
1955:							
Oct.	41.0	4.2	9.9	1.8	58.0	139.0	65
Nov.	44.5	3.8	9.0	0.0	61.3	136.7	68
Dec.	45.3	2.6	6.0	0.0	67.5	137.4	77

TABLE VII

SOLAR WATER HEATER, MELBOURNE — TEST RESULTS

Mo. ('56)	Mean daily hot water discharge (gal)	Daily electrical energy consumption (kwh)			Mean cold water temp. (°F)	Mean hot water temp. (°F)	Mean solar contribution (%)
		Mean	Max.	Min.			
Jan.	47.7	2.9	8.7	0.0	66.8	136.5	75
Feb.	45.8	0.5	1.8	0.0	72.5	138.2	95
Mar.	44.1	2.6	5.3	0.0	70.6	134.2	74
April	44.4	5.2	7.5	0.0	64.0	133.5	52
May	43.2	6.2	6.7	2.9	56.8	135.2	47
1955:							
June	44.5	7.7	11.4	2.8	53.5	135.8	39
July	44.9	8.1	11.8	4.8	51.3	136.2	38
Aug.	44.7	6.1	9.8	3.5	52.4	132.0	50
Sept.	44.3	4.9	7.8	1.2	55.5	134.5	59
Oct.	45.3	3.9	7.8	0.0	59.6	134.6	67
Nov.	46.1	3.7	7.9	0.0	61.9	134.8	68
Dec.	50.5	3.5	7.4	0.0	66.4	137.6	72

DISCUSSION OF RESULTS

On the basis that the number of square feet of the absorber area is equal to the number of gallons of hot water used daily, the mean yearly contribution of solar energy in per cent is shown in Table I. This contribution represents the net saving in the fuel bill for heating water.

TABLE VIII

SOLAR WATER HEATER, SYDNEY — TEST RESULTS

Mo. ('56)	Mean daily hot water discharge (gal)	Daily electrical energy consumption (kwh)			Mean cold water temp. (°F)	Mean hot water temp. (°F)	Mean solar contribution (%)
		Mean	Max.	Min.			
Jan.*	38.6	2.9	7.9	0.0	74.3	135.0	66
Feb.	45.2	4.9	10.5	1.2	70.8	134.3	52
Mar.†	46.2	3.6	6.4	0.4	69.0	133.6	66
April	48.2	3.6	8.1	0.0	64.5	137.6	70
May	46.2	6.2	13.9	3.8	58.8	138.3	51
June‡	45.7	6.2	—	—	53.9	137.0	53
July	45.2	6.3	11.7	4.2	49.0	135.6	54
Aug.	44.3	4.4	10.8	1.7	50.3	135.4	66
Sept.	45.0	4.8	9.5	2.1	53.3	136.6	63
Oct.	45.1	4.6	9.6	2.2	61.1	135.7	61
Nov.	45.0	2.6	7.8	0.1	66.0	134.6	76
Dec.	45.0	3.1	7.6	0.4	71.3	135.2	61

*Readings started on January 17.
†Readings not taken between March 6 and 22.
‡Readings not available for June. Interpolated from May and July figures.

TABLE IX

RATIO OF MONTHLY LOWEST TO HIGHEST SOLAR ENERGY CONTRIBUTION OR UNIFORMITY FACTOR OVER THE TEST PERIOD

Adelaide	Brisbane	Canberra	Deniliquin	Geelong	Melbourne	Sydney
0.47	0.61	0.44	0.57	0.49	0.40	0.68

TABLE X

MEAN DAILY VALUES FOR BRIGHT SUNSHINE HOURS AND SOLAR ENERGY COLLECTED WITH 45 SQ. FT. ABSORBERS AT VARIOUS LOCALITIES

Month	Adelaide		Brisbane*		Canberra		Melbourne	
	Sunshine (hr)	Solar energy collected (kwh)	Sunshine (hr)	Solar energy collected (kwh)	Sunshine (hr)	Solar energy collected (kwh)	Sunshine (hr)	Solar energy collected (kwh)
Jan.	8.9	10.3	7.3	8.6	10.3	10.3	6.8	8.7
Feb.	10.3	12.3	5.2	8.1	6.3	9.5	9.7	10.2
Mar.	7.3	10.3	6.1	7.2	4.7	8.6	5.6	7.5
April	5.5	7.9	7.1	8.9	6.0	9.4	4.0	5.7
May	4.5	7.3	7.5	10.6	4.1	7.6	2.7	5.5
June	3.3	6.2	6.1	6.9	4.4	7.7	3.5	4.9
July	2.2	6.1	5.8	8.5	4.1	5.7	3.1	4.9
Aug.	4.0	7.0	8.9	9.9	6.1	9.2	5.3	6.1
Sept.	5.0	8.5	8.5	9.6	7.4	11.3	5.4	7.1
Oct.	5.9	8.9	8.6	9.8	7.5	10.2	6.5	7.9
Nov.	8.4	8.9	9.0	9.4	9.4	11.8	7.2	8.0
Dec.	7.9	9.0	7.7	8.3	11.0	12.1	7.0	8.9

*12 per cent added to solar energy collected to compensate for loss of radiation due to hail protection.

TABLE XI

MEAN DAILY NUMBER OF SUNSHINE HOURS OVER AT LEAST 30 YEARS COMPARED WITH SUNSHINE HOURS PREVAILING DURING THE TEST PERIOD

Month	Adelaide	Brisbane	Canberra	Melbourne
January	10.0	7.6	8.1	7.8
February	9.3	7.4	7.5	7.4
March	7.9	7.0	7.1	6.5
April	6.0	7.1	6.6	5.0
May	4.8	6.6	5.2	4.1
June	4.2	6.3	4.3	3.4
July	4.3	6.8	4.7	3.7
August	5.4	7.9	5.8	4.6
September	6.3	8.2	7.2	5.5
October	7.3	8.4	7.7	5.8
November	8.6	8.2	7.9	6.2
December	9.5	8.2	8.2	7.0
Yearly mean	7.0	7.5	6.7	5.6
Yearly mean during test	6.1	7.3	6.8	5.6

The monthly variations are evident from Tables II to VIII.

It will be seen that the highest value is for Deniliquin, where the saving is 81 per cent, and the lowest Melbourne, amounting to 61 per cent.

The absorber area can, of course, be increased to provide enough heating throughout the year without a booster. This, however, would be an economic proposition only where the insolation throughout the year is sufficiently uniform.

The ratio of monthly lowest to highest per cent contribution of solar energy, taken from Tables II to VIII, is shown in Table IX, and it may be called "uniformity factor." It may be seen from this Table that the highest value of uniformity during the test period was in Sydney and Brisbane, and the lowest in Melbourne and Canberra. In general, the uniformity factor increases with decreasing latitude, eliminating the necessity of a booster.

It was shown by Angstrom;[3] Black, Bonython, and Prescott;[4] and others that a correlation exists between bright sunshine hours and total incident solar radiation on a horizontal surface. In the following, an attempt is made to correlate the number of bright sunshine hours with the solar energy collected and transferred to the water in the experimental solar water heaters at Adelaide, Brisbane, Canberra, and Melbourne. From the values shown in Table X, the regression equation[5] was calculated taking the mean daily number of bright sunshine hours in each month as the independent variable, and the mean daily solar energy contribution to heat water in the corresponding period with a 45 sq ft absorber as the dependent variable. The regression equation is then

$$Q_s = 3.74 + 0.736h \qquad [5]$$

where:

Q_s = mean daily solar energy contribution (kwh),
h = mean daily number of bright sunshine hours.

The correlation coefficient in this calculation was found to be $r = 0.865$, and the standard deviation from the regression line

$$\sigma_r \times t = 0.92 \text{ kwh}$$

Equation [5] can also be written as

$$q_s = 284 + 56h \qquad [6]$$

where q_s is the mean daily solar energy collected, Btu per sq ft per day. This equation is plotted in Fig. 4, and the 95 per cent confidence limits are drawn.

It must be borne in mind that the relationship shown in Fig. 4 can be used only for prediction of q_s from a known value of h if the conditions for collection are equivalent to the conditions prevailing during the experiments, since the efficiency of collection depends largely on such factors as type of absorber, rate of water flow through the absorber, temperature of water entering the absorber in relation to the ambient temperature, and angle of inclination of the absorber.

An accurate prediction on the performance of a solar absorber is possible only if the amount of incident solar radiation and the efficiency of collection of the absorber is known. Lacking these data, a prediction of performance

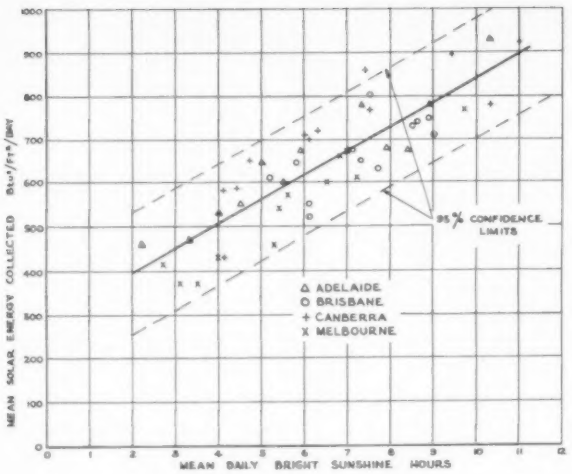

FIG. 4 — Regression of bright sunshine hours upon mean daily solar energy collected.

of a conventional absorber from the mean daily bright sunshine hours may serve as a rough guide in the design of a solar water heater. The method of such a prediction may be illustrated in the following example.

A solar water heater is required for a holiday house for operation during the summer months only. The mean daily sunshine hours over each of these months are known from the meteorological records to be not less than eight. The heater should be able to supply 30 gal of water daily at a nominal temperature of 135°F, and it should not include any booster. Cold water temperature during the period of operation is never below 65°F.

From Fig. 4 it is found that for eight hours of sunshine the rate of collection with a conventional absorber q_s is 730 Btu per sq ft per day.

The heat needed to raise the temperature of 30 gal of water from 65°F to 135°F is

$$Q_n = 30(135 - 65)\ 10 = 21{,}000 \text{ Btu per day.}$$

Hence the minimum absorber area required

$$A = \frac{Q_n}{q_s} = \frac{21{,}000}{730} = 28.8 \text{ sq ft}$$

Two absorbers of the standard design,[2] having 16-sq ft absorbing area each are chosen, together with a 60-gal insulated storage tank. A slightly larger total absorbing area than calculated will provide some compensation for the heat loss from the storage tank to the environment. The 60-gal tank stores two days' supply of hot water, ensuring hot water after a cloudy day.

Table XI shows the mean daily number of sunshine hours over at least 30 years for Adelaide, Brisbane, Canberra, and Melbourne as published by the Metorological Bureau.[6]

It may be seen that the number of sunshine hours prevailing during the test period and shown in Table X deviated considerably in many cases from the sunshine hours shown in Table XI over a corresponding month. The yearly means, however, do not deviate much except for Adelaide, where an unusually cloudy year was experienced.

REFERENCES

1. R. N. Morse, "Solar water heaters." *Proceedings of the World Symposium on Applied Solar Energy*. Stanford Research Institute, 1956. p. 191-200.
2. R. N. Morse, "Solar water heaters for domestic and farm use." *C.S.I.R.O., Engineering Section, Report* E.D. 5, Sept. 1957.
3. A. Angstrom, "Solar and terrestrial radiation." *Quart. J. Roy. Met. Soc.* 50:121, 1924.
4. J. N. Black, C. W. Bonython, and J. A. Prescott, "Solar radiation and the duration of sunshine." *Quart. J. Roy. Met. Soc.* 80:231-5, 1954.
5. K. A. Brownlee, *Industrial Experimentation*. London, H.M.S.O., 1949.
6. Australia, Meteorological Bureau, "The climate and meteorology of Australia." *Bull.* No. 1. Canberra, Commonw. Govt. Printer, 1951.

A SIMPLE REACTION TURBINE AS A SOLAR ENGINE

By S. T. HSU and B. S. LEO

Department of Mechanical Engineering, University of Wisconsin, Madison

This article describes the design of a simple reaction turbine operating on saturated low pressure steam that could be generated by a solar boiler. The turbine was developed primarily to obtain a small power unit for irrigation purposes. Tests were therefore performed with the combination of turbine and a centrifugal pump. Horsepower curves and rotational loss curves are shown, and a comparison with five other small prime movers of varied design is also presented.

INTRODUCTION

In recent years, a growing interest has been shown by scientists and engineers in utilizing the sun's energy for power generation. Because of the practical limitations of collector size, the development of solar engines has been confined to lower-output units such as small engines for pumping water in rural areas. Attempts have been made to obtain electrical energy directly from solar radiation by means of thermopiles,[6] and a few hot-air engines have also been built.[6] However, for the time being, it is believed that a steam engine or turbine offers more advantages than other types of prime movers. There are small horsepower steam engines and turbines available on the market, but their cost is probably too high for underdeveloped areas and their maintenance may require mechanically trained personnel.

A study was therefore made in the Mechanical Engineering Department at the University of Wisconsin to develop a simple reaction turbine which can be manufactured at a relatively low price, will be easy to operate, and will require little maintenance.

FIG. 1 — Reaction turbine.

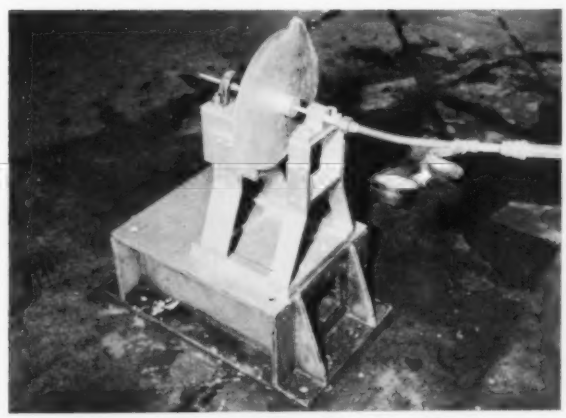

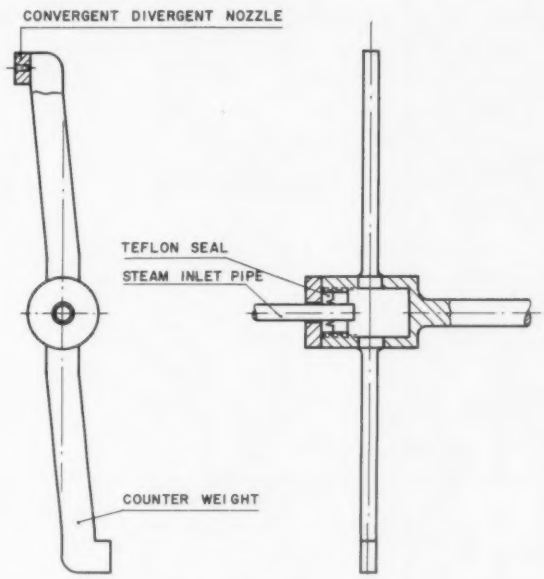

FIG. 2 — Turbine rotor.

The working principle of the turbine is not new. A turbine of similar design was built about a century ago, but was not considered practical because of its low efficiency. However, it may well be that an inexpensive, simple and rugged prime mover with comparatively low efficiency will have immediate use as a solar engine in arid sections of the world.

TURBINE DESIGN

A solar boiler is assumed to deliver saturated steam at 50 psia to the turbine which is shown in Fig. 1 and 2. It consists of a base, two ball-bearing pillow blocks, a rotor which is constructed of a ⅜-in. shaft with a ⅝-in. S-shaped pipe, a convergent divergent nozzle, a teflon seal, a seal housing, and a steam-inlet pipe. The S-shaped pipe is enclosed with two shields in order to reduce heat and windage losses. The nozzle is soldered in the pipe end and can be replaced by others to suit the different steam pres-

sures. All parts are made of low-carbon steel except the cast iron pillow blocks and the brass nozzle. The pillow blocks can be dismounted from the shaft by releasing the setscrews. The diameter of the turbine rotor is 1 ft, and it is statically balanced.

CALCULATIONS

Reaction Force and Horsepower

The jet of steam is discharged from the nozzles with the relative velocity w, while the nozzle moves in the opposite direction with the absolute velocity u. Hence, the absolute velocity of the jet is $C = (w - u)$ ft per sec.

The velocity of the steam entering the nozzle is negligible; its momentum at the entrance section is $M_1 = 0$. Let the steam flow rate be G lbs per sec; then the change in momentum in pounds per second is given by

$$R = M_2 - M_1 = \frac{G}{g} \times C = \frac{G}{g}(w - u) \qquad [1]$$

where:

g = acceleration due to gravitation, [2]
$w = \sqrt{2gJ\,(h_1 - h_2)}$ ft per sec,
h_1 = enthalpy per lb of steam at nozzle entrance,
h_2 = enthalpy per lb of steam at nozzle exit,
J = conversion factor between Btu and ft-lb.

The velocity of the nozzle in feet per second is

$$u = \frac{\pi \times D \times n}{60} \qquad [3]$$

where:

D = diameter of turbine rotor,
n = RPM = number of revolutions per minute.

The horsepower produced by the turbine is $\frac{R \times u}{550}$, or

$$HP = \frac{G}{g \times 550}(w - u)u \qquad [4]$$

$$\frac{d(HP)}{du} = \frac{G}{g \times 550}(w - 2u) \qquad [5]$$

Hence, the turbine develops the maximum horsepower when $(w - 2u) = 0$, or $u = w/2$ ft per sec.

The nozzle was designed for a flow of 30 lbs per hr of saturated steam, expanding isentropically from 50 psia at the entrance to 14.7 psia at the exit.

Rotational Loss

The rotational loss due to air resistance was calculated from the equation[3]

$$N = \frac{3.32 \times D^2 \times u^{2.85}}{10^9} \qquad [6]$$

in which N is the horsepower, D is the diameter of a disc in feet, and u is the peripheral volicity of the disc in ft per sec.

For the different values of the diameter of the turbine rotor, 0.5 ft, 0.8 ft, 1.0 ft, 1.2 ft, and 2.0 ft, a set of five rotational loss curves was constructed and superimposed on the horsepower curves at a steam-flow rate of 30 lbs per hr and a pressure of 50 psia. From these curves it was found that the maximum net horsepower in the speed

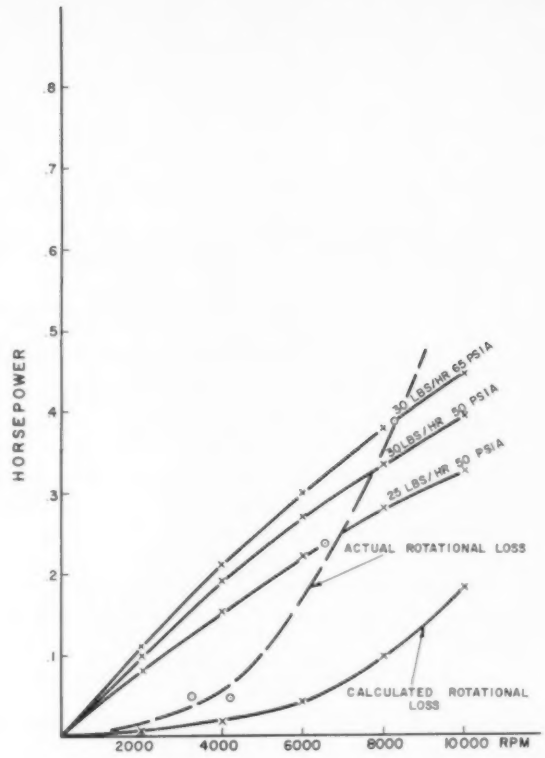

FIG. 3 — Horsepower curves vs. RPM for the pressures 50 psia, 65 psia, and a steam rate of 25 and 30 lb per hour.

range of 0 to 10,000 RPM is obtained with a rotor diameter of approximately 1 ft. This size was, therefore, chosen for the turbine rotor.

Thermal Brake Efficiency

The thermal brake efficiency is

FIG. 4 — Horsepower curves vs. RPM for the pressure range 20 psia to 170 psia and a steam rate of 30 lb per hour.

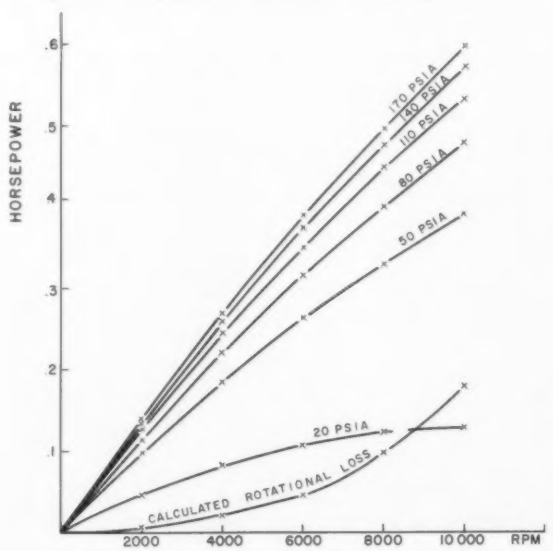

$$n = \frac{\text{BHP} \times 2544}{G \times h} \qquad [7]$$

where:

BHP = brake horsepower,

G = number of pounds of steam per hour flowing through the turbine,

h = enthalpy per pound of steam entering the turbine.

Horsepower Curves

The theoretical horsepower vs. number of revolutions per minute from 0 to 10,000 for saturated steam with steam rates of 30 and 25 lbs per hr expanding from 65 and 50 psia to 14.7 psia is shown in Fig. 3. Fig. 4 shows the horsepower vs. number of revolutions per minute from 0 to 10,000 for saturated steam with a steam rate of 30 lb per hr expanding from 170, 140, 110, 80, 50, and 20 psia to 14.7 psia. The maximum thermal brake efficiency vs. psia obtained from these curves is shown in Fig. 5.

TESTING PROCEDURE

The turbine was connected to a steam line and tested at 65 and 50 psia. The steam quality was determined by a Peabody calorimeter. A Prony brake was used to determine the brake horsepower at various speeds of the noncondensing turbine. To measure the steam consumption, the turbine was prevented from rotating at the operating pressure, and the steam from the nozzle was condensed and measured. The brake horsepower is

$$\text{BHP} = \frac{G \times L \times 2\pi \times n}{33{,}000} \qquad [8]$$

where:

BHP = brake horsepower,

G = weight on brake,

L = brake arm,

n = number of revolutions per minute of turbine.

The nozzle, designed for 50-psia pressure, was also used at 65-psia pressure. A small centrifugal pump was connected to the turbine, and measurements were made to determine the quantity of water that could be pumped against a head of 12 ft.

FIG. 5 — Efficiency vs. pressure for reaction turbine using saturated steam with a steam rate of 30 lb per hour expanding from 170, 140, 110, 80, 50, and 20 psia to 14.7 psia.

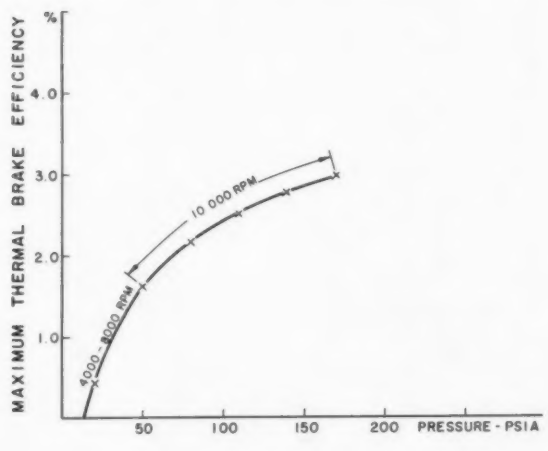

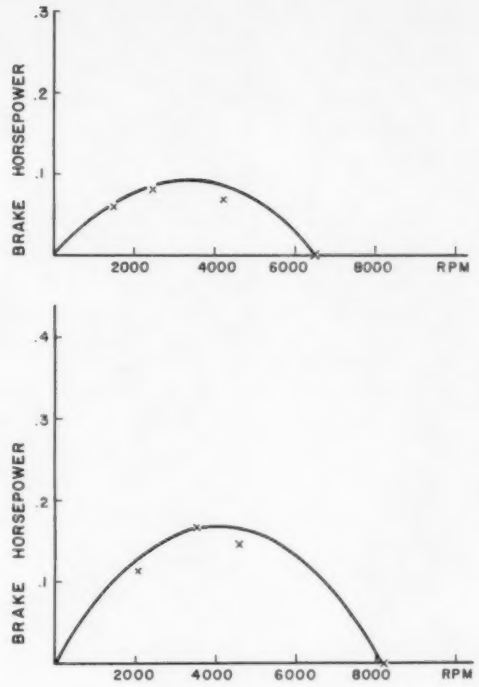

FIG. 6 — Brake horsepower vs. RPM for reaction turbine. Upper curve is for 50 psia, curve below is for 65 psia.

TEST RESULTS

The following data were obtained at 65 and 50 psia pressure with a steam quality of 98.0 per cent and 97.5 per cent respectively.

RPM	BHP	Pressure (psia)	Steam consumption (lb per hr.)
8250	0	65	30
4495	0.146	65	30
3500	0.167	65	30
2045	0.114	65	30

RPM	BHP	Pressure (psia)	Steam consumption (lb per hr.)
6500	0	50	25
4200	0.0666	50	25
2540	0.0805	50	25
1500	0.0594	50	25

The curves of BHP vs. RPM are shown in Fig. 6. The combination of turbine and pump is shown in Fig. 7. The pump delivered 730 gal of water per hour against a head of 12 ft when the turbine was operating at 50 psia and 1800 RPM, and 1120 gal per hour when the turbine operated at 65 psia, 2100 RPM.

TURBINE PERFORMANCE

The turbine was connected to an experimental solar boiler which delivered steam at 50 psia when heated by a

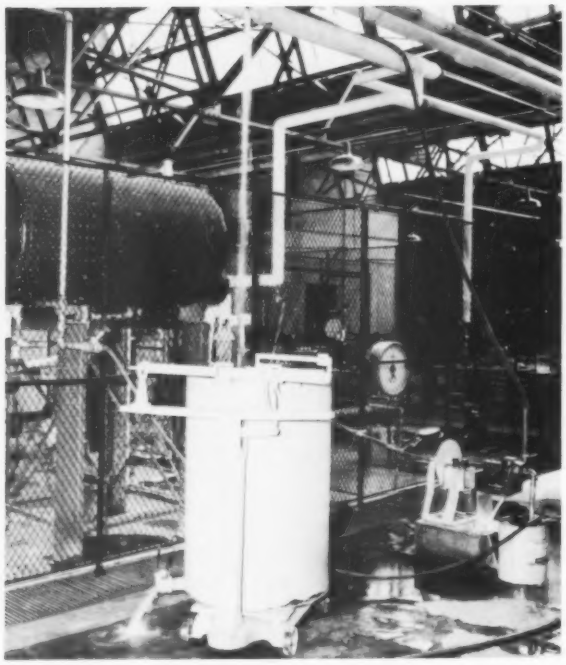

FIG. 7 — Combination of reaction turbine and centrifugal pump.

FIG. 8 — Reaction turbine running on steam generated by a solar boiler.

spherical reflector. The turbine could be operated only for short periods because of the lack of sufficient steam supply. The turbine and part of the reflector are shown in Fig. 8.

The maximum thermal brake efficiency was found to be 0.8 per cent at 50 psia and 1.2 per cent at 65 psia. The turbine ran smoothly without any appreciable vibration. Its power output and rotational losses balanced each other at 6500 RPM and 8200 RPM at 50 psia and 65 psia, respectively. No maintenance work was necessary on either turbine or pump during an operation period of 50 hours.

PERFORMANCE OF OTHER SMALL ENGINES

For the purpose of comparison, a collection of five small steam engines of varied design was also tested to determine the individual performance of the engines at 50- and 65-psia pressure. The collection included an impulse turbine (1), a larger and a smaller slide-valve steam engine (2) and (3), a rotary steam engine (4), and a poppet-valve-type steam engine (5). The engines are shown in Fig. 9.

The turbine was designed to give 1 HP at 115-psia pressure and 3000 RPM. The larger steam engine was designed for 50- to 135-psia pressures. The smaller steam engine was designed for saturated steam at 65 psia; the rotary engine and the poppet-valve engine were both designed for saturated steam at 135-psia pressure. All engines were oil-lubricated except the rotary engine.

The maximum thermal brake efficiency of these engines at the pressures 50 and 65 psia was 0.44 per cent and 0.5 per cent for the impulse turbine, 0.28 per cent and 0.47 per cent for the rotary engine, 1.38 per cent and 1.8 per cent for the larger steam engine, 1.29 per cent and 1.22 per cent for the smaller steam engine, and 0.46 per cent and 1.18 per cent for the poppet-valve engine.

The impulse turbine, the poppet-valve steam engine, and the larger steam engine had a maximum thermal

FIG. 9 — Engines tested for performance. Top (left to right): larger steam engine (2), impulse turbine (1), reaction turbine. Bottom (left to right): smaller steam engine (3), rotary engine (4), poppet-valve-type steam engine (5). Note 2-ft scale.

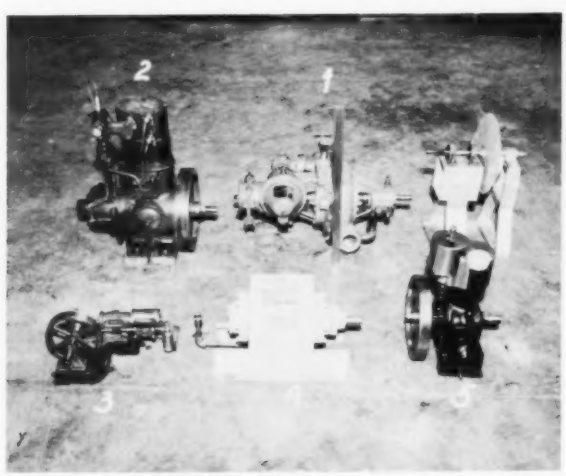

brake efficiency of 1.13, 1.18, and 1.4 per cent; 2.04, 2.5, and 4.5 per cent; and 3.3, 3.0, and 3.6 per cent at the respective pressures 90, 115, and 140 psia. The rotary engine stalled at these pressures and efficiency data could, therefore, not be obtained. The smaller steam engine was not tested since it was not designed for higher pressure than 65 psia.

The steam engines and the rotary engine had to be turned to get started. The smaller steam engine had leaks, and the exhaust of the poppet-valve engine contained oil.

The manufacturing cost of these five engines ranges from 75 to 500 dollars a piece, the smaller steam engine having the lowest cost; the manufacturing cost of the reaction turbine is about twenty dollars.

DISCUSSION OF RESULTS

It can be seen from Fig. 3 that the actual rotational-loss curve, which includes heat and friction loss besides windage loss, is considerably steeper than the calculated rotational loss curve at speeds above 4000 RPM. The largest part of the deviation is probably due to the air resistance by the nozzle end of the turbine rotor.

The teflon seal has functioned very well. It can be replaced easily at low cost in case of failure.

The ball bearings are very satisfactory. They reach a maximum temperature of approximately 100°F when the turbine was running at 65 psia pressure.

It was difficult to find a collection of engines all designed for 50 and 65 psia pressure. The efficiency data are, therefore, not complete.

CONCLUSIONS

It is evident that the reaction turbine does not have a high efficiency. However, its efficiency for pressures up to 65 psia is not much smaller than the efficiency of other steam prime movers for this pressure range. The great advantage of the reaction turbine is its low manufacturing cost, simple design, easy maintenance, and high reliability.

ACKNOWLEDGEMENT

The authors wish to acknowledge the financial support for these studies supplied from the Rockefeller Foundation through a grant for research on the utilization of solar energy.

REFERENCES

1. *Solar energy research;* ed. by Daniels and Duffie. Madison, Univ. of Wisconsin Pr., 1955.
2. M. J. Zucrow, *Jet propulsion and gas turbines.* N.Y., Wiley.
3. Stodola and Loewenstein, *Steam and gas turbines.* N.Y., McGraw-Hill, 1927. Vol. I, p. 197.
4. Rudolf Mewes, *Dampfturbinen.* Berlin, Verlag von M. Krayn.
5. Charles Henry Pope, *Solar heat; its practical applications.* Boston, A.B.C.H. Simonds & Co., 1903.
6. *Proceedings of the World Symposium on Applied Solar Energy.* Stanford Research Institute, 1956.
7. John I. Yellott, "Energy from the sun." *Power Eng.* Feb. 1957:94.
8. John I. Yellott, "Power from solar energy." *Trans. Am. Soc. Mech. Engr.* 79:1349, Aug. 1957.

SOLAR COLLECTOR SURFACES WITH WAVELENGTH SELECTIVE RADIATION CHARACTERISTICS*

By T. F. IRVINE, JR., J. P. HARTNETT, and E. R. G. ECKERT

Department of Mechanical Engineering, University of Minnesota, Minneapolis

The use of porous materials through which a coolant is forced for the protection of surfaces exposed to high temperature gas streams has been discussed in a number of recent papers. The knowledge of the radiation properties of these materials is required if the designer is to be able to predict the porous wall temperatures to determine whether metallurgical limitations have been exceeded. With this application in mind, measurements were previously reported for the absorptivity for solar radiation of a number of porous surfaces.[1] Since that time total normal emissivity data have been obtained for the same surfaces. In viewing these results, it was discovered that these surfaces combined high absorptivity for solar radiation with a low emissivity value, and consequently their use as solar collectors is suggested. It is the purpose of this paper to describe the experimental apparatus used to obtain the radiation data and to compare the recent emissivity measurements with the solar absorptivity data for the same surfaces. For specified conditions, an efficiency is defined which allows a quantitative comparison of these with other surfaces as solar collectors.

DESCRIPTION OF APPARATUS

Total Normal Emissivity Measurements

The equipment used for the measurement of the total normal emissivity is shown in Fig. 1 and has previously been discussed in detail.[2] Only a brief description will be given here. The most essential piece of equipment is the radiometer, which is so designed that radiant energy entering the opening (a) is collected by a 6-in.-diameter, gold-surface mirror (b) and directed to the receiving surface of a thermopile (c), which in turn is connected to a galvanometer. The porous test specimen (e) is held tightly against an electrically heated copper plate, and the entire assembly is supported in a transite frame. A reference for the radiation measurements is provided by the black body (d). The blackbody and the test sample temperature are controlled by varying the electrical power input to individual heaters. A double-walled container (f) with the inner and outer walls coated with a black paint of high absorptivity for long wavelength radiation surrounds the test specimen. Cooling water flows through this guard container, thereby creating a surrounding with well-defined temperature and radiation characteristics. A cylindrical opening in the guard permits the radiometer to view the test sample. In addition, an indentation of 1¼-in. diameter and 4½-in. deep in the guard creates a blackbody (g) at the surrounding guard temperature.

After equilibrium conditions have been reached, the radiometer is sighted, in turn, on the porous surface (e) and the two black bodies (d) and (g). The resulting galvanometer deflections are recorded. These readings, in conjunction with the corresponding temperature measurements, allow the calculation of the emissivity from the relations:

$$\epsilon_s = \frac{T_b^4 - T_g^4}{T_s^4 - T_g^4} \times \frac{\Delta_2 - \Delta_3}{\Delta_1 - \Delta_3} \qquad [1]$$

where:

ϵ_s = total normal emissivity of test specimen (e),
T_b = temperature of black body (d), deg R,
T_g = temperature of guard opening (g), deg R,
T_s = temperature of test specimen, deg R

*Publication from the Heat Transfer Laboratory, Mechanical Engineering Department, University of Minnesota, Minneapolis, Minnesota.

FIG. 1 — Apparatus for measuring total normal emissivities.

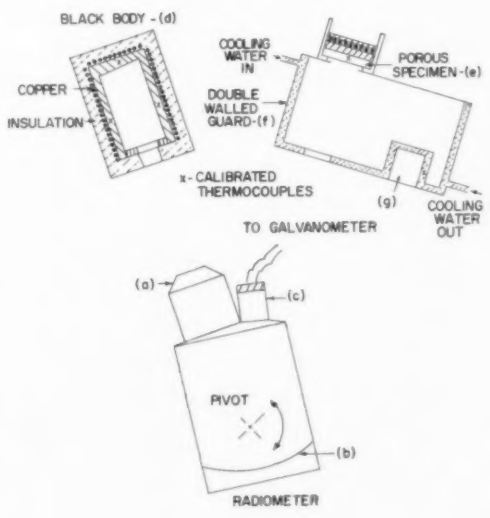

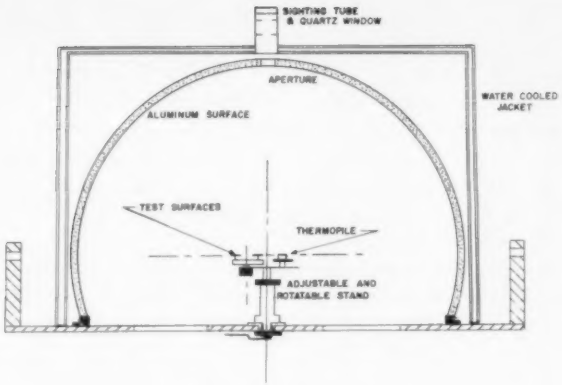

ABSOLUTE INTEGRATING RADIOMETER

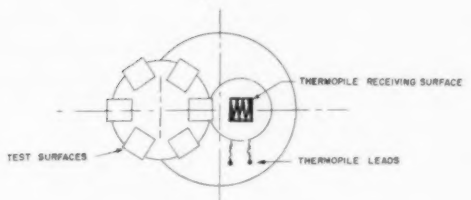

TOP VIEW

THERMOPILE AND TEST SURFACE ADJUSTABLE STAND

FIG. 2 — Apparatus for solar absorptivity measurements.

Δ_1 = galvanometer reading when radiometer is sighted at black body (d),

Δ_2 = galvanometer reading when radiometer is sighted at test surface (e),

Δ_3 = galvanometer reading when radiometer is sighted at guard opening (g),

Solar Absorptivity Measurements

The absorptivity values of the porous materials as reported in Ref. 1 were determined with an absolute integrating radiometer as shown in Fig. 2. A thermopile and a test surface are located on conjugate foci on the diameter of the hemisphere. If solar energy passes through the aperture directly onto the receiving surface of the thermopile, the reading of the galvanometer connected to the thermopile is an indication of the amount of incident solar energy. If the solar energy is next reflected off the test surface and onto the thermopile, the necessary integration of energy reflected at all angles is accomplished by the hemispherical surface. By taking the ratio of the energy reflected onto the thermopile from the test surface to that energy directly incident onto the thermopile and applying minor corrections,[1] the reflectivity and hence the absorptivity can be determined.

DESCRIPTION AND PREPARATION OF TEST SURFACES

Measurements have been obtained with the following classes of porous surfaces: (a) Poroloy surfaces, (b) modified Tyler materials.

The Poroloy materials[3] used in this investigation were fabricated commercially of stainless-steel wire wound on a mandrel one layer over another to yield the desired porosity. The material was then sintered. A chemical analysis yielded the proportions given in Table I of chromium and nickel for the stainless-steel Poroloy specimens tested.

TABLE I
A CHEMICAL ANALYSIS OF POROLOY SPECIMENS

Porosity of material (per cent)	Nickel (per cent)	Chromium (per cent)
28	8.86	18.7
31	8.87	18.6
43	8.78	18.3

The modified Tyler materials[4] are composed of screens which have been fabricated by a special weaving process. The screens are then rolled to give the desired porosity. The base material is AISI type 304 stainless steel.

All samples were so dense that no light could be seen through them when they were held against a light bulb. Prior to the measurements, all test surfaces were washed with benzol and then with acetone. To further specify the Poroloy and Tyler surfaces, photomicrographs are shown in Fig. 3.

FIG. 3 — Photomicrographs of porous surfaces.

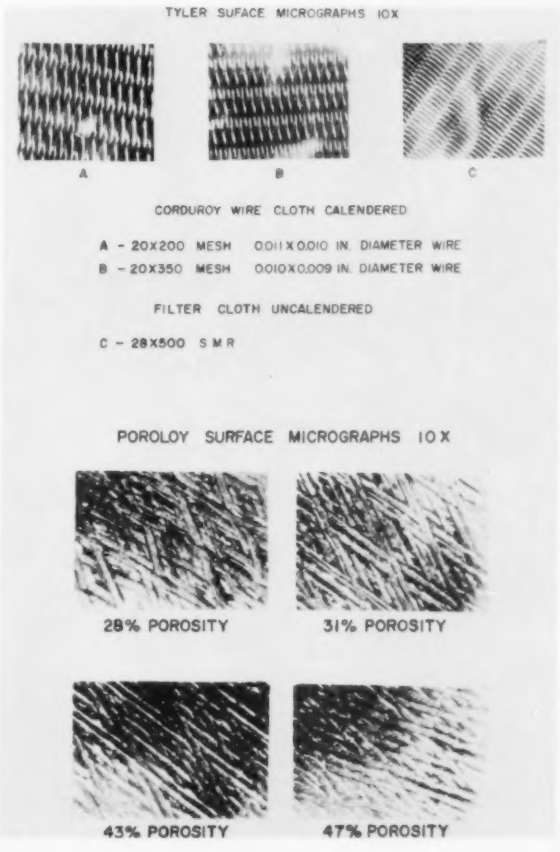

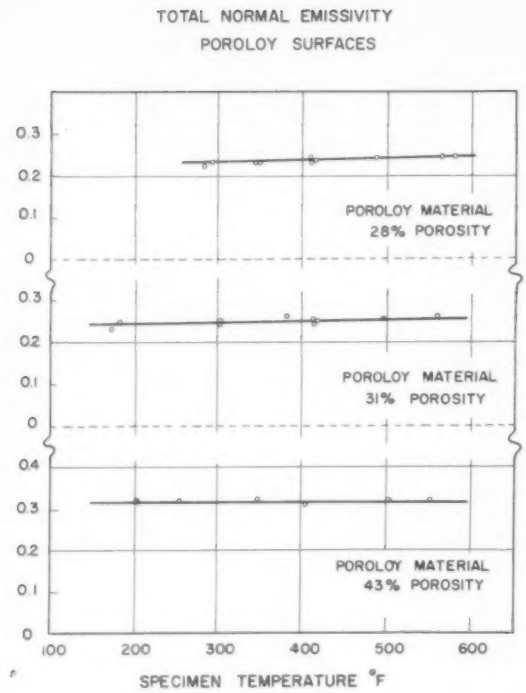

FIG. 4 — Total normal emissivities for Poroloy surfaces.

FIG. 5 — Total normal emissivities for Tyler surfaces.

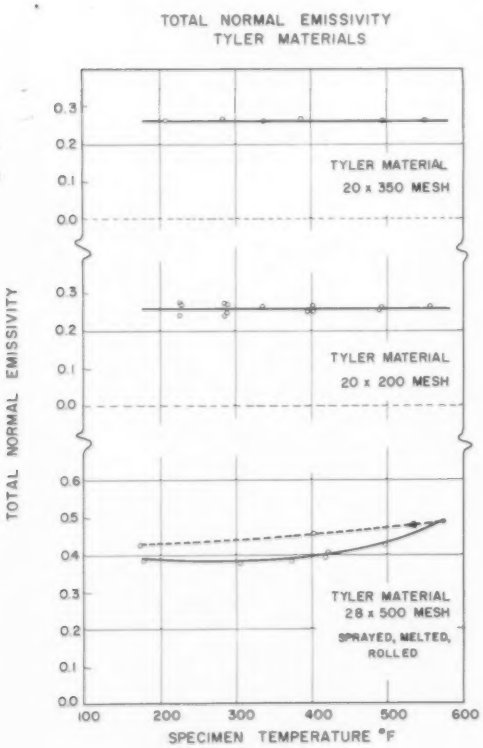

RESULTS AND DISCUSSION

The measured total normal emissivity values are shown in Figs. 4 and 5 for the Poroloy and Tyler materials, respectively. The total normal emissivity values for the Poroloy surfaces were found to be approximately 0.25 for the 28 and 31 per cent porosities. The 43 per cent porosity surface shows a somewhat higher value of 0.32. A slight increase with temperature for any one specimen is also apparent. It is of interest to note that measurements of solid stainless-steel specimens using the same apparatus yielded values ranging from 0.13 for a highly polished surface to 0.22 for a dull surface finish.

Two of the Tyler surfaces, the 20 x 350 mesh and the 20 x 200 mesh, yield values of total normal emissivity of approximately 0.26, which is quite constant over the temperature range of the measurements (100°-600°F). The third material, the 28 x 500 mesh, shows much higher values of emissivity, which increases with temperature from 0.38 at 175°F to 0.48 at 575°F. The emissivity difference between the various Tyler materials may be understood by referring to the photomicrographs, Fig. 3, which show that two of these surfaces, the 20 x 200 mesh and the 20 x 350 mesh, are of similar weave, differing only in one dimension of mesh size. The third Tyler surface which is sprayed with soldering material, melted, and rolled, presents a markedly different surface appearance.

These recent emissivity values along with the earlier solar absorptivity results are summarized in Table II.

TABLE II
EMISSIVITY AND ABSORPTIVITY OF POROLOY AND TYLER SURFACES

Surface	Total absorptivity for normally impinging solar radiation (surface at 100 °F)[1]	Total normal emissivity (surface at 200 °F)
Poroloy		
28%	0.63	0.23
31%	0.63	0.24
43%	0.66	0.32
Tyler		
20 x 350 mesh	0.73	0.26
20 x 200 mesh	0.77	0.25
28 x 500 mesh	0.86	0.38

These values emphasize that the emissivity of a surface, in general, is not equal to the absorptivity of the surface for impinging radiation. This point, often misunderstood in the radiation literature, can be seen clearly by referring to the equations which define the total emissivity and the absorptivity.

Emissivity

$$\epsilon = \frac{\int_0^\infty \epsilon_{\lambda T}\, e_{b\lambda T}\, d\lambda}{\int_0^\infty e_{b\lambda T}\, d\lambda} \qquad [2]$$

where:

ϵ = total emissivity of surface at temperature T,
$\epsilon_{\lambda T}$ = monochromatic emissivity of the surface at temperature T,
$e_{b\lambda T}$ = monochromatic emissive power of a black body

at temperature T,
λ = wavelength.

Absorptivity

$$a = \frac{\int_0^\infty a_{\lambda T} G_{\lambda T_0} d\lambda}{\int_0^\infty G_{\lambda T_0} d\lambda} \qquad [3]$$

where:

a = total absorptivity of surface at temperature T,
$a_{\lambda T}$ = spectral absorptivity of surface at temperature T,
$G_{\lambda T_0}$ = monochromatic intensity of incoming radiation from a source at temperature T_0.

Kirchhoff's law in its basic form may be written

$$\epsilon_{\lambda T} = a_{\lambda T} \qquad [4]$$

The total emissivity ϵ is, according to Equation [2], a function of the surface properties and the surface temperature. The total absorptivity is, according to Equation [3], a function of these two parameters, but in addition is dependent on the wavelength distribution of the impinging radiation $G_{\lambda T}$. Thus, the total absorptivity is, in general, equal to the total emissivity only for the following conditions: (a) the body is gray (i.e., $\epsilon_{\lambda T}$ and $a_{\lambda T}$ are independent of the wavelength λ) allowing $\epsilon_{\lambda T}$ and $a_{\lambda T}$ to be removed from inside the integral sign, or (b) the incoming radiation, $G_{\lambda T}$, is equal to $e_{b\lambda T}$, that is, when the incoming radiation is blackbody radiation at the temperature of the receiving surface. The assumption of grayness is applicable only to a limited number of engineering materials and, at best, represents an approximation. Generally this assumption of grayness will lead to incorrect results of the incoming radiation and the emitted radiation are concentrated in different portions of the spectrum.

The incoming radiation for the solar absorptivity temperature measurements is essentially blackbody radiation at a temperature of 10,000°F, which is markedly different in its wavelength distribution from the distribution of blackbody radiation at the surface temperature of 100°F. The results of Table II indicate that the monochromatic emissivity of the two classes of metal surfaces increases with decreasing wavelength.

EFFECTIVENESS OF POROUS MATERIALS AS SOLAR COLLECTORS

It is clear that solar collector surfaces should possess large solar-absorption coefficients and low emissivities. This point has been discussed by Tabor,[5] who has developed a surface having such characteristics by means of coating techniques.

In order to evaluate quantitatively the performance of selective surfaces, it is of interest to define a collector model. Such a model is illustrated in Fig. 6. The surface consists of a flat plate oriented normal to the direction of the sun's rays. For simplicity, it is specified that the plate temperature is constant and that useful energy is being removed from the rear of the plate by means of an appropriate circulating fluid. An energy balance written on a unit area of the surface takes the following form:

$$a_s Q_s = \epsilon_{T_c} \sigma T_c^4 + h_a (T_c - T_a) + Q_c \qquad [5]$$

In this equation, a_s is the collector absorptivity to solar radiation, Q_s the impinging solar radiation, ϵ_T the emissivity of the surface at the plate temperature T_c, σ is Boltzmann's constant for black body radiation, h_a the heat transfer coefficient between the plate and the surrounding air at temperature T_a, and Q_c the useful heat energy removed from the rear of the surface.

Since the object of the collector is to make Q_c as large as possible in comparison with Q_s, it is natural to define a collector efficiency η_c, as the following ratio:

$$\eta_c = \frac{Q_c}{Q_s} \qquad [6]$$

A combination of Equations [5] and [6] produces the following expression for collector efficiency:

$$\eta_c = a_s \left[1 - \frac{\epsilon_{T_c} \sigma}{a_s Q_s} T_c^4 - \frac{h_a}{a_s Q_s} (T_c - T_a) \right] \qquad [7]$$

Equation [7] indicates that the collector efficiency increases as either ϵ_{T_c}/a_s or the convective heat loss decreases, with a maximum collector efficiency reached when

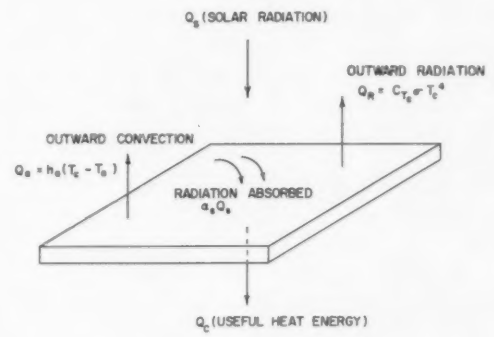

FIG. 6 — Flat-plate collector model.

FIG. 7 — Collector efficiency vs. collector temperature for a number of surfaces: (1) lamp-black paint; (2) graphite; (3) Tyler 20 x 350; (4) Tyler 20 x 200; (4A) Tyler 20 x 200 — no convection; (5) Tyler 28 x 500; (6) coated surface (described in Ref. 8); (6A) Coated surface (Ref. 8) — no convection.

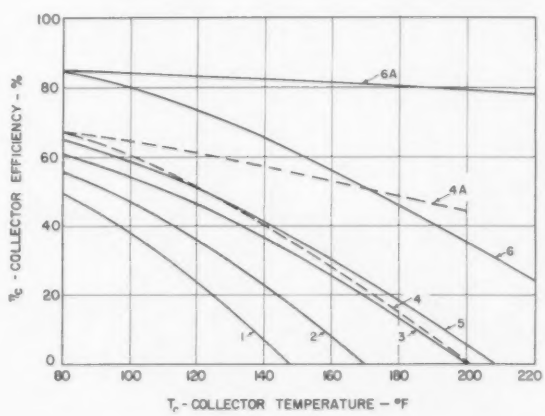

TABLE III

DATA USED FOR CALCULATING CURVES IN FIG. 6

$$Q_s = 300\ \frac{\text{Btu}}{\text{ft}^2 - \text{hr}},\quad T_a = 80^\circ\text{F},\quad h_a = 0.22\ (T_c - T_a)^{1/3}$$

Material	Tyler 20x350 mesh	Tyler 20x200 mesh	Tyler 28x500 mesh	Graphite[6]	Lamp-black paint[7]	Coated surface[8]
α_s	0.73	0.77	0.86	0.85	0.97	0.9
ϵ_{T_c}	0.26	0.25	0.38	0.60	0.97	0.1

these two quantities go to zero. This maximum value for the collector efficiency is numerically equal to the solar absorptivity, thereby emphasizing the desirability of high absorptivity values.

An interesting comparison of surfaces can be made with Equation [7]. If Q_s and T_a are specified, and h_a evaluated as turbulent-free convection from an upward-facing plate,[6] it is possible to relate the collector efficiency to the plate temperature as is done in Fig. 7. The data used in calculating Fig. 7 are shown in Table III. Since both η_c and T_c are measures of successful collection, i.e., in general both should be as large as possible, Fig. 7 illustrates over a range of possible operating conditions the relative merits of the surfaces.

Fig. 7 illustrates that dull black paint, although frequently used in solar collectors, is a poor surface, especially at higher temperatures. Next in order of increasing efficiency are graphite, the porous surfaces, and the coated surfaces. It will be noted that the differences are significant among the various surfaces where, for instance, at a collector temperature of 120°F the black paint has an efficiency of 24 per cent and the Tyler T-28-500 an efficiency of 51 per cent.

A recent paper[8] has discussed the desirability of facing the collector in a downward direction to reduce convective heat losses from the collector surface. As a limiting case of no convection losses, curves 4-A and 6-A in Fig. 6 show the performance of a porous and a coated surface under such conditions.

As seen in Fig. 7, the coated surface has a collector efficiency higher than the porous surfaces. Two factors, however, continue to make the porous surfaces attractive. The aging and mechanical strength characteristics of the coatings have been a disadvantage in their use. The porous surfaces may overcome these difficulties. Also, the porous surfaces discussed in the present paper were not chosen beforehand for desirable wavelength characteristics. It is possible that a systematic investigation may reveal porous surfaces with even better radiation properties from a solar collector standpoint.

ACKNOWLEDGEMENT

The financial aid of the Graduate School of the University of Minnesota made this research possible, and the authors gratefully acknowledge this support. In addition, the authors are indebted to Mr. Richard O'Neill for obtaining the test data and to F. J. Bradac for his help in the fabrication of the test equipment.

REFERENCES

1. Richard C. Birkebak and J. P. Hartnett, "Measurements of the total absorptivity for solar radiation of several engineering materials." *Trans. Am. Soc. Mech. Engr.* 80:373, 1958.
2. E. R. G. Eckert, J. P. Hartnett, and T. F. Irvine, "Measurement of total emissivity of porous materials in use for transpiration cooling." *Jet Propulsion*, April 11, 1956.
3. *Poroloy Catalog*. Poroloy Equipment, Inc., Pacioma, Calif.
4. *Tyler Catalog*. W. S. Tyler Company, Cleveland, Ohio.
5. H. Tabor, "Selective radiation I: wavelength discrimination." *Bull. Res. Conc. Israel* 5A:119, April 1956.
6. W. H. McAdams, *Heat transmission*. N.Y., McGraw-Hill, 1954.
7. W. W. Coblenz. *Bull. Nat. Bur. Stand.*, No. 9, 1912.
8. H. Tabor, "Solar energy research." *Solar Energy* 2(1):3, Jan. 1958.

THE EFFECT OF SURFACE COATINGS ON THE SOLAR RADIATION EQUILIBRIUM SKIN TEMPERATURE OF AN EARTH SATELLITE

By JAMES R. JENNESS, JR.

Haller, Raymond, and Brown, Inc., State College, Pennsylvania

The skin temperature of an earth satellite is governed mainly by equilibrium between absorbed solar radiation and re-emitted infrared radiation. A polished metal surface will reflect a large portion of the incident solar radiation but will give a relatively high skin temperature because its infrared emissivity is low. A coating of white nonmetallic material will give a lower skin temperature, even though it absorbs a greater portion of the incident solar radiation, because its infrared emissivity is much greater.

INTRODUCTION

At stable-orbit altitudes, collisions of an earth satellite with residual gas molecules produce a negligible amount of "aerodynamic" heating. The satellite's skin temperature depends mainly on the balance between radiation absorbed from the sun, earth, and moon, and radiation emitted by the satellite. The amount of radiant energy received from the moon is very small compared to that from the sun; it will therefore be neglected. Although it is not negligible, the radiation received from the earth is less intense than direct solar radiation, and the error resulting from disregarding radiation reflected and emitted by the earth will not be great. A first-order estimate of a satellite's skin temperature can be obtained by considering the sun as the only heat source.

HEAT FLOW IN SPHERICAL SHELL

Consider a spherical shell of radius r and thickness s as shown in Fig. 1. Radial temperature gradients will be neglected, and radiation exchange between different parts of the inner surface will be neglected also, with the realization that tangential temperature gradients will be slightly reduced by this effect.

The heat gained by a ring element of area $2\pi r^2 \sin\theta \, d\theta$ is equal to the solar radiation absorbed plus the heat conducted from the adjacent ring element whose temperature is higher. The heat lost is equal to the radiation emitted plus the heat conducted to the adjacent ring element whose temperature is lower. The solar radiation absorbed by a ring element of the sphere's surface is

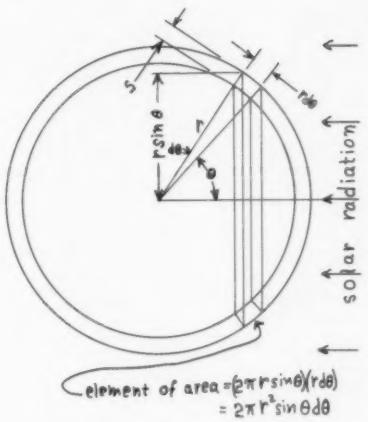

FIG. 1 — Spherical shell exposed to solar radiation.

$$(2\pi r^2 \sin\theta \, d\theta) \cos\theta \int_0^\infty \epsilon_\lambda I_\lambda \, d\lambda$$

and the radiation emitted by the ring is

$$2\pi r^2 \sin\theta \, d\theta \int_0^\infty \epsilon_\lambda W_{T\lambda} \, d\lambda$$

where:

ϵ_λ is the spectral emissivity (and absorptivity) of the sphere's surface for radiation of wavelength λ,

I_λ is the intensity of solar radiation per unit wavelength increment at wavelength λ,

and

$W_{T\lambda}$ is the radiating power per unit wavelength increment at wavelength λ of a black body at temperature T.

The rate of flow of heat through a segment of cross sectional area a and thickness D with is opposite faces at temperatures T_1 and T_2 is $k(T_2 - T_1)a/D$, where k is the thermal conductivity of the material. It is assumed that the shell thickness s is small relative to the radius r, so that the cross sectional area of a ring element of the sphere is $(2\pi r \sin\theta)\, s$. For a very narrow ring, $D = r\,d\theta$ and $T_2 - T_1 = -dT$, since it is obvious that T decreases

with increasing θ. Thus, the tangential rate of flow of heat at an angle θ from the direction of incident solar rays is

$$k(-dT)\ (2\pi rs\sin\theta)/rd\theta = -2\pi ks\sin\theta\frac{dT}{d\theta}$$

(The negative sign indicates that heat flows in the direction opposite to that of the temperature gradient, from higher to lower temperatures.)

In the steady state, the rate of flow of energy into each ring element of the spherical shell is equal to the outward rate of flow, so that

$$2\pi r^2\sin\theta\cos\theta\,d\theta\int_0^\infty \epsilon_\lambda I_\lambda\,d\lambda - 2\pi ks\sin\theta(dT/d\theta)_\theta =$$

$$2\pi r^2\sin\theta\,d\theta\int_0^\infty \epsilon_\lambda W_{T\lambda}\,d\lambda - 2\pi ks\sin\theta(dT/d\theta)_{\theta+d\theta}$$

Removing the common factor $2\pi\sin\theta$ and rearranging,

$$ks\,[(dT/d\theta)_{\theta+d\theta} - (dT/d\theta)_\theta] = r^2d\theta\int_0^\infty(W_{T\lambda} - I_\lambda\cos\theta)\,\epsilon_\lambda\,d\lambda$$

Now,

$$\frac{(dT/d\theta)_{\theta+d\theta} - (dT/d\theta)_\theta}{d\theta} = \frac{d}{d\theta}\frac{dT}{d\theta}$$

so

$$\frac{d^2T}{d\theta^2} = \frac{r^2}{ks}\int_0^\infty(W_{T\lambda} - I_\lambda\cos\theta)\,\epsilon_\lambda\,d\lambda \qquad [1a]$$

from $\theta = 0$ to $\theta = \pi/2$, and

and

$$\frac{d^2T}{d\theta^2} = \frac{r^2}{ks}\int_0^\infty W_{T\lambda}\,\epsilon_\lambda\,d\lambda \qquad [1b]$$

from $\theta = \pi/2$ to $\theta = \pi$. (Two equations are required for an adequate description of the heat flow in the spherical shell, since no solar radiation is incident on the surface from $\theta = \pi/2$ to $\theta = \pi$.)

Now I_λ is not a function of θ, and, for a given surface, ϵ_λ is determined, so that

$$\int_0^\infty I_\lambda\,\epsilon_\lambda\,d\lambda = A = \text{constant}$$

This constant is the rate of absorption of energy per unit area by a given surface exposed to normally incident solar radiation unfiltered by the earth's atmosphere. For most materials, ϵ_λ varies over a fairly wide range in the spectral region (0.3μ to 3.0μ wavelength) wherein 95 per cent of the sun's radiation is concentrated, so that the evaluation of A is somewhat involved. In the spectral region beyond 3μ, where most radiation is emitted by the spherical shell, ϵ_λ is more nearly constant, and

$$\int_0^\infty W_{T\lambda}\,\epsilon_\lambda\,d\lambda = \int_{3\mu}^\infty W_{T\lambda}\,\epsilon_\lambda\,d\lambda = \bar{\epsilon}\sigma T^4$$

where $\bar{\epsilon}$, the average value of ϵ_λ for $\lambda > 3\mu$, is taken as the effective value of total emissivity, and σ is the Stefan-Boltzmann constant. With these simplifying assumptions, Equations [1a] and [1b] become

$$\frac{d^2T}{d\theta^2} = \frac{r^2}{ks}(\bar{\epsilon}\sigma T^4 - A\cos\theta) \qquad [1a']$$

from $\theta = 0$ to $\theta = \pi/2$, and

$$\frac{d^2T}{d\theta^2} = \frac{r^2}{ks}\,\epsilon\,\sigma\,T^4 \qquad [1b']$$

from $\theta = \pi/2$ to $\theta = \pi$.

The total radiation emitted by the sphere is equal to the total radiation absorbed, so that

$$\int_0^\infty \epsilon_\lambda\,d\lambda\int_0^\pi W_{T\lambda}\,(2\pi r^2\sin\theta\,d\theta) = \int_0^\infty \epsilon_\lambda I_\lambda\,d\lambda\int_0^{\pi/2}(\pi r^2\sin\theta\,d\theta)\cos\theta$$

Removing the common constant factor $2\pi r^2$,

$$\int_0^\infty \epsilon_\lambda\,d\lambda\int_0^\pi W_{T\lambda}\sin\theta\,d\theta = \int_0^\infty \epsilon_\lambda I_\lambda\,d\lambda\int_0^{\pi/2}\sin\theta\cos\theta\,d\theta. \qquad [2]$$

With the simplifying assumptions in Equations [1a'] and [1b'], this becomes

$$A = 2\int_0^\pi \bar{\epsilon}\sigma T^4\sin\theta\,d\theta \qquad [2']$$

A solution for T as a function of θ has been obtained for only two limiting cases. In the first, k and/or s is zero, causing Equation [1'] to become indeterminate. This is the case of a very thin spherical shell of low thermal conductivity which must re-emit all absorbed solar energy at the spot where it is absorbed. Then $\epsilon\,\sigma\,T^4 - A\cos\theta = 0$, or

$$T = \left[\frac{A\cos\theta}{\bar{\epsilon}\sigma}\right]^{1/4} = T_{\max}(\cos\theta)^{1/4} \qquad [3]$$

from $\theta = 0$ to $\theta = \pi/2$, and $T = 0$ from $\theta = \pi/2$ to $\theta = \pi$. The average temperature of the sphere's surface is

$$\bar{T} = \frac{1}{4\pi r^2}\int_0^{\pi/2}\left[\frac{A\cos\theta}{\bar{\epsilon}\sigma}\right]^{1/4}(2\pi r^2)\sin\theta\,d\theta$$

$$= \tfrac{1}{2}\left[\frac{A}{\epsilon\,\sigma}\right]^{1/4}\int_0^{\pi/2}(\cos\theta)^{1/4}\sin\theta\,d\theta$$

$$= \tfrac{2}{5}\left[\frac{A}{\epsilon\,\sigma}\right]^{1/4} = \tfrac{2}{5}\,T_{\max} \qquad [4]$$

The other extreme occurs if the sphere rotates about an axis perpendicular to the incident solar rays so that it is at uniform temperature over its entire surface. Then T is not a function of θ, and Equation [2'] becomes $A = 4\bar{\epsilon}\sigma T^4$, from which

$$T = \bar{T} = \left[\frac{A}{4\epsilon\,\sigma}\right]^{1/4} = (1/4)^{1/4}\,T_{\max} = 0.707\,T_{\max} \qquad [5]$$

These two cases will never hold true exactly, but establish limits within which actual results are to be expected.

Assuming graybody conditions, i.e., $\epsilon_\lambda = \bar{\epsilon} =$ constant for all λ, Wilson[1] has found 418°K as the value of $T_{\max}$ in Equations [3], [4], and [5], and 296°K as the value of $T = \bar{T}$ given by Equation [5]. Considering in some detail the variation of ϵ_λ with λ, it will now be shown how these values are modified by the characteristics of the satellite's surface.

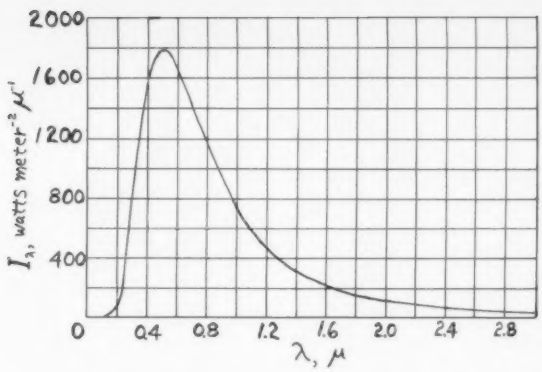

FIG. 2 — Spectral intensity of solar radiation.

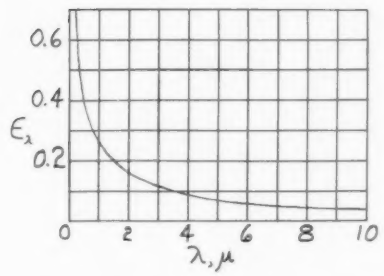

FIG. 3 — Spectral emissivity of a polished nickel surface.

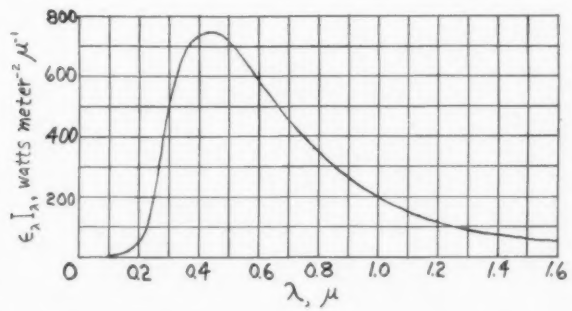

FIG. 4 — Spectral absorption of solar radiation by a polished nickel surface.

TEMPERATURE OF A SPHERE WITH A POLISHED NICKEL SURFACE

To determine the temperature to be expected for a spherical satellite with a polished nickel surface, it is first necessary to estimate the total absorption A for a polished nickel surface normal to the sun's rays above the earth's atmosphere. Fig. 2 shows I_λ as a function of λ. The integration of $I_\lambda\, d\lambda$ from $\lambda = 0$ to $\lambda = \infty$ would give the solar constant, 1.35 (10^3) w per sq m. Fig. 3 shows the spectral emissivity ϵ_λ for a nickel surface as a function of wavelength, found by subtracting from unity the spectral reflectivities of nickel given by the *Handbook of Chemistry and Physics*.[2] Fig. 4 shows the result of point-by-point multiplication of the curves of Fig. 2 and Fig. 3 to give a curve of the quantity $\epsilon_\lambda I_\lambda$ as a function of λ. The integration of a major portion of this function is carried out graphically, counting the squares under the curve to give (in watts per square meter)

$$\int_0^{1.6\mu} \epsilon_\lambda I_\lambda\, d\lambda = 424.5$$

About 10 per cent of the sun's radiation, or 1.35 (10^2) w per sq m is at wavelengths greater than 1.6μ, and from Fig. 3 it is seen that 0.1 is a reasonable estimate for the average absorptivity of the nickel surface from $\lambda = 1.6\mu$ to $\lambda = \infty$, so the total rate (in watts per square meter) of absorption of solar radiation by the polished nickel surface is $A_{Ni} = 424.5 + 13.5 = 438$.

A significant portion of the radiation re-emitted by the sphere is at wavelengths greater than 10μ, so it will be assumed that $\bar{\epsilon} = 0.06$ for emission of radiation by the nickel surface, as a relatively small portion of the re-emitted radiation is in the spectral region ($\lambda < 6\mu$), where ϵ_λ is greater than 0.06. Then, by Equation [3], for a thin spherical shell which keeps the same side toward the sun, the temperature T_{max} of the "hot spot" toward the sun is

$$\left[\frac{438 \text{ watts meter}^{-2}}{(0.06)\,(5.672)\,(10^{-8}) \text{ watts meter}^{-2}\,(^\circ\text{K}^{-4})}\right]^{1/4} = 600^\circ\text{K} = 327^\circ\text{C}$$

and the average temperature is, from Equation [4],

$$\tfrac{2}{5}(600^\circ\text{K}) = 240^\circ\text{K} = -33^\circ\text{C}$$

If the sphere rotates about an axis perpendicular to the incident solar rays so that it is uniformly exposed to solar radiation, its temperature is, from Equation [5],

$$(0.707)\,(600^\circ\text{K}) = 423^\circ\text{K} = 150^\circ\text{C}$$

SURFACE COATINGS TO MODIFY EMITTING AND ABSORBING CHARACTERISTICS

Similarly an estimate was made of the equilibrium temperature which would be attained by a spherical shell coated with a white porcelain enamel. The absorptivity in the visible was taken as unity minus the reflectivity for one of several porcelain enamels measured by Iliff[3] and was assumed to be unity (although it should be slightly less because of surface reflection) for ultraviolet radiation of wavelengths less than 0.3μ, as the shorter wavelength radiation is strongly absorbed by silica and other components of ceramic coatings. At wavelengths greater than 4.5μ, the emissivity was assumed to be approximately equal to that of typical silica glasses measured by McMahon.[4] Graphical integration similar to that carried out in Fig. 4 gives a total absorbing power $A_{coated} = 587$ w per sq m for the surface with a white porcelain enamel coating.

The average emissivity at wavelengths greater than 4μ is approximately 0.9, and this value will be taken for $\bar{\epsilon}$, as very little radiation is emitted at wavelengths less than 4μ. Then, for a satellite of low thermal conductivity which keeps the same side toward the sun, the temperature of the "hot spot" found by Equation [3] is

$$\left[\frac{587 \text{ watts meter}^{-2}}{(0.9)(5.672)\ 10^{-8} \text{ watts meter}^{-2}\ ^{\circ}\text{K}^{-4}}\right]^{1/4}$$
$$= 327^{\circ}\text{K} = 54^{\circ}\text{C}$$

and the average temperature from Equation [4] is

$$\tfrac{2}{3}(327^{\circ}\text{K}) = 131^{\circ}\text{K} = -142^{\circ}\text{C}$$

If the satellite is at uniform temperature by virtue of high thermal conductivity or uniform exposure to solar radiation, the temperature is

$$(0.707)(327^{\circ}\text{K}) = 232^{\circ}\text{K} = -41^{\circ}\text{C}$$

CONCLUSIONS

The temperatures computed above are not precise because of the simplifying assumptions involved. However, the case described by Equation [5] can be considered a first-order estimate, as it is highly improbable that a satellite will keep the same side toward the sun or have no redistribution of heat by conduction. It is seen that a polished metal surface, even though it reflects a greater portion of incident solar radiation, will result in a higher equilibrium skin temperature than will a nonmetallic coating because its infrared emissivity is much lower than that of a nonmetallic coating.

It is possible to provide an ambient temperature within the desired range for satellite instruments by a proper surface on the satellite's skin. The skin temperature can be set at any value between those for a white nonmetallic coating and a polished metal surface by dividing the total area in the proper proportions between polished metal and white coating in a regular pattern. An alternate method of controlling the temperature is variation of the thickness of a transparent coating of high infrared emissivity over a polished metal surface as described by Tousey.[4] Surface coatings such as paints, ceramic glazes, evaporated coatings, or anodized coatings should provide the desired absorbing and emitting characteristics, so that the coating material is restricted only by satisfactory adhesion to the satellite's skin during launching and orbit.

REFERENCES

1. Raymond H. Wilson, Jr. *Science* 127:811-812, April 11, 1958.
2. *Handbook of Chemistry and Physics,* 38th Edition. Cleveland, Ohio, Chemical Rubber Publishing Co., 1956. p. 2713.
3. John W. Iliff. *J. Am. Ceram. Soc.* 24:97-99, March 1941.
4. Howard O. McMahon. *J. Am. Ceram. Soc.* 34:91-96, March 1951.
5. R. Tousey. *J. Opt. Soc. Am.* 47:266, April 1957.

WAVELENGTH-DEPENDENT (SELECTIVE) PROCESSES FOR THE UTILIZATION OF SOLAR ENERGY

By L. H. SHAFFER

Central Research Laboratory, American Machine & Foundry Company, Stamford, Conn.

The theoretical maximum work obtainable from solar-powered selective absorber thermal devices is calculated. Selective thermal devices are compared with quantum devices and the optimum cut-off wavelengths and other operating parameters are calculated for both types of device. Selective thermal devices are capable of an exceedingly high over-all efficiency. Theoretically, as much as 55 per cent of the average sunlight received at the earth's surface may be converted to useful work. The effects of imperfect absorbing and reflecting surfaces and the effects of small convection and conduction losses are considered briefly.

INTRODUCTION

H. Tabor[1] has suggested that the efficiency of thermal processes for capturing solar heat, or for producing useful work from solar radiation, can be improved by using a selective absorbing surface. This surface is such that the absorptivity and emissivity are high up to some cut-off wavelength and are low for all wavelengths beyond the cut-off wavelength. It is the purpose of this paper to examine the theoretical consequences of using such a selective absorber. From a theoretical point of view it makes no difference whether the selectivity is obtained by some coating on the actual absorber surface or by inserting a suitable filter in front of a blackbody absorber. In practice, it may be desirable to obtain the necessary selectivity by combining both a selective filter and a selective absorber. If this is done, the net emissivity of the combination will be

$$1 \Big/ \left(\frac{1}{\epsilon_1} + \frac{1}{\epsilon_2} - 1 \right).$$

Quantum processes for recovering useful work from solar radiation are also characterized by a cut-off wavelength. For completeness, and because it is instructive to compare the performance of selective thermal absorbers with quantum devices, a brief discussion of the behavior of quantum devices is also included.

DISCUSSION

Efficiency of Solar-Powered Selective Absorber Thermal Device

A significant improvement in the efficiency of a solar-powered thermal device can be obtained if a selective absorber is used to collect the radiation. To determine the theoretical maximum efficiency, it is simplest to start by considering a device that is perfectly insulated. All of the heat absorbed by the collector is either reradiated or transferred without loss to a Carnot engine. We will assume that the engine discharges its heat to a resevoir at 300°K. In this case, the maximum work rate is

$$W' = \left\{ a\,G' - \epsilon\,\sigma(T_1^4 - 300^4) \right\} \left(1 - \frac{300}{T^1} \right) \quad [1]$$

and the over-all efficiency is

$$\eta'' = \eta'\,\eta = \frac{W'}{G'} = a \left\{ 1 - \frac{\epsilon\,\sigma}{a\,G'} (T_1^4 - 300^4) \right\} \eta \quad [2]$$

where:

W' = power (per sq cm of collector),
a = absorptivity for solar radiation,
G' = solar constant at earth's surface (assumed average value = 1 cal per sq cm per min = 6.97×10^5 ergs per sq cm per sec),
ϵ = emissivity for self-radiation,
σ = Stefan-Boltzmann constant = 5.673×10^{-5} ergs per sq cm per °K^4 per sec,
η'' = overall work efficiency,
η' = collection efficiency for solar radiation

$$= a \left\{ 1 - \frac{\epsilon\,\sigma}{a\,G'} (T_1^4 - 300^4) \right\},$$

η = efficiency of ideal (Carnot) engine =

$$\left(1 - \frac{300}{T_1} \right),$$

T_1 = receiver operating temperature, °K.

Assuming for the moment that a and ϵ are not appreciably affected by the operating temperature T_1, the temperature corresponding to maximum work rate is given by

$$T_1^4 = \frac{\frac{300}{4\,\sigma} \cdot G' \cdot \frac{a}{\epsilon} - \frac{300^5}{4}}{T_1 - \frac{900}{4}} \quad [3]$$

The optimum temperature and heat and work efficiencies for various possible values of a and ϵ are tabulated in Table I.

TABLE I

OPERATING TEMPERATURE FOR MAXIMUM WORK AND OTHER PERFORMANCE FACTORS, FOR VARIOUS ASSUMED VALUES OF a AND ϵ

a/ϵ	1	5	9	13	90
T_1 (°K)	340	410	450	475	662
η' (%)	57.2		63.1		75.1
η'' (%)	6.72		21.0		41.1
a	1.0		0.9		0.9
ϵ	1.0		0.1		0.01

The data in Table I show that very high temperature and exceptionally high efficiencies can be obtained as a/ϵ increases. It is not, however, possible to make ϵ arbitrarily small. This is illustrated by Fig. 1, which shows schematically the relationships between the ideal selective surface, the distribution of energy in the solar radiation curve, and the energy distribution of the self-radiation of a black body at T_1. In this case, we assume that $a_\lambda = \epsilon_\lambda = 1$ up to the cut-off wavelength, λ_c, and $a_\lambda = \epsilon_\lambda = 0$ for $\lambda_c \leqq \lambda \leqq \infty$. The average value of the absorptivity for solar radiation is a_λ times the shaded area under the spectral curve for solar radiation divided by the entire area under the solar curve or[2]

$$a = \frac{\displaystyle\int_0^{\lambda_c} \frac{8\pi ch}{\lambda^5} \cdot \frac{1}{e^{ch/\lambda kT} - 1} \cdot d\lambda}{\displaystyle\int_0^{\infty} \frac{8\pi ch}{\lambda^5} \cdot \frac{1}{e^{ch/\lambda kT} - 1} \cdot d\lambda} = -\frac{15}{\pi^4} \int_x^{\infty} \frac{y^3\, dy}{e^y - 1} \qquad [4]$$

FIG. 1 — Relationships between ideal selective surface, incident solar radiation, and self-emission of black body receiver. ———Absorptivity and emissivity of ideal selective surface. - - - - - Solar energy incident on receiver, approximate intensity, and wavelength distribution. —·—·—. Normal self-emission of blackbody receiver operating at high temperature, approximate intensity and wavelength distribution.

Energy emitted by selective surface.

Input energy accepted by selective surface.

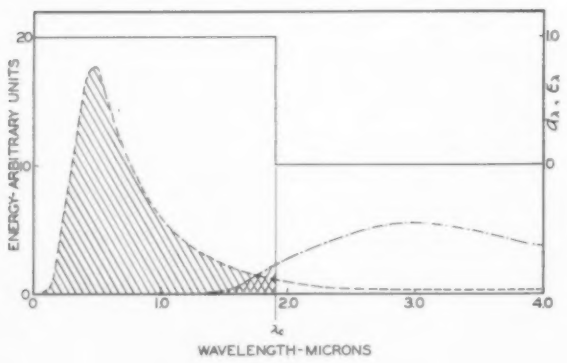

$$\cong \frac{15}{\pi^4} e^{-x}(x^3 + 3x^2 + 6x + 6)$$

where $x = ch/\lambda_c\, kT_s$ and T_s = apparent temperature of sun. Similarly[2]

$$\epsilon = -\frac{15}{\pi^4} \int_x^{\infty} \frac{y^3\, dy}{e^y - 1} \cong \frac{15}{\pi^4} e^{-x}(x^3 + 3x^2 + 6x + 6) \qquad [5]$$

where $x = ch/\lambda_c\, kT_1$ and T_1 = absorber temperature.

In most practical cases, it is convenient to find a directly from a plot of cumulative energy vs. wavelength constructed from measured solar intensities. Complete solar energy vs. wavelength data for various atmospheric conditions have been given by Moon.[3] Fig. 2 is a plot of Moon's data for $m = 2$.

Since a depends on λ_c and ϵ depends on T_1 and λ_c, it should be possible to express the over-all efficiency, Equation [2], as a function of λ_c and T_1, and to maximize this equation with respect to λ_c and T_1. It seems much simpler, however, to obtain a rough estimate of the best value of λ_c by considering quantum processes and then to solve for η'', η', T_1, etc., for several wavelengths in the vicinity of the best λ_c estimated from a consideration of quantized systems. Quantized systems are taken here to be systems which have a characteristic energy gap that is greater than kT, i.e., $(hc/\lambda_c) > kT$, where T is the absolute temperature of the system. It will be seen below that the maximum in the η'' vs λ_c curve is quite broad for either selective absorber thermal processes or for quantum processes; therefore, no significant error will be made if the best λ_c for selective absorber thermal devices is chosen from a consideration of the theory of quantum devices.

Efficiency and Optimum Cut-off Wavelength for Solar-Powered Quantum Device

Trivich and Flinn[4] have given an expression for the optimum cut-off wavelength for quantum processes using unconcentrated solar energy. If the sun's effective temperature is taken as 6,000°K, Trivich and Flinn find that the optimum cut-off is 1.11 microns. The treatment of quantum processes outlined below and summarized in Fig. 3 differs in some respects from that given by Trivich

FIG. 2 — Cumulative per cent of total incident solar energy vs. wavelength for air mass equal to two (after Moon).

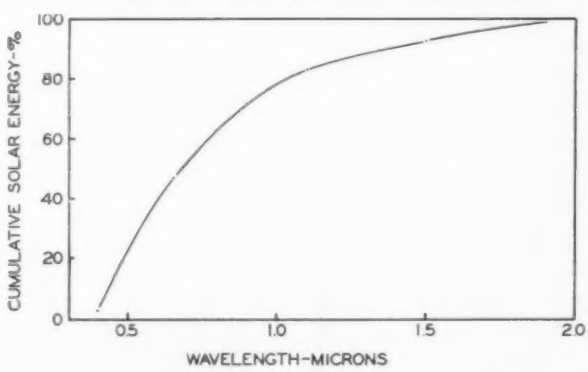

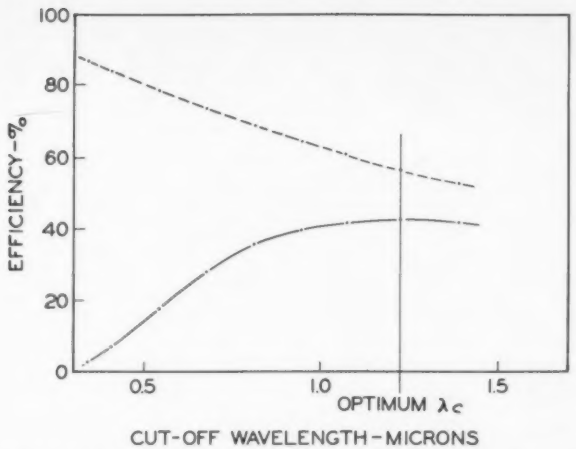

FIG. 3 — Theoretical maximum efficiencies of quantum conversion of solar radiation to useful work. ----- Based on portion of spectrum received by quantum device. ——— Based on total incident solar energy. Solar temperature assumed equal to 5,550°K.

and Flinn, but it appears to be based on the same principles.

In a quantum system, all quanta with energies greater than the cut-off energy can excite a chemical or physical change. However, only a part of each quantum with energy greater than the cut-off energy is used in exciting the quantum change; the remainder of the energy in these high energy quanta is, in general, dissipated as heat (or light). For any wavelength $\lambda < \lambda_c$, the fraction of the incoming energy convertible to work is $(hc/\lambda_c)/(hc/\lambda)$; no energy arriving at wavelengths $\lambda > \lambda_c$ can be used by the system. Therefore, the maximum over-all work efficiency obtainable, assuming that each quantum with energy greater than the cut-off is utilized to the fullest extent possible, is

$$\eta'' = \frac{\int_0^{\lambda c} \frac{8\pi ch}{\lambda^5} \cdot \frac{1}{e^{ch/\lambda kT} - 1} \cdot \frac{hc}{\lambda_c} \cdot \frac{Y}{hc} \cdot d\lambda}{\int_0^{\infty} \frac{8\pi ch}{\lambda^5} \cdot \frac{1}{e^{ch/\lambda kT} - 1} \cdot d\lambda} \qquad [6]$$

This can be simplified to

$$\eta'' = \frac{ch}{\lambda_c kT_s} \cdot \frac{\int_x^{\infty} \frac{y^2\,dy}{e^y - 1}}{\int_0^{\infty} \frac{y^3\,dy}{e^y - 1}} \cong \frac{15}{\pi^4}\, x\, e^{-x}(x^2 + 2x + 2) \qquad [7]$$

where $x = ch/\lambda_c kT_s$ and T_s is the apparent temperature of the sun. The numerical value of Equation [7] has been plotted in Fig. III. A similar treatment permits calculation of the work efficiency based on the portion of the solar spectrum received at wavelengths $0 \leqq \lambda \leqq \lambda_c$. This has been shown as a dotted line in Fig. 3. The calculations summarized in Fig. 3 were made assuming that the equivalent temperature of the sun was 5,550°K. The maximum in the efficiency vs. wavelength curve occurs at 1.224μ and the greatest efficiency possible is 42 per cent. The maximum is very broad and apparently any wavelength between 1.075 and 1.375μ would permit a maximum theoretical efficiency of at least 41.5 per cent. The maximum possible efficiency of any quantum device can be read directly from Fig. 3 if its characteristic cut-off wavelength is known.

Comparison of Thermal Device with Quantum Device

It is instructive at this point to consider the efficiency of a selective absorber thermal device characterized by a cut-off wavelength of 1.224μ. Using the same assumed solar spectrum, $T_s = 5{,}550$°K; a evaluated as in Equation [4] is 0.734. The best values of T_1, η', η'' etc., can be readily obtained by finding ϵ, Equation [5], for several temperatures and then substituting these values in Equation [2] and calculating the efficiencies at the temperatures assumed. The performance curves for a selective absorber receiving radiation from a black body at 5,550°K are shown in Fig. 4. Curves for an ideal black receiver are included for comparison. The maximum values are summarized in Table II.

TABLE II

COMPARISON OF OPTIMUM PERFORMANCE FACTORS FOR BLACK BODY, IDEAL SELECTIVE ABSORBER THERMAL DEVICE ($\lambda_c = 1.224\ \mu$) AND QUANTUM DEVICE ($\lambda_c = 1.224\ \mu$), ASSUMING $T_s = 5{,}550$ °K AND $G' = 1$ CAL PER SQ PER MIN

	Black body	Ideal selective absorber	Quantum device
T_1 (°K)	340	850	
η' (%)	57.2	71.5	
η'' (%)	6.72	46.1	42.0
a	1.0	.734	.734
ϵ	1.0	4.9×10^{-4}	

It will be noted that the selective absorber thermal device has a slightly higher theoretical maximum efficiency, 46 per cent, than the quantum device, 42 per cent. It is beyond the scope of this paper to give a complete discussion of the relationship between η'' quantum and

FIG. 4 — Work (———) and heat (-----) efficiencies of blackbody and of ideal selective absorber thermal device as a function of operating temperature. Based on theoretical spectrum for sun at apparent temperature of 5,550°K, total incident solar energy taken as 1 cal per sq cm per min.

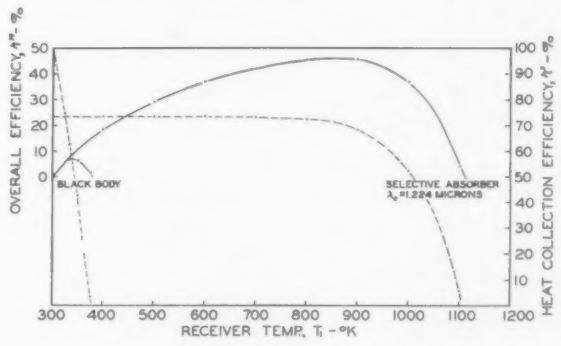

η'' selective-thermal. However, the physical phenomena responsible for the result obtained above can be illustrated by considering two radiant energy receivers connected to an infinite sink at 0 °K. Receiver number one is imagined to be a quantum device, say a photoelectric converter, with cut-off frequency λ_c, and it is maintained at 0 °K by contact with an infinite reservoir. Receiver number two is imagined to consist of a Carnot engine connected between a black body and the infinite sink at 0 °K. The black body is supposed to be surrounded by a selective filter such that only wavelengths shorter than λ_c reach the black body. Both devices then only receive a fraction of the energy radiated by the source. The fraction received will be proportional to $-\int_x^\infty \frac{y^3\,dy}{e^y-1}$ where $x = hc/\lambda_c kT_s$ and T_s is the temperature of the source. We can imagine that the work rate of the Carnot engine is adjusted to maintain the black body at some low temperature, say 100°K. At this temperature, even in the absence of the selective filter, only 1 per cent of the input from the sun would be lost through reradiation; with the selective filter in place, the loss through reradiation becomes vanishingly small. Under these conditions, the Carnot engine-black body-selective filter combination will be able to turn 100 per cent of the energy transmitted by the filter into work. However, the work that can be done by the quantum device will only be proportional to

$$-x\int_x^\infty \frac{y^2\,dy}{e^y-1} \qquad [8]$$

and therefore

$$\frac{\eta''_{\text{quantum}}}{\eta''_{\text{selective-thermal}}} = \frac{x\int_x^\infty \frac{y^2\,dy}{e^y-1}}{\int_x^\infty \frac{y^3\,dy}{e^y-1}}$$

This quantity is $\leqq 1$; it approaches 1 when $x \to \infty$, i.e., when $\lambda_c \to 0$. When $\lambda_c \to \infty$, the quantum device becomes indistinguishable from an ordinary black body-thermal device.

Optimum Cut-off Wavelength and Operating Parameters for Selective Absorber Thermal Device

To confirm that 1.224μ is the optimum cut-off for the thermal case and to show that the maximum is also broad in the thermal case, the optimum temperature and the other performance factors have been calculated for several cut-off wavelengths. Since the figures obtained in this calculation of the ideal case will be useful in computing performance factors in more practical cases, a was obtained graphically from Fig. 2. Fig. 2 is based on Moon's curves for $m = 2$, and the final practical figures will provide the basis for a conservative estimate of the performance of a selective absorber thermal device during a clear day. The results for an ideal selective absorber, i.e., $a_\lambda = 1$ for $0 \leqq \lambda \leqq \lambda_c$, $\epsilon_\lambda = 0$ for $\lambda_c \leqq \lambda \leqq \infty$, and conduction losses = 0, are given in Table III.

TABLE III

OPTIMUM PERFORMANCE FACTORS FOR IDEAL SELECTIVE ABSORBER THERMAL DEVICES POWERED BY ACTUAL SOLAR RADIATION. SEVERAL CUT-OFF WAVELENGTHS

λ_c (μ)	1.1	1.224	1.37
T_1 (°K)	925	875	810
η' (%)	80.6	83.4	81.5
η'' (%)	54.6	54.9	54.5
a	0.831	0.867	0.900
ϵ	3.8×10^{-4}	6.8×10^{-4}	9.9×10^{-4}

Effect of Nonideal Reflecting and Absorbing Surfaces on Optimum Parameters

In actual practice, it may be impossible to obtain a surface for which $a_\lambda = 1$ or $\epsilon_\lambda = 0$. Therefore, the calculations for $\lambda_c = 1.37\mu$ have been modified to represent the following conditions: $a_\lambda = a_1 = 0.9$ for $0 \leqq \lambda \leqq \lambda_c$, and $\epsilon_\lambda = a_2 = 0.01$ and 0.02 for $\lambda_c \leqq \lambda \leqq \infty$. Whenever $a_\lambda \neq 1$ at wavelengths shorter than cut-off and $\epsilon_\lambda \neq 0$ at wavelengths longer than cut-off, the average values of a and ϵ for use in Equation [2] can be obtained as follows*

$$a = a_1 Fc + a_2(1 - Fc) \qquad [9]$$

$$\epsilon = a_1 fc + a_2(1 - fc) \qquad [10]$$

where:

Fc = the fraction of the solar energy arriving at wavelengths $0 \leqq \lambda \leqq \lambda_c$,

fc = the fraction of the self energy emitted at wavelengths $0 \leqq \lambda \leqq \lambda_c$,

= ϵ_{ideal} as calculated from Equation [5].

Efficiency vs. temperature curves for $\lambda_c = 1.37\mu$ and $a_\lambda = 1$, $\epsilon_\lambda = 0$; and $a_\lambda = 0.9$, $\epsilon_\lambda = 0.02$ are shown as upper curves in Figs. 5 and 6. Values of the principal parameters at the optimum operating temperature can be found in Table IV.

TABLE IV

EFFECTS OF CONDUCTION AND CONVECTION HEAT LOSSES ON PERFORMANCE FACTORS OF IDEAL AND REAL SELECTIVE SURFACES WHEN $\lambda_c = 1.37\ \mu$

$a_\lambda(\lambda < \lambda_c) = 1.0$,

$\epsilon_\lambda(\lambda > \lambda_c) = 0.0$

H_c †	0.00000	0.00033	0.001	0.003
T_1 (°K)	810	780	600	425
η' (%)	86.5	71.7	60.0	52.0
η'' (%)	54.5	44.2	30.0	15.5
a	0.90	0.90	0.90	0.90
ϵ	9.9×10^{-4}	6.7×10^{-4}	2.5×10^{-5}	5×10^{-5}

$a_\lambda(\lambda < \lambda_c) = 0.90$,

$\epsilon_\lambda(\lambda > \lambda_c) = 0.01$

H_c †	0	0.00033	0.001	0.003
T_1 (°K)	650	600	515	410
η' (%)	67.0	61.0	54.2	47.0
η'' (%)	36.2	30.5	22.8	15.0
a	0.811	0.811	0.811	0.811
ϵ	0.01007	0.01002	0.010	0.010

*A more elaborate treatment is required if a and ϵ actually vary with wavelength in any manner more complicated than a simple step at λ_c.

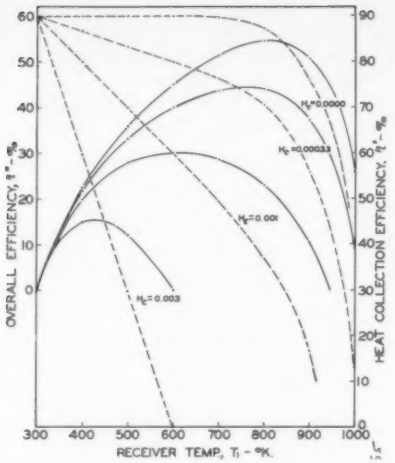

FIG. 5 — Work (———) and heat (- - - - -) efficiencies of ideal selective absorber thermal device as a function of operating temperature. $\lambda_c = 1.37\mu$ and $\alpha_\lambda(\lambda < \lambda_c) = 1.00$, $\epsilon_\lambda(\lambda > \lambda_c) = 0.00$. Convection and conduction losses, H_c, given in cal per sq cm per min per °C.

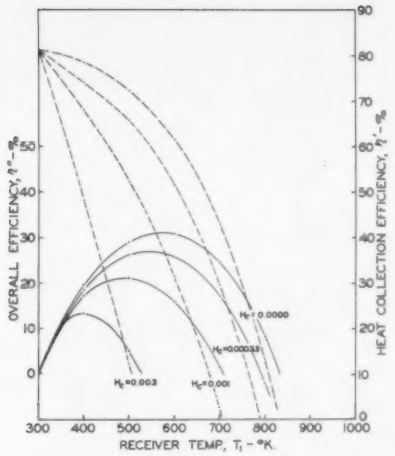

FIG. 6 — Work (———) and heat (- - - - -) efficiencies of real selective absorber thermal device as a function of operating temperature. $\lambda_c = 1.37\mu$ and $\alpha_\lambda(\lambda < \lambda_c) = 0.90$, $\epsilon_\lambda(\lambda > \lambda_c) = 0.02$. Convection and conduction losses, H_c, given in cal per sk cm per min per °C.

$$\alpha_\lambda(\lambda < \lambda_c) = 0.90,$$
$$\epsilon_\lambda(\lambda > \lambda_c) = 0.02$$

H_c †	0	0.00033	0.001	0.003
T_1 (°K)	575	540	480	400
η' (%)	64.5	60.7	56.0	48.2
η'' (%)	31.1	26.8	21.1	13.2
α	0.812	0.812	0.812	0.812
ϵ	0.02002	0.020	0.020	0.020

†Cal per sq cm per min per °C.

Effects of Convection and Conduction Losses

Up to this point, there has been no consideration of the effects of thermal losses other than radiation. Equation [2] can be modified as follows to include the effects of convection and conduction heat losses in a practical selective absorber thermal device:

$$\eta'' = \frac{W'}{G'} \qquad [11]$$
$$= \alpha \left\{ 1 - \frac{\epsilon\,\sigma}{\alpha\,G'}(T_1^4 - 300^4) - \frac{H_c}{\alpha\,G'}(T_1 - 300) \right\} \times \left(1 - \frac{300}{T_1} \right)$$

where the symbols have the same significance as in Equation [2] and H_c is the unit heat-loss coefficient. H_c may be a mild function of temperature,[5] but for the purposes of illustrating the effects of conduction and convection losses on the performance of flat collectors, numerical solutions to Equation [1] were obtained for several assumed values of H_c. H_c was taken as equal to 0.003, 0.001, and 0.00033 cal per sq cm per min per °C. The convection-conduction heat-loss values reported by other investigators in general range from 0.001 to 0.006 cal per sq cm per min per °C.

The results obtained for the selective surface described in the previous paragraph are plotted in Figs. 5 and 6. Values of the principal parameters at the temperatures corresponding to maximum efficiency for each case are given in Table IV.

Although results for the effect of convection and conduction losses at only one cut-off wavelength have been presented here, it should be noted that as these losses increase, the optimum cut-off shifts to longer wavelengths and the optimum temperature and the over-all maximum efficiency decrease.

SUMMARY

Solar-powered selective thermal devices can theoretically be operated at an exceedingly high over-all efficiency. The fullest capabilities of such devices can be realized only if the receiver is perfectly insulated, for example, enclosed in a transparent evacuated envelope.

The maximum theoretical over-all efficiency of a solar-powered selective thermal device operated under optimum conditions in an environment at 300°K is greater than the theoretical maximum over-all work efficiency of a quantum conversion system with only one operative energy gap.

A theoretically perfect selective thermal device, on earth, receiving energy from the sun at an average rate of 1 cal per sq cm per min can convert 55 per cent of this energy into useful work at an operating temperature of 875°K.

Using a technically feasible selective surface, $\alpha_\lambda = 0.9$ for $0 \leqq \lambda \leqq \lambda_c$ and $\epsilon_\lambda = 0.02$ for $\lambda_c \leqq \lambda \leqq \infty$, 31 per cent of the incident solar radiation can be converted to useful work at an operating temperature of 575°K.

If the miscellaneous convection and conduction losses in the device above are taken as 0.001 cal per sq cm per min per °C, then the maximum theoretical amount of work will be 21 per cent of the incident solar radiation, and the best operating temperature will be 480°K.

REFERENCES

1. H. Tabor, "Selective radiation I: wavelength discrimination." *Bull. Res. Coun. Israel* 54:119-28, 1956.
2. See, for example, F. K. Richtmeyer and E. H. Kennard, *Introduction to modern physics,* 3rd ed. N.Y., McGraw-Hill, 1942. p. 200 *ff.*
3. Parry Moon, "Proposed standard solar-radiation curves for engineering use." *J. Franklin Inst.* 230(5):583-617, 1940.
4. *Solar energy research;* ed. by Daniels and Duffie. Madison, Univ. of Wisconsin Pr., 1955. p. 143.
5. H. C. Hottel and B. B. Woertz, "The performance of flat-plate solar-heat collectors." *Trans. ASME* 64:91-104, 1942.

STATIONARY MIRROR SYSTEMS FOR SOLAR COLLECTORS

By H. TABOR

National Physical Laboratory of Israel, Jerusalem

An angle in solar geometry termed the EWV altitude is defined, and its variation with time and season is shown. This variation indicates the necessary acceptance angle of a stationary mirror system for solar collectors. It is shown that a completely stationary mirror cannot give any useful concentration, but that if the tilt is varied with the seasons, an east-west cylindrical parabolic mirror without diurnal movement can yield a concentration of approximately three. This may be increased to about four with the aid of a small auxiliary (fixed) mirror to provide a second stage of optical concentration.

INTRODUCTION

Flat-plate collectors without concentrating mirrors are limited in the useful temperature that can be reached because of the heat losses from the irradiated surface. The use of selective black (low emissivity) surfaces[1] improves the situation, but temperatures much above 100°C with efficiencies of the order of 50 per cent are not readily obtainable.

Thus for higher temperatures — as are, for example, required for power generation — it has been necessary to use mirrors for concentrating the solar energy, thereby reducing the relative heat losses.

The instantaneous collection efficiency η_1 of a collector at temperature T is given by [2]

$$\eta_1 = \alpha\beta N_1 = \alpha\beta \left[1 - \frac{Q_x}{Q_i} \right] \qquad [1]$$

$$= \alpha\beta \left[1 - \frac{v_e(T)}{\alpha\beta P} \cdot \frac{1}{Q_i} \right] = \alpha\beta - \frac{v_e(T)}{PQ_i}$$

where:

α = absorptivity to solar radiation,

β = transmissivity of any optical elements between incoming sunshine and the absorbing surface,

$v_e(T)$ = rate of heat loss (per unit area) from absorbing surface, at temperature T,

P = optical concentration, i.e., ratio of area of solar aperture to area of irradiated absorber,

Q_x = cut-off intensity = $v_e(T)/\alpha\beta P$,

Q_i = intensity of incoming solar radiation measured at the aperture of the collector,

N_1 = retention efficiency = $1 - Q_x/Q_i$.

Omitting the effect of a number of correction terms (which will be discussed elsewhere), Equation [1] may be used for average efficiencies by using $\overline{Q}_{im}$, the mean value of Q_i, i.e.,

$$\eta_1 = \alpha\beta - \frac{v_e(T)}{P\,\overline{Q}_{im}} \qquad [1a]$$

(where the bar indicates average values).

From this it is seen that if $v_e(T)$ is not a small fraction of the mean solar intensity, optical concentration is essential if a reasonable collection efficiency is to be obtained.

Thus, mirror systems have almost invariably been proposed for solar collectors designed for power production. Apart from the reduction in the value of β in Equation [1] or [1a] resulting from the use of a mirror,* the question of moving the mirror to follow the sun involves considerable increase in the cost of the equipment and in its maintenance.

An interesting question arises: can a mirror system be employed which does not have to follow the sun, and, if so, what is the greatest concentration power that can be obtained?

To answer this question, we must consider: (a) some aspects of solar geometry and (b) some geometrical properties of the parabola.

SOLAR GEOMETRY

In the course of a day, the sun moves over a large angle as it sweeps the sky from sunrise to sunset. A much smaller angular motion is that of the rise and fall of the sun. The chance of being able to focus the sun during the day with a stationary mirror is thus far greater if we are concerned with altitude movements than azimuthal movements.

On the day of the equinox, the sun appears to describe an exact semicircle in a plane passing through the observer, the tilt of the plane to the vertical being equal to the geographical latitude of the site of the observer. If a camera using a thin horizontal slit lying east-west instead of a lens were pointed at the sun at noon, a horizontal line image would be formed which during the day would

*Surfaces with a stable reflectivity above 80 per cent are extremely expensive.

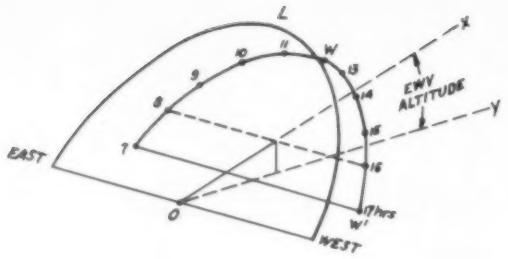

FIG. 1a

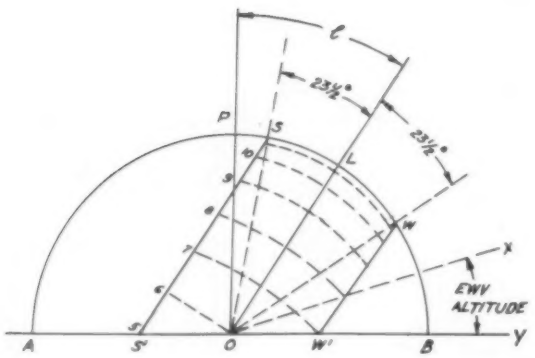

FIG. 1b

move along its own length but would not suffer displacement. A cylindrical mirror would give the same effect, so that concentration of the beam becomes possible without moving the mirror, provided that the system is very long in the east-west direction. However, on any other day it is found that if the camera is pointed at the sun at noon a sideways translation of the image occurs in the mornings and evenings. Thus, if the system is to catch the image all day the receiving screen must be quite wide so that the possible concentration of the mirror is reduced. Exactly how wide the receiver must be is indicated in Fig. 1b which is a projection on a N-S vertical plane of the apparent motion of the sun for the equinox and solstice days.

APB represents the heavens to an observer at *O*, *P* being the zenith point. *OL* represents the plane of the ecliptic at the equinoxes. Angle *LOP* equals the geographical latitude. *WW'* represents the ecliptic plane at the winter solstice. *SS'* represents the ecliptic plane at the summer solstice.

OL and *WW'* are shown in perspective view in Fig. 1a, which shows the hourly positions. These hours are also shown in Fig. 1b.

If we draw a line *OX* from *O* through any given time and month on Fig. 1b — for example through 8 a.m. on the winter solstice, then the angle *BOX* may be called the EWV altitude of the sun at that time, for if a long horizontal V channel faces the equator with one face on the ground, sunshine will just enter the V. The EWV altitude is, of course, the altitude as generally defined projected onto a vertical N-S plane.

It may be shown that

$$\text{EWV altitude} = \tan^{-1}[\tan \text{altitude} \times \sec \text{azimuth}] \quad [2]$$

The change in EWV altitude with time is called the EWV altitude swing, and it is this swing which must be accommodated by any cylindrical mirror system mounted in the E-W direction.

If this swing, measured from the equinox* position, is called V it may be shown that, to a first approximation,

$$\tan V = \frac{\tan\left[23\tfrac{1}{2} \sin \frac{2n\pi}{365}\right]}{\cos 15t} \quad [3]$$

where:

n is the number of days from the equinox,

t is the time in hours, measured from solar noon,

$\pm 23\tfrac{1}{2}°$ is the swing of the noon altitude of the sun during the year.

The values of V are plotted in Fig. 2.

From this figure it can be seen that to accept all solar radiation say from at least 8 a.m. to 4 p.m., all the year, involves a total swing of V of $\pm 41°$, or $82°$. If we are prepared to lose half an hour's sunshine in the morning and evening of the solstice months then a swing of $\pm 36°$ is sufficient.

It will now be shown that acceptance angles of the order of $72°$ or $82°$ cannot be accommodated by mirrors with a concentration power greater than one, so that a mirror fixed during the whole year cannot provide any useful concentration.

However, if we are prepared to make periodic adjustments in the tilt of the mirror, then the situation is improved. For example, from Fig. 2, an acceptance angle of $17°$ will collect sunshine for ± 4 hours on the solstices (and even longer on other days), while only $12°$ is required to collect sunshine for $\pm 3\tfrac{1}{2}$ hours on the solstices.

*By measuring V from the equinox instead of from the ground we eliminate the need to know the latitude, for Fig. 1b is the same for all sites except for a rotation about the point *O*.

FIG. 2

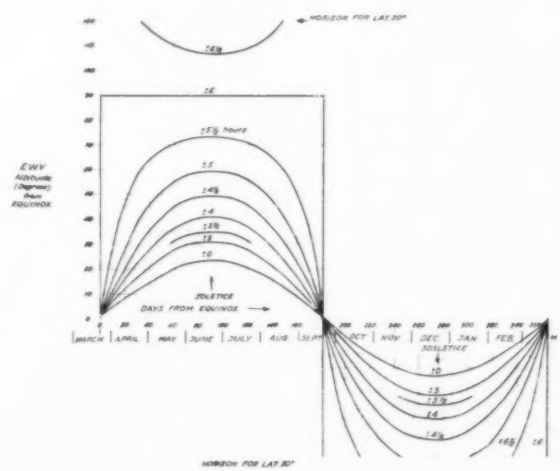

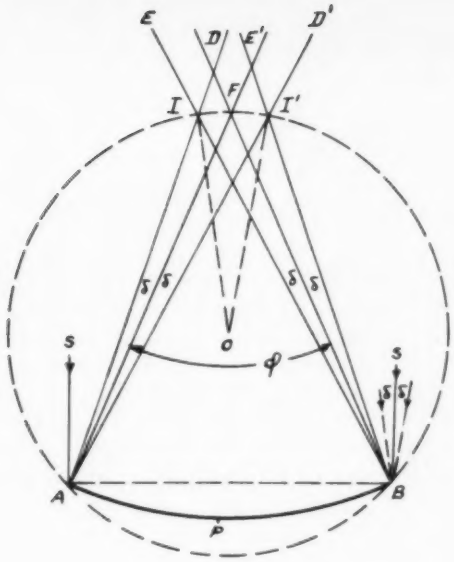

FIG. 3a — Symmetrical case.

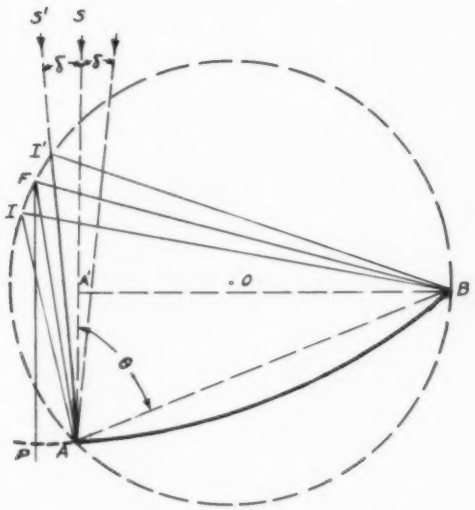

FIG. 3b — Tilted (shadowless) case.

GEOMETRY OF THE CYLINDRICAL PARABOLA

We consider, at this stage, only concentration in the plane of the diagram as produced, for example, by cylindrical mirrors. There are three main cases of interest — the symmetrical case, the tilted (shadowless) case, and the symmetrical diametral case. These are illustrated in Figs. 3(a), 3(b), 5(a), and 5(b).

Consider first a symmetrical mirror of aperture AB (Fig. 3a) capable of focusing a parallel beam of light SS to a sharp focus at F. If the incoming beam is deflected an angle δ to the left, the extreme reflected rays from A and B are AD and BE, which lines make angles δ with AF and BF respectively. If the beam is now deflected δ to the right we get extreme rays AD' and BE'.

The minimum width of traverse of the image spot is clearly II', where I is the intersection of AD and BE and I' the intersection of AD' and BE'.*

The optical geometrical concentration ratio P_g is AB/II'.

Because angle DAD' = angle $EBE' = 2\delta$, it follows that I, I', A, B, and F lie on a circle whose center we call O and radius R. Then because the angle subtended at the center is double the angle subtended at the circumference, we obtain at once, since angle $IOI' = 4\delta$,

$$II' = 2R \sin 2\delta \qquad [4]$$

$$AB = 2R \sin \phi \qquad [5]$$

where ϕ is the angle AIB or $AI'B$ or AFB, i.e., the angular aperture of the mirror measured from the focus. Thus

$$P_g = \frac{AB}{II'} = \frac{\sin \phi}{\sin 2\delta} \qquad [6]$$

and the maximum value occurs for $\phi = 90°$, i.e.

$$P_{g\,\max} = \frac{1}{\sin 2\delta} \qquad [6a]$$

where 2δ is the total swing of the incoming beam.

The geometrical concentration ratio P_g is not necessarily the same as the useful optical concentration P. Thus, if in Fig. 3a a receiver plate placed at II' is insulated on the side away from the mirror, a shadow is cast on the mirror and the useful aperture of the system becomes $AB - II'$.

Thus the actual concentration becomes approximately

$$P = P_g - 1 = \frac{\sin \phi}{\sin 2\delta} - 1 \qquad [7]$$

or

$$P_{\max} = \operatorname{cosec} 2\delta - 1 \qquad [7a]$$

Furthermore, if we call U the utilization factor of the mirror, i.e., the ratio of the actual width of intercepted solar radiation to the width of the mirror, we have, for this case

$$U = 1 - \frac{1}{P_g} = 1 - \frac{\sin 2\delta}{\sin \phi} \qquad [8]$$

or

$$U_{\max} = 1 - \sin 2\delta \qquad [8a]$$

If the receiver plate is not insulated on the side facing the sun (except by glass panes), then the full concentration P_g and the full aperture AB are utilized, but the heat losses are increased.

Whether to insulate the rear side of II' or not can be decided from a knowledge of the heat losses. Let the extra heat loss at temperature of operation T resulting from exposing the rear side be $\Delta v_c(T)$ and let the mean value of solar incidence intensity be $\overline{Q_{in}}$. Then exposure of the rear side is justified if the net additional incoming solar radiation is greater than the extra heat loss, i.e., if

*It can be shown that, if the mirror focuses at F, then all parts of the mirror between A and B will produce rays that are inside II'.

$$(\alpha\beta)_\gamma \overline{Q_{im}} > \Delta v_c(\tau) \qquad [9]$$

where $(\alpha\beta)_\gamma$ is the over-all transmission-absorption coefficient for the glass cover and the rear side.

We note that the concentration power of the mirror does not appear here though it will influence the *magnitude* of the difference of efficiency between the two cases.

The shadow cast on the mirror, which is important in cases of low concentration, can be avoided by using a tilted mirror as shown in Fig. 3b. The tilt is such that the extreme incident ray $S'A$ just coincides with the extreme image point I'.

Because of the tilt, the effective width of the mirror AB becomes $A'B$, the projection of AB normal to the (central) solar beam, or

$$\text{effective width} = AB \sin\theta$$

or
$$U = \sin\theta \qquad [10]$$

where θ is the angle $A'AB$.

The useful concentration is given by

$$P = P_g \sin\theta = \frac{\sin\phi \sin\theta}{\sin 2\delta} \qquad [11]$$

since the amount of sunshine falling on the mirror has been reduced by the utilization factor U.

The maximum value of P is not necessarily that given for $\phi = 90°$ — as in the case of the symmetrical mirror — because of the strong influence of the $\sin\theta$ term. θ and ϕ are related because of the requirement that A and B shall lie on a parabola with focus at F and optic axis FP parallel to the central solar beam.

FIG. 4 — Performance of stationary cylindrical parabolic mirrors.

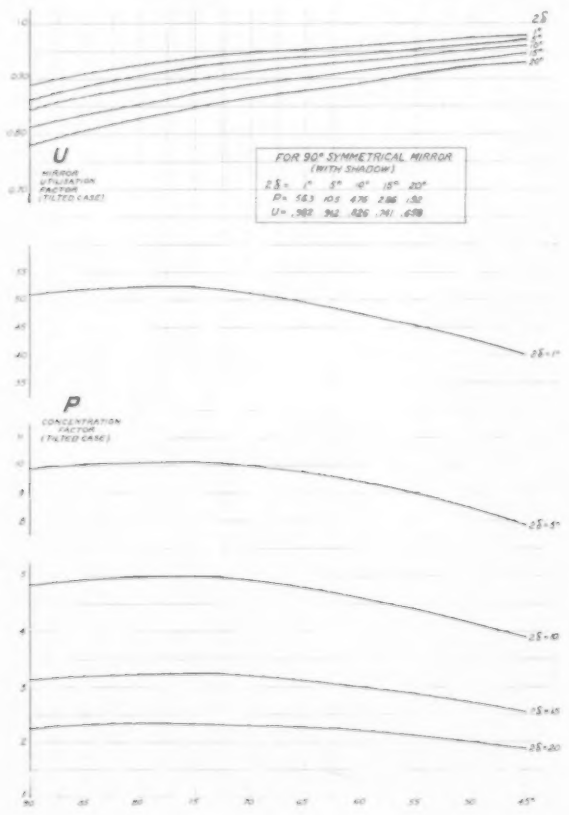

It may be shown that θ and ϕ are related by the equations

$$\theta = \gamma - 2\delta \qquad [12a]$$

where

$$\cot\gamma = g \operatorname{cosec}\phi - \cot\phi \qquad [12b]$$

where

$$g = \frac{1 + \cos(2\delta + \phi)}{1 + \cos 2\delta} \qquad [12c]$$

From these equations, Fig. 4 has been prepared to show the utilization factor and the useful optical concentration for different values of the incoming beam swing 2δ. The maxima in P for the shadowless case are due to the relative importance of ϕ and θ in Equation [11], for an increase of θ is accompanied by a decrease in ϕ. This latter feature means that, as we decrease ϕ still further, we get a better utilization factor but at the expense of a reduced concentration power. The optimum design depends upon the cut-off value Q_x. When this is low, it is more important to utilize as much of the mirror as possible than to get a little more concentration; but when the losses are high, the extra concentration power may be worthwhile even at the loss of some of the incoming sunshine.

(In the practical cases considered, ϕ, the aperture of the mirror, is between 45-70°). It is at once seen from Fig. 4 that if the solar beam swing 2δ is small, the symmetrical system gives the highest utilization and concentration factors because the effect of the shadow is small. But for 2δ above about 10°, the shadowing becomes serious and the tilted system without shadow gives higher factors.

It is clear that a mirror in the form of a paraboloid of revolution (or a cylindrical parabola with its cylindrical axis north-south, whether horizontal or tilted) cannot be used in a fixed position since its concentration factor would be less than unity on account of the solar-beam moving of the order of 180° in a day across the sky. Thus, for example, for the symmetrical mirror with shading, Equation [7a] gives $2\delta = 30°$ for a maximum concentration factor of unity, and in the tilted unshadowed case 2δ is approximately 42° for a concentration of unity.

It is clear, therefore, that a fixed mirror can only be considered if the solar swing is less than 42°. This leads to the use of cylindrical parabolic mirrors with the cylindrical axis lying horizontally east-west in which, as we have seen from the section on solar geometry, useful collection can occur with 2δ of the order of 15°, the mirror being adjusted periodically, say once a week. As seen in Fig. 4, concentration factors of the order of three are then possible.

There is an alternative method of using a cylindrical parabola, i.e., by having the collector symmetrically placed on the optic axis, the collector being double-sided or irradiated on both sides. Can this give better results than the case of the symmetrical (single-sided) case or the tilted shadowless case already considered?

We consider first the case of a symmetrical parabola, as shown in Fig. 5a. As before, we assume a central posi-

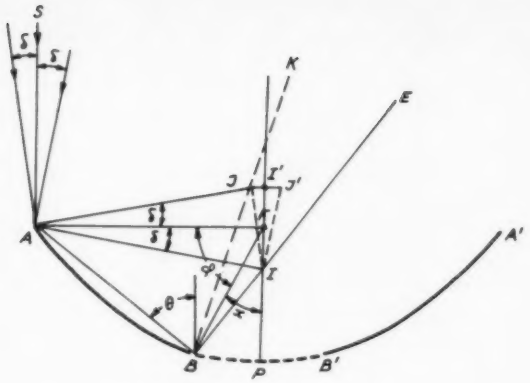

FIG. 5a — Symmetrical diametral case.

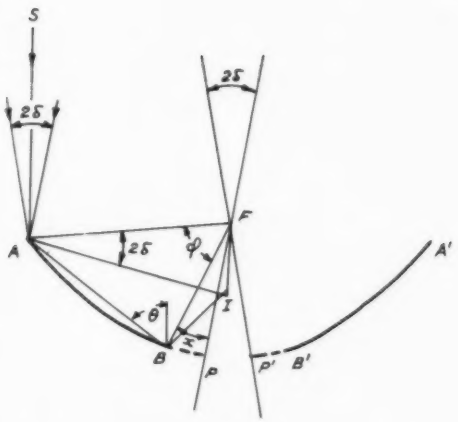

FIG. 5b

tion of the solar beam and a deflection of this beam $\pm\ \delta$. A point near the outer part of the parabola such as A gives rise to an image spread II', and it may be shown* that the ratio of mirror width AA' to image spread II' is a maximum when AA' passes through the focus F, i.e., the mirror aperture AFA' is 180°. In this case we have

$$\frac{AA'}{II'} = \frac{1}{\tan \delta} \qquad [13]$$

or the concentration ratio, remembering that the receiver II' has an area $2II'$, becomes $1/2 \tan \delta$.

Unfortunately, the central portions of the mirror give rise to reflected rays such as BK (angle $FBK = \delta$), and it may readily be shown that such rays strike the optic axis at a point outside FI'. Furthermore, the reflected rays coming from area B near the apex P strike any receiver placed at II' with very high angles of incidence. There are two solutions to this problem.

(1) The first is to place the receiver plate at an angle as shown at IJ. This means that a double-sided receiver will have a triangular section JIJ' with the portion JJ' also being irradiated and also being added to the cooling surface.**

As in the case treated in Fig. 3b, the points $ABJF$ lie on a circle, and the geometry becomes very similar to that already studied. The point B is also defined in position, for the ray BE must not fall below I.

It may be shown that, without limiting the points A, A' (Fig. 5a) to lie on a line through F, the geometry leads to the following equations:

$$P = \frac{\sin \theta \sin \phi + \sin 2\delta \sin \delta}{\sin 2\delta\ (1 + \sin \delta)} \qquad [14]***$$

where ϕ is the angular aperture of each half of the mirror AB, $A'B'$ measured from the focus and θ is the tilt of each half of the mirror to the central solar beam; i.e., the mirror utilization factor is, as before, $U = \sin \theta$. ϕ and θ are not freely chosen, being linked by the following equations

$$[1 + \cos (\phi + x)]\ [\sin (\phi + x + \delta)] = (1 + \cos x) \sin (x + \delta) \qquad [15a]$$

$$\theta = 180 - (\phi + \delta + 2x) \qquad [15b]$$

where x is the angle BFP. The angle JIJ' emerges from the geometry as equal to 2δ.

For a given value of δ, pairs of values of x and ϕ are obtained from Equation [15a], and the values are chosen which lead to the best values of P and $\sin \theta$. The general results are similar to those obtained for the tilted case of Fig. (3b) with slightly inferior values for P and $\sin \theta$. As an example, for $2\delta = 15°$, the optimum value for ϕ is about 80° ($x = 15$ to 18°) leading to $\theta = 57°$, $U = 0.839$, and $P = 2.71$. By comparison we see from Fig. 4 that for $2\delta = 15°$, $\phi_{\text{optimum}} \sim 65°$; $U \sim 0.9$; $P \sim 3.1$.

(2) Alternatively to making the receiver of triangular section as in (1) above, a flat receiver can be used if the parabolic mirror is comprised of two halves, each half having its optic axis tilted an angle δ to the central solar beam (Fig. 5b). In this way, no reflected ray ever falls above the focus point F.

In this case, it may be shown that

$$P = \frac{\sin \phi \sin \theta}{\sin 2\delta} \qquad [16]$$

and θ and ϕ are related by the two equations

$$(1 + \cos x)\ [\sin (x + 3\delta)] = [1 + \cos (\phi + x)]\ [\sin (\phi + x + 3\delta)] \qquad [17a]$$

$$\theta = 180 - (\phi + 2x + 4\delta) \qquad [17b]$$

where x is the angle BFP.

As in the case (1) we choose values of ϕ leading to the best compromise of P and U. The results are very similar to those obtained for the case of the tilted mirror (Fig. 3b) and just a little inferior. Thus for the case of $2\delta = 15°$, we find optimum value of $\phi = 80°$, $\theta \sim 54°$, leading to $U = 0.81$ and $P = 3.07$. This compares with $U = 0.9$ and $P = 3.1$ for $\phi = 65°$ in Fig. 4.

*For any point B, $II'/XN = \sin 2\delta / (\cos^2 \delta - \cos^2 x)$, which is a minimum when $x = 90°$.

**A small improvement in concentration would occur if the section JJ' were insulated, but in practice it would be very difficult to carry this out effectively.

***The terms in $\sin \delta$ are omitted if the portion JJ' is covered with insulation material.

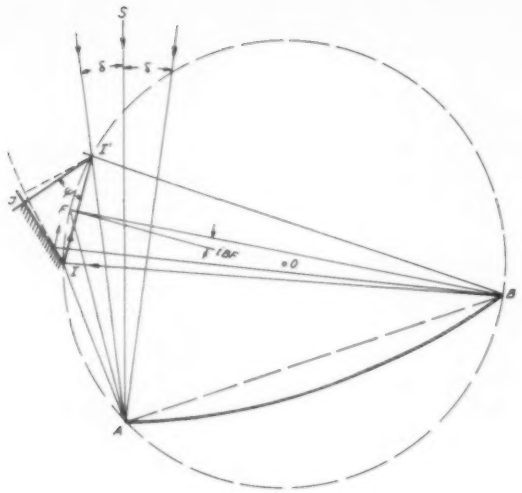

FIG. 6

We thus see that the symmetrical diametral case with the receiver irradiated on both sides yields results approaching those obtained with the single-sided tilted case, with the advantage that because the receiver is irradiated on both sides it is only half as large — for a given sunshine aperture — as the single-sided case. However, the single-sided case also has certain practical merits: the mirror can be very low, i.e., near the ground, thereby reducing the effect of wind and facilitating manual cleaning; a second stage of concentration is possible as described below.

SECOND STAGE CONCENTRATION

We have seen that, for a given value of the solar-beam swing 2δ, there is a limit to the concentration power obtainable with a single cylindrical parabolic mirror. Thus for $2\delta = 15°$, P is approximately equal to 3. Can we obtain further optical concentration by use of a second optical stage?

Clearly we cannot apply a second stage of optical concentration to the double-sided receiver, and as we have shown that for $2\delta \sim 15°$ the tilted case of Fig. 3b is more satisfactory than the symmetrical case of Fig. 3a, we will limit the discussion to the case illustrated in Fig. 3b, which is redrawn in Fig. 6.

In Fig. 6 it can be seen that the angle of incidence of ray AI on a receiver plane II' is greater than the angle of incidence of the ray BI' because of a lack of symmetry.

It may be shown from the geometry of Fig. 6 that the angle of incidence i_{BF} of the ray BF on a plane (normal to the plane of the diagram) through II' is given by

$$\tan i_{BF} = \operatorname{cosec} \phi - \cot \phi - \sin 2\delta \qquad [18]$$

and the other angles of incidence are

$$\begin{aligned} i_{BI}' &= i_{BF} - \delta \qquad [19] \\ i_{AF} &= \phi - i_{BF} \\ i_{AI} &= \phi - i_{BF} - \delta \\ i_{BI} &= i_{BF} + \delta \\ i_{AI}' &= \phi - i_{BF} + \delta \end{aligned}$$

Let us now swing the receiver plate at II' through an angle ψ to a position $I'J$. Also, from I to J we place a plane mirror. It is clear that if the mirror position corresponds to the external bisector of the angle BII' the ray BI will be reflected to I' and rays from points between B and A falling on the mirror will be reflected onto the area $I'J$.

If $I'J$ is less than II', second stage optical concentration is achieved.

We have, in the triangle IJI', two conditions to satisfy: (a) ψ should be such that the angle of incidence of BI' on $I'J$ should not exceed say 60°; (b) The angle JII' is the external bisector of angle BII' — or greater, if all rays falling on the mirror are to be reflected onto $I'J$. Clearly, it is disadvantageous to make angle JII' more than necessary since this results in a larger receiver dimension $I'J$. Thus we fix angle JII' as the external bisector of BII'.

Now $BII' = 90 - i_{BI} = 90 - i_{BF} - \delta$, whence the external bisector of angle JII' is

$$45 + \tfrac{1}{2}(i_{BF} + \delta) \qquad [20]$$

For condition (a) we have

$$\begin{aligned} \angle\, BII' &= i_{BI}' + 90 = i_{BF} - \delta + 90 \\ \therefore \angle\, JI'B &= i_{BF} + 90 - \delta + \psi - 90 + i_o \end{aligned}$$

where i_o is the angle of incidence of BI' on $I'J$, which we wish to limit to about 60°,* i.e.,

$$\psi = \angle\, JI'B - \angle\, BI'I = i_o - i_{BF} + \delta \qquad [21]$$

It is also clear from the triangle IJI' that for a fixed position of IJ, the smallest value of $I'J$ occurs when IJI' is a right angle, i.e., when angles $I'IJ$ and ψ are complementary.

If possible, we require

$$\begin{aligned} 90 &= \angle\, JII' + \psi \qquad [22] \\ &= 45 + \tfrac{1}{2}(i_{BF} + \delta) + i_o - i_{BF} + \delta \\ i_o &= 45 - \tfrac{1}{2} i_{BF} - 3/2\delta \end{aligned}$$

Thus, unless i_{BF} is negative — which from Equation [18] will only occur for large values of δ (ϕ being in practice between 45° and 70°) — we have i_o less than 45°, which is very satisfactory.

We also note that the extreme angle of incidence from rays reflected from the mirror is that of the ray II', i.e., the angle of incidence $= 90 - \psi$. So ψ should not be below about 30°. From Equation [20] and the requirement of being complementary we obtain

$$\psi = 45 - \tfrac{1}{2}(i_{BF} + \delta) \qquad [23]$$

and the second stage concentration

$$P_2 = II'/IJ \qquad [24]$$

or

$$P_2 = \sec \psi$$

TABLE I

	2δ			
φ	5°	10°	15°	20°
90°	42.4	39.6	36.5	33.4
80°	36.9	33.7	29.3	26.4
70°	31.5	27.8	23.7	19.7
60°	26.1	22.0	17.6	13.3
50°	20.8	16.3	11.7	7.1
45°	18.1	13.5	8.6	4.1

*More correctly we wish to limit the largest angle of incidence — ray BJ — to 60°.

TABLE II

ϕ	90°	80°	70°	60°	50°	45°	Notes
U	0.812	0.853	0.885	0.912	0.933	0.942	From Figure 4
P_1	3.13	3.24	3.21	3.05	2.75	2.57	
i_{BF}	36.5	29.3	23.7	17.6	11.7	8.6	From Table I
ψ	23.0	26.6	29.4	32.45	35.4	36.95	Equation [23]
P_2	1.086	1.118	1.148	1.185	1.227	1.251	Equation [24]
P_1P_2	3.40	3.62	3.69	3.62	3.38	3.22	

From Equation [18] we obtain the values of i_{BF}, in degrees, given in Table I.

Equations [23] and [24] then give the second stage concentration.

Consider a practical case, where $2\delta = 15°$. We can then prepare Table II.

This table shows the maximum concentration factor for ϕ, about 70°, with a slight falling off for smaller or larger values of ϕ. In practice it is probably better to use a value of ϕ smaller than 70° because of the better utilization factor of the mirror. Furthermore it is, as stated earlier, desirable to keep ψ greater than 30° in order to avoid large angles of incidence on JI'.

Slightly greater values of P_2 are obtained if the side mirror IJ is curved. Thus, if IJ is curved to form part of a parabola of which B is the focus and whose optic axis is parallel to II', then all rays from B falling on the mirror IJ strike JI' at the constant angle ψ. P_2 can be increased to about 1.3 (for the case of $2\delta = 15°$), leading to a total concentration factor P_1P_2 of nearly four. Of course, allowance must be made for the reflection losses introduced by the extra mirror, but as only about half* the rays strike this mirror it causes only half the loss. Thus if the reflectivity of the mirror is about 0.86, then if half the rays strike it, the value 0.93 may be used in the computation of β, the transmission coefficient of the system.

As will be shown in another paper, the use of second stage optical concentration has another advantage: it permits the receiver to be set exactly horizontal (face downwards).

The geometry shown in Figs. 3a and 3b, 5a, 5b, and 6 is based upon a given direction of the solar beam, i.e., a given mean EWV altitude. As this altitude varies with the seasons, the mirror tilt must be altered. In order to maintain the specified geometry, this means that the tilt of the receiver must also be altered. However, it will be shown in another paper that by careful choice of conditions it becomes unnecessary to rotate the receiver when the mirror angle is altered, a result of considerable practical importance.

CONCLUSIONS

(1) A completely fixed mirror cannot provide any useful concentration.

*Strictly speaking, an hour-by-hour analysis should be carried out for the different seasons of the year and the results weighted with the intensity of the sunshine.

(2) Useful concentration can be obtained from a mirror which has no diurnal movement but whose tilt is adjusted at certain periods of the year — say once a week. The mirror has the form of a cylindrical parabola with the cylindrical axis mounted horizontally east-west.

(3) For a collection of ± 4 hours on any day of the year, the acceptance angle of the mirror must be at least 17°:* for ± 3½ hours on the solstices (and longer periods on other days) the acceptance angle must be at least 12°. The angles are obtained from Fig. 2.

(4) A useful yield will be obtained if the acceptance angle is of the order of 15°. In this case, the maximum optical concentration obtainable is 3.

(5) By use of an auxiliary side mirror for second stage concentration this concentration power can be increased to about 4.

*This angle should be increased by: (a) about 0.5° to allow for the angular size of the sun; (b) about 1°-2° to allow for errors in setting.

Note

Figs. 3, 5, and 6 show the relationship between incident and reflected rays lying in the plane of the diagram. It may be shown that, for mirrors, the same relationships apply to incident rays tilted out of the plane of the diagram, the reflected rays giving the same projection onto the plane of the diagram as produced by the corresponding projection of the incident rays. Thus, if for a given EWV altitude the position of the solar image is established, this position remains the same for all rays with the same EWV altitude (whether in the plane of the diagram or tilted with respect to it) with only a drift of the image along its own length. This property is a consequence of the universal equality of the angle of reflection and the angle of incidence.

The same result is *not* obtained in the case of cylindrical *lenses*. If the incident beam is tilted out of the plane of the diagram, the refracted image moves closer to the lens, resulting in defocusing of the image on a fixed receiving screen. A stationary cylindrical lens mounted with its cylindrical axis horizontal east-west will, in general, produce a very poor result.

REFERENCES

1. H. Tabor, *Bull. Res. Counc. Israel* 5A (2) :129-134, 1956.
2. H. Tabor, *Bull. Res. Counc. Israel* 5C (1) :5-26, 1955.

EVIDENCE FOR THE NEED OF A CHEAP SIMPLE SOLAR RADIATION RECORDER

By G. T. WARD

University of California, Berkeley

The recording of solar radiation data in eight tropical countries is surveyed. The author urges the development of an inexpensive solar radiation recorder with an accuracy of plus or minus five percent which would provide reliable data for engineers and agriculturalists.

In many parts of the world, engineers and physicists are engaged in the development of equipment for the commercial utilization of solar energy. Its means of utilization vary: solar radiation may be absorbed as heat energy, it may be used to generate electricity by the thermoelectric effect, the photovoltaic cell, or the photogalvanic effect, or it may be used by *Chlorella* and other organic material in the manufacture of digestible protein. Agricultural scientists are also concerned with solar energy, for not only do they require radiation data to correlate surface evaporation when studying problems of soil erosion, but they have also recently come to the conclusion that solar radiation is, in many cases, the limiting factor in the growth of crops and in the health of farm animals.

Although the World Meteorological Organization, realizing the lack of information concerning the incidence of solar radiation over the earth's surface, has urged its member countries to install equipment to record solar radiation, the implementation of its recommendations is limited by the high cost of recording apparatus. To date, all thermopiles and pyrheliographs have been developed by physicists with the object of obtaining accurate physical data at a very few locations for the study of purely physical problems such as the value of the "solar constant" and the preferential absorption of radiant energy in the atmosphere by ozone, oxygen, water vapour, etc., in various parts of the spectrum. Consequently, in roughly half of the countries in the world, solar radiation is recorded at one or two stations only, while in the rest equipment has been unobtainable because of its high cost. The small amount of information which is available is not of great use to the applied scientist whether he be an engineer or an agriculturist; for instance, no matter how accurate may be the records of solar radiation at Poona and Delhi, they are of little help to the Indian engineer concerned with the scattered areas of India, who wishes to assess the economic advisability of installing either solar water heaters or pumping machines driven by solar hot-air engines, since the intensity and duration of solar radiation varies greatly even over relatively short distances. Likewise, although it is recognized that radiation is the most important factor in the acclimatization of cattle to tropical conditions, the agriculturalist considering this problem in Kenya is provided only with solar radiation figures for Nairobi.

It is evident that the applied scientist requires information covering a wide area, although it need not necessarily be as exact as that which a physicist would demand. In order that a government meteorological department might provide the information required, the best distribution of instruments would appear to be thus: at the central office in the country's capital, Moll-type thermopiles or Eppley pyrheliometers, plus a substandard for calibration checks on the thermopiles; and, at every meteorological station in the provinces, a cheap type of instrument with an accuracy of approximately plus or minus five per cent. The performance of these secondary recorders could then be checked regularly by sending them to the central office for comparison with the thermopiles. Each country's meteorological service would then provide the necessary information, not only for physical work concerning the value of the solar constant, absorption of radiant energy, etc., based upon the records available at the capital, but also for the construction of radiation maps containing data of sufficient reliability for engineers and agriculturalists.

As evidence of the insufficiency of present data concerning solar energy, the difficulties of the various meteorological departments, and the requirements of applied scientists, the following information is offered.

Malaya

The Meteorological Department has no equipment for recording solar radiation. The purchase of such equipment was considered but was turned down because of the high cost involved. However, the Physics Department of the

*Now at the University of Malaya, Kuala Lumpur, Malaya.

University of Malaya has also been interested in meteorological research. For several years both total and direct radiation have been recorded using Moll thermopiles, the calibration being checked periodically by a temperature-drift radiometer of N.P.L. pattern, while during the past year a study of the spectral distribution of incoming radiation has been initiated. During the past two years the utilization of solar energy for heat and power has been studied. The performance of solar water and air heaters has been evaluated and correlated with the radiation incident at Singapore. Experiments are also being carried out concerning air conditioning and refrigeration using solar energy in an absorption cycle. It is now possible to predict the performance of a solar heater in any location where the rate of radiation is known, and it is hoped that it will soon be possible to make similar predictions for air conditioning and refrigeration. The information regarding incident solar radiation, however, is not available although a good coverage of the Federation of Malaya could be obtained by installing recorders at each of the meteorological stations in the provinces.

India

Solar radiation has been recorded by the Meteorological Department for many years at Poona, and these records have been used for predicting the insolation throughout India.[1] Equipment has recently been installed at Delhi consisting of two Kipp and Zonen Moll thermopiles and an Abbot silver-disc pyrheliometer. The Delhi records to date indicate that the insolation predicted by extrapolation from Poona is inaccurate. No information is available for the rest of India, Pakistan, and Ceylon. The National Physical Laboratory of India at New Delhi has been active in studying the application of solar energy to cooking, distillation, the pumping of water, and boiling water by optical concentration, but so far the work has been purely empirical and practical trials of each application have to be carried out in each locality before the performance of the equipment is known. As a typical example, near the desert of Sind there is a stretch of arid waste land where the sap of a type of palm tree is concentrated to obtain sugar. Fuel is scarce and expensive, and it was suggested that solar heat be used. In this case, before an assessment could be made of the value of solar energy, it was necessary for special equipment to be built and for scientists to transport it several hundreds of miles in order to carry out an empirical experiment. Had the meteorological department been able to install a simple type of radiation recorder no expensive and laborious practical experiment would have been necessary because the information would have been available to enable a rapid and simple calculation to be carried out.

Egypt

Solar energy is recorded at Helwan Observatory, Cairo, only. The National Research Council, realizing the enormous possibilities of utilizing solar energy for water heating, cooking, air conditioning, and especially for the lifting of water from canals and artesian wells for irrigation purposes, has formed a special committee to co-ordinate all research in Egypt. Experimental work has begun on solar heating at Cairo University under the supervision of Professor Iskander and Dr. Khalil of the Faculty of Engineering, and on the production of protein for human consumption from local species of *Chlorella* by Dr. Ezz-Eldin, Taha. The generation of electricity is being studied by Dr. Nesr and Dr. Sakr of the University of Ain Shams. The results of this work, however, will be applicable only to Cairo unless a series of stations is set up for recording solar radiation throughout the country.

Sudan

No records of solar radiation are taken in the Sudan, although it is realized that it is one of the countries which is most suited to the utilization of solar energy. The Physics Department of the University College, Khartoum, is taking an active interest in the subject and Dr. Hamouda is initiating a research program. It is probable that the University will purchase thermopiles in the near future to record radiation at Khartoum, but the Sudan is a vast country with three or four completely different climatic zones. It will be necessary for the Meteorological Department or the Department of Agriculture to record radiation at a number of provincial centres with a simple type of apparatus. These figures would then be available for the specialists in Khartoum, and indeed in other parts of the world, to assesss the performance of various types of equipment throughout the country.

Uganda

There is no recording of solar radiation, although Mr. Bargman, the head of the Meteorological Department, would be able to arrange for the installation of suitable equipment should it be available. K. Rose of the Physics Department of the University College, Makerere, and H. G. Farbrother of the Cotton Research Institute, Namulonge, are engaged in the investigation of the effect of solar radiation on the evaporation of moisture from soils and various crops, with reference to erosion by surface run-off, and also on the health and yield of cotton plants. They suffer seriously from the lack of insolation data throughout the colony and would greatly appreciate any information which could be supplied.

Kenya

No records of solar radiation are taken by the Meteorological Department, although equipment will be installed in the near future at the meteorological station at Nairobi. The East African Agricultural and Forestry Research Organization near Nairobi, however, has taken records with a Callender thermopile since 1936. This method proved too tedious and a Gorczynski thermopile with a Cambridge recorder was installed at the beginning of 1954. This equipment is being calibrated every two years at the National Physical Laboratory, Great Britain. Work has been carried out to prove the effect of insolation on the growth of the potato (J. Glover), and investigations are proceeding regarding other crops. Moisture evapora-

tion is being studied by Dr. Pereira while Dr. French is making a study of the effect of radiation on the health of cattle. On the engineering side, the utilization of solar energy for water heating, distillation, salt concentration, and coffee drying is being investigated by N. Ramsey of the Anglo-Baltic Corporation. F. S. Strongman of the Materials Branch of the Public Works Department, Nairobi, is attempting to record solar energy in conjunction with the design of a domestic solar water-heater for African housing. The East African Housing Committee is considering installing solar water heaters in twenty thousand houses in Nairobi alone, as well as in Mombasa and elsewhere in Kenya. Installation of an electric water heater would necessitate an increase of one hundred per cent in the rent and, provided that solar heaters of approximately thirty gallons capacity can be installed for £30 or less, the Public Works Department will go ahead with the plan. In each of the above cases, experimental work is only being carried out over a limited area, usually near Nairobi. Before the results of these experiments can benefit other parts of the country, it is essential that adequate data be available regarding regional insolation.

Madagascar

Solar radiation is recorded only at the capital, Tananarive, the Meteorological Department running the equipment provided by the South African Weather Bureau at Pretoria. The country comprises several distinct climatic zones, and if the Meteorological Department could provide radiation maps it would be possible for the scientists of the Research Institute, Tananarive, and the Department of Agriculture to utilize the information available in other countries to assess the performance of various types of solar heating cycles in Madagascar.

Mauritius

Solar radiation is not recorded. There is a possibility of using solar energy for salt production, the processing of sugar-cane cuttings to prevent the spread of disease, and for coffee drying and tobacco curing. Again, although it would not be expected that basic research would be carried out in such a small colony, the facilities are available in the Agricultural Engineering Section of the Department of Agriculture for applying knowledge gained elsewhere, provided that the radiation is known in the island.

The above survey is by no means complete and applies only to the eight tropical countries which it was possible for me to visit. However, it does appear that the applied scientist, whether he be an engineer or an agriculturalist, and the physicist require a different type of information. The physicist must have maximum accuracy, usually regardless of cost, and sufficient information may be obtained by an intensive study at a few selected points. The applied scientist, however, is concerned with large areas of land. He must be able to assess the economics of the application of his research work over hundreds of square miles, and it is necessary to supply him with radiation data covering the whole region in which he is interested. On the other hand, he does not demand the same degree of accuracy as the physicist. The applied scientist has urgent need of a simple but reliable apparatus which is capable of recording solar radiation with an accuracy of the order of plus or minus five per cent, which could be installed at the provincial meteorological and agricultural stations throughout each country to supply the necessary information.

It is hoped that this short article will stimulate interested individuals and organizations to develop an inexpensive solar radiation recorder to satisfy this pressing need.

REFERENCES

1. L. A. Ramdas and S. Yegnanarayanan, "Solar energy in India." Paper presented at the Symposium on Solar Energy and Wind Power, New Delhi, October, 1954.

BASIC OPTICAL CONSIDERATIONS IN THE CHOICE OF A DESIGN FOR A SOLAR FURNACE*

By W. A. BAUM** AND J. D. STRONG***

Simple relationships exist between the aperture of a solar furnace, the target size, the angle of convergence, the maximum attainable concentration ratio, the over-all efficiency, and the amount of spill light surrounding the target. For optical systems having continuous unobstructed surfaces and no spherical aberration, the concentration ratio is determined solely by the angle of convergence. Various systems differ considerably, however, in the amount by which their apertures exceed that of an ideal system of equal performance; in the resulting efficiency at which they operate; in the associated amount of waste light spilled outside the target; in the distribution of this spill light; and in the relative convenience with which they can be fabricated and adjusted. A paraboloidal mirror with heliostat does not seem to be an optimum choice. The optical possibilities afforded by other two-mirror systems are discussed and illustrated by example. We also present structural design for a two-mirror system which appears to possess some practical advantages over the heliostat-paraboloid combination.

I. INTRODUCTION

The purpose of a solar furnace is to concentrate as much flux as possible onto a specified target area. There are many different optical systems which might be used for this purpose, and they differ considerably both in performance and practicability. The use of a paraboloid, which has been given first consideration for the Cloudcroft furnace, does not appear to be an optimum choice. The purpose of this report is to call attention to the range of possible alternatives and to show by example what might be achieved. It would be regrettable indeed if design and construction were to proceed without recognition of these alternatives.

For a specified target size and a specified solid angle from which flux converges toward the target, there is (as shown below) a fundamental upper limit on the amount of flux which can be concentrated onto the target. No optical system, however ideal it may be, can exceed this upper limit. If an optical system receives more than this amount of flux, it cannot deliver all of the received flux onto the specified target area, and it accordingly has two faults: (a) It is bigger than theoretically necessary. (b) It spills the excess flux into a halo around the target where it is not wanted. In these terms, a paraboloidal mirror of the proportions now under consideration for the Cloudcroft furnace (say, 104-ft aperture and 120° cone of convergence) is more than 1.7 times larger than ideally necessary, and it spreads the excess light (44 per cent of the total received) over an area 7 times as large as that of the target. While we know of no practical furnace system exactly meeting the conditions required for ideal performance, we do know of practical systems which excel a paraboloid.

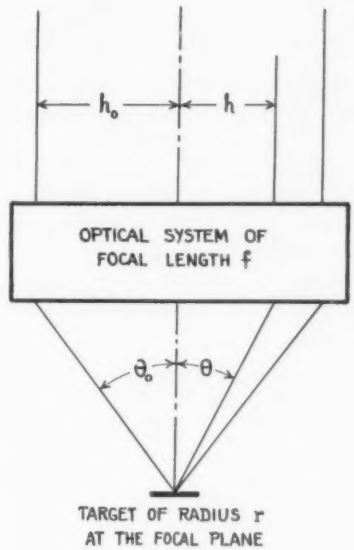

FIG. 1.

The criteria of an ideal system would be that it have no spherical aberration and no coma — in short, that it meet the Abbe sine condition. This situation is represented by

*Originally published as Holloman Air Force Missile Development Center, *Technical Memorandum* No. HDGR-57-14, September 25, 1957.

**Mount Wilson and Palomar Observatories, Carnegie Institution of Washington, and California Institute of Technology.
***Professor of Experimental Physics, John Hopkins University.

Fig. 1, where the sine condition requires, for any particular ray, that

$$h = f \sin \theta$$

If the angular radius of the sun is taken to be 16 minutes of arc, and if the target radius is r, we have

$$f = 215r$$

The aperture under these conditions is

$$2h_o = 430\, r \sin \theta_o$$

If the target diameter is 5 in. ($r = 2.5$), as contemplated for the Cloudcroft furnace, and if the peripheral angle θ_0 is 60°, the aperture turns out to be about 78 ft. This is the maximum aperture of an ideal system for which *all* of the light can be delivered to a 5-in. target. If there were no reflection or absorption losses, the maximum possible concentration ratio for $\theta_0 = 60°$ would be

$$\frac{\pi h_o^2}{\pi r^2} = (215)^2 \sin^2 (60°) = 34600$$

Any optical system with continuous unobstructed surfaces and free of spherical aberration can produce the same concentration ratio for the same value of θ_o, but the associated aperture will automatically be greater than $2h_o$ if the sine condition is not also met. One can also arrive at the foregoing conclusions from purely geometrical arguments without invoking the sine condition *per se*.

The geometrical efficiency of an optical system having continuous unobstructed surfaces and free of spherical aberration will be simply

$$\epsilon = h^2/Y^2$$

where Y is the radius of the aperture. For a paraboloid with $\theta = 60°$ and with a 5-in. paraxial solar image, we find $2Y$ is about 104 ft, yielding:

$$\epsilon = \left(\frac{78}{104}\right)^2 = 56\%$$

This result can be laboriously verified by dividing the paraboloid (or any other system having the same Y, f, θ) into annular zones, computing the image profile for each zone, finding what fraction of this image actually hits the target, weighting these zonal efficiences in proportion to the relative areas of the zones, and finally summing the zonal contributions. This procedure was actually carried out for two very different systems, and the results (with suitable allowance for obstructed areas) have checked the conclusions above.

The actual efficiency of a system will be considerably less than the geometrical efficiency discussed above because of losses due to glass absorption, imperfect reflection, obstructed areas, and interstices between the facets that comprise the optical elements. Optimistically assuming two reflections of 0.9 efficiency and other losses totaling 0.1, we find that an actual efficiency of 41 per cent is unlikely to be exceeded by any system with a 104-ft aperture, a 5-in. target, and a 120° cone of convergence ($\theta = 60°$).

Four important conclusions can be summarized:

(a) If we are interested in a 5-in. target with $\theta = 60°$, a 104-ft aperture is not necessarily needed. Only 56 per cent of the flux received by a 104-ft aperture can be geometrically utilized. A somewhat smaller aperture (theoretically minimum = 78 ft) can achieve equal performance if a suitable and practical optical system can be found. We do not need to belabor this possibility — its importance is appreciated when one recalls that costs of large constructions vary roughly as the cube of the aperture. Or, turning the argument around, we can say that a 104-ft aperture should be capable of performing efficiently on a target larger than 5 in. (theoretical maximum = 6.6 in.).

(b) We noted that *all* 104-ft optical systems with continuous unobstructed surfaces and with no spherical aberration will put 56 per cent of their unabsorbed or unobstructed flux onto a 5-in. target if $\theta = 60°$. They are all basically equal in that respect. They differ considerably, however, in where the 44 per cent spillage goes. A 104-ft paraboloid spreads this spillage over a 13-in. disc, whereas an alternative system discussed in Section III, confines nearly all of the spillage to an 8-in. disc. In the latter case, the spillage lies close enough to the 5-in. central disc to be of frequent practical use.

(c) It is possible to design optical systems which not only are superior to the paraboloid with respect to a and b above, but which in addition possess certain advantages with respect to simplicity of optical fabrication and convenience of adjustment. For example, the cases discussed in Section III employ surfaces which are either spherical or nearly spherical over most of their area.

(d) A substantial gain in concentration ratio is potentially available by allowing θ to exceed 60°. Since the concentration ratio varies as $\sin^2 \theta$, one can theoretically gain a factor of 1.18 by making $\theta = 70°$, a factor of 1.29 by making $\theta = 80°$, or a factor of 1.33 by making $\theta = 90°$ (which is the absolute limit for a flat target). However, values of θ beyond 70° are probably not optically practical. At $\theta = 70°$, the maximum attainable concentration ratio (neglecting losses) is 40,700, and the associate aplanatic aperture $2h_o$ is 84 ft if a 5-in. target is used.

The remainder of this report is divided into four parts. Section II concerns the characteristics of a paraboloidal mirror, Section III explores what might be achieved with a two-mirror system consisting of a large primary and a small secondary, Section IV discusses a structural design suited to the type of optical system presented in Section III, and Section V presents an alternate arrangement for using a paraboloid with a heliostat. The structural designs, prepared with the excellent artistic collaboration of Mr. Roger Hayward, appear to possess certain practical advantages over the proposed heliostat-paraboloid combination.

It should be emphasized that the present report does not pretend to be a complete survey of the optical or structural possibilities. Its primary purpose has been to show that the various possibilities of devising a solar furnace are not yet exhausted.

II. CHARACTERISTICS OF A PARABOLOID

Fig. 2 is the axial section through a paraboloid of rotation with various pertinent quantities labeled. In rec-

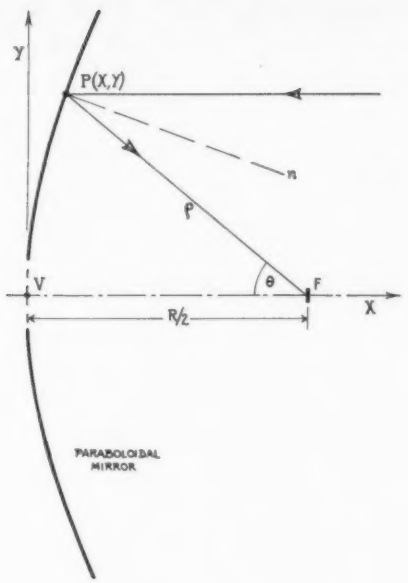

FIG. 2.

tangular coordinates the equation for this section is simply:

$$Y^2 = 2RX$$

where the origin is at the vertex V of the paraboloid, and where R is its radius of curvature in that neighborhood. The distance from the vertex to the focus is $R/2$. In polar coordinates the equation of the paraboloid is

$$\rho = \frac{R}{1 + \cos\theta}$$

where the pole is at the focus. The normal to the surface at P makes an angle $\theta/2$ with the axis, and the radius of curvature at P is given by

$$R\left(\frac{2}{1+\cos\theta}\right)^{3/2}$$

in the meridional plane, and by

$$R\left(\frac{2}{1+\cos\theta}\right)^{1/2}$$

in the sagittal plane. A pencil of rays parallel to the axis and incident at P is brought to an anastigmatic focus at F, so that the effective focal length in both the meridional plane and the sagittal plane is simply ρ. If a target surface is placed normal to the axis at F, the sagittal half-width of the solar image produced by a single facet at P is the product of ρ and the sun's angular radius:

$$b = 0.004654\,\rho = \frac{0.004654\,R}{1+\cos\theta}$$

and the projected meridional half-width of the image is

$$a = b\sec\theta$$

For paraxial rays, $a = b = 0.002327\,R$. If the target is made to coincide with this paraxial image, the optical efficiency of any annular zone at angle θ is accordingly

$$\epsilon = \frac{(0.002327)^2R^2}{ab} = 0.25\,(1+\cos\theta)^2\cos\theta$$

The fraction of the aperture area contained within a narrow zone of width ΔY is

$$\Delta A = \frac{2Y\,\Delta Y}{Y_1^2} = 2\left(\frac{R}{Y_1}\right)^2\frac{\sin\theta\,\Delta\theta}{(1+\cos\theta)^2}$$

where Y_1 is the radius of the full aperture. The over-all efficiency of the system is therefore

$$E = \int_0^{\theta_1}\epsilon\,dA = 0.5\left(\frac{R}{Y_1}\right)^2\int_0^{\theta_1}\sin\theta\cos\theta\,d\theta$$

which yields

$$E = 0.25\,(1+\cos\theta_1)^2$$

For a 104-ft paraboloid with a 5-in. paraxial image, we have $Y_1 = 52$ ft, $R = 89.5$ ft, $\theta = 60°$, and we obtain $E = 56$ per cent. This is in agreement (as we should expect) with the result derived from the Abbe sine condition in Section I.

The 44 per cent spillage of a paraboloid having $\theta = 60°$ is spread over a disc 13.3 in. in diameter, or an area of 140 sq. in. The distribution of this spill light can be computed by finding what fractions of the elliptical solar images ($2a$ long and $2b$ wide) formed by facets at various values of θ fall inside concentric circles of various diameters between 5 in. and 13.3 in. at the focal plane. When the elliptical image falls entirely inside a circle of radius r, the efficiency for the associated zone and for this value of r is 100 per cent. When the circle lies entirely inside the elliptical image, the zonal efficiency is r^2/ab. When the circle intersects the ellipse, as sketched in Fig. 3, the efficiency is $S/\pi\,ab$, where S is the area which the circle and the ellipse have in common. If $\alpha = a/r$ and $\beta = b/r$, it can be shown that the area in common is

$$S = \pi + 2\,\alpha\,\beta\arcsin\left(\frac{1-\beta^2}{\alpha^2-\beta^2}\right)^{1/2} - 2\arcsin\left[\alpha\left(\frac{1-\beta^2}{\alpha^2-\beta^2}\right)^{1/2}\right]$$

This expression is rather complex for practical computation, and the following approximation is more expedient:

FIG. 3.

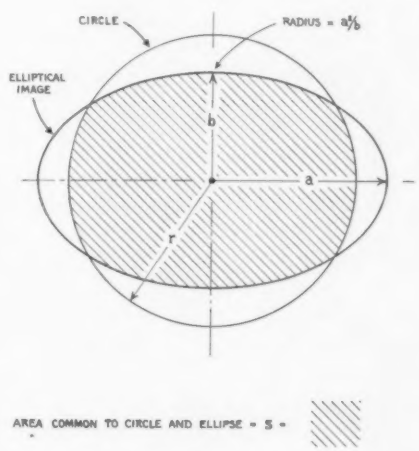

TABLE I

ZONAL EFFICIENCIES AND THE DISTRIBUTION OF SPILL LIGHT SURROUNDING THE TARGET OF A PARABOLOID

Aperture $= 2Y_1 = 100$ ft, peripheral $\theta = 60°$, paraxial image $= 4.84$ in.

Zone No.	1	2	3	4	5	6	7	8	9	10	
Inner Y (ft)	6.00	16.91	23.15	28.03	32.18	35.86	39.20	42.26	45.12	47.81	
Outer Y (ft)	16.91	23.15	28.03	32.18	35.86	39.20	42.26	45.12	47.81	50.36	
Mean θ	15°9′	26°2′	32°53′	38°20′	42°50′	46°45′	50°25′	53°32′	56°24′	59°5′	
a (in.)	2.549	2.836	3.131	3.455	3.808	4.200	4.631	5.106	5.630	6.220	% flux
b (in.)	2.460	2.548	2.629	2.710	2.791	2.873	2.953	3.034	3.114	3.194	inside r
ϵ for various r: 2.5 in.	0.988	0.865	0.759	0.667	0.588	0.518	0.457	0.403	0.356	0.314	59.1
3.0 in.	1.000	1.000	0.986	0.910	0.826	0.737	0.656	0.581	0.513	0.452	76.6
3.6 in.	1.000	1.000	1.000	1.000	0.985	0.922	0.848	0.767	0.692	0.623	88.4
4.2 in.	1.000	1.000	1.000	1.000	1.000	1.000	0.975	0.905	0.834	0.757	94.7
4.8 in.	1.000	1.000	1.000	1.000	1.000	1.000	1.000	0.987	0.937	0.871	98.0
6.0 in.	1.000	1.000	1.000	1.000	1.000	1.000	1.000	1.000	1.000	0.994	99.9

$$\epsilon \approx \frac{r^2}{ab}\left\{1 - \left[\frac{(r-b)^3}{r^2\,(r - br^2/a^2)}\right]^{1/2}\right\}$$

When $b \to r$, $\epsilon \to r/a$; and when $a \to r$, $\epsilon \to 1$.

Some sample results are listed in Table I and plotted in Fig. 6. These data were assembled primarily for comparison with similar results for another system discussed in Section III.

III. TWO-MIRROR SYSTEMS

When only one mirror participates in the focusing, it must necessarily be a paraboloid, unless the mirror surface is a discontinuous curve. In general, discontinuous curves result in the utilization of less solid angle for the same peripheral θ and Y, and they consequently offer no gain over continuous curves.

When more than one mirror participates in the focusing, an infinite number of combinations become possible, and specific cases must be selected for investigation. Several combinations involving a large primary mirror and a small secondary mirror were investigated in varying degrees of detail. A particularly interesting case, diagrammed in Fig. 4, provides a suitable example for discussion in the present report. A blend of this case with another one will also be discussed to show how the good features of two systems might be combined. It must be remembered that these cases are merely examples with arbitrarily chosen parameters, and that they do not represent optimum choices. Much additional computing and comparing would be required to afford a basis for the selection of an optimum case.

FIG. 4.

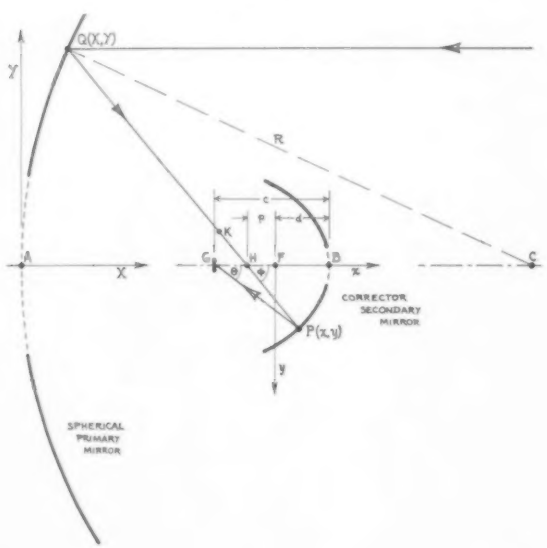

In Fig. 4 the primary mirror, which includes about 90 per cent of the total mirror area of the system, is a sphere of radius R. Such a choice would clearly be convenient both for construction and for adjustment. Except for the inner zone hidden by the secondary, the facets of the spherical primary can be adjusted very simply by autocollimation, using a small light source at the center of curvature C.

The secondary mirror, which amounts to about 10 per cent of the total mirror area, serves to correct the spherical aberration of the primary. It is roughly paraboloidal in form, and its facets can be adjusted with adequate precision by means of a template.

Strangely, the spherical aberration of the primary mirror serves a useful purpose. It prevents the effective focal length of the combination from increasing with θ, and it thereby keeps the solar image small for the outer zones of the system. It is especially effective in the meridional plane, where it also compensates for the sec θ factor due to the oblique incidence of the zonal images on the target. As a consequence, the outer zones of the system are the most efficient ones, and the spillage around the target is confined to a much smaller disc than in the case of the paraboloid.

The exact shape of the secondary mirror can be derived by imposing the condition that optical path lengths must be the same for all rays that come to a focus at the center of the target. For any value of ϕ, the path is

$$L\phi = \underbrace{-R\left(1 - \cos\frac{\phi}{2}\right)}_{\text{to } Q} + \underbrace{\frac{R}{2}\sec\frac{\phi}{2}}_{\text{to } H} + \underbrace{(x+p)\sec\phi}_{\text{to } P} + \underbrace{\left[(x-d+c)^2 + (x+p)^2\tan^2\phi\right]^{1/2}}_{\text{to } G}$$

TABLE II

SAMPLE TWO-MIRROR SYSTEM HAVING AN ALL-SPHERICAL PRIMARY

$c = 0.21\ R$, $d = 0.1\ R$, aperture = 100 ft, $R = 93$ ft

ϕ	20.0	27.5	35.0	42.5	50.0	57.5	65.0	deg
p	0.72	1.37	2.26	3.39	4.81	6.54	8.64	ft
X	1.41	2.67	4.30	6.32	8.71	11.47	14.56	ft
Y	16.15	22.10	27.96	33.70	39.30	44.73	50.00	ft
x	8.82	8.25	7.49	6.24	4.44	1.92	−1.44	ft
y	3.47	5.01	6.82	8.86	11.02	13.28	15.42	ft
θ	10.330	15.181	21.060	28.266	36.915	47.543	60.326	deg
(QH)	47.22	47.87	48.76	49.89	51.31	53.04	55.13	ft
(QK)	45.79	45.26	44.35	43.34	42.14	40.77	39.22	ft
(HP)	10.16	10.85	11.89	13.07	14.39	15.75	17.01	ft
(KP)	11.58	13.56	16.30	19.62	23.55	28.02	32.93	ft
(GP)	19.37	19.15	18.98	18.70	18.35	18.00	17.75	ft
$2a$	8.70	7.38	6.18	5.24	4.59	4.33	4.77	in.
$2b$	10.06	9.44	8.69	7.98	7.31	6.77	6.42	in.
ϵ (5 in.)	28.5	35.8	46.5	59.8	72.7	79.6	80.5	%

where the spherical aberration of the primary is

$$p = \frac{R}{2}\left(\sec\frac{\phi}{2} - 1\right)$$

For paraxial rays, $\phi \to 0$ and

$$L_o = \frac{R}{2} + d + c$$

Setting $L\phi = L_o$, we obtain

$$X = \frac{A^2 - p^2\tan^2\phi - (c-d)^2}{2(c-d) + 2A\sec\phi + 2p\tan^2\phi}$$

where $A = c + d + p\ (2\cos\phi/2 - 1 - \sec\phi)$.

It follows that

$$y = (x + p)\tan\phi$$

and the final angle of convergence is

$$\theta = \arctan\left(\frac{y}{x + c - d}\right)$$

In terms of R and ϕ, the coordinates of the primary sphere with the origin at the vertex are

$$X = R\left(1 - \cos\frac{\phi}{2}\right);\ Y = R\sec\frac{\phi}{2}$$

The solar image formed by a facet of the primary mirror at Q is strongly astigmatic, the meridional image falling at K and the sagittal image at H, but the secondary mirror puts these component images back together again at F. The magnification of the secondary mirror is therefore different for the two axes of the solar image, and (as remarked earlier) it has the desirable feature of decreasing with increasing ϕ and θ. For any particular P and Q, the final solar image formed on a plane normal to the optic axis at F is an ellipse similar to that formed by a facet of a paraboloid, except that its meridional dimension is now the smaller axis instead of the larger axis of the ellipse. To compute the dimensions of the image ellipses associated with the various zones of the system, one must make use of the following expressions for the pertinent segments of the light path:

$$(QH) = 0.5\ R\sec\frac{\phi}{2}$$

$$(QK) = 0.5\ R\sec\frac{\phi}{2} - 0.5\ Y\tan\frac{\phi}{2}$$

$$(HP) = y\csc\phi$$

$$(KP) = y\csc\phi + 0.5\ Y\tan\frac{\phi}{2}$$

$$(GP) = y\csc\theta$$

On a plane normal to the optic axis at F, the meridional half-width of the image (semi-minor axis) is

$$a = 0.004654\ (QK)\left(\frac{GP}{KP}\right)\sec\theta$$

and the sagittal half-width of the image (semi-major axis) is

$$b = 0.004654\ (QH)\left(\frac{GP}{HP}\right)$$

Some sample data for an optical system of this type are listed in Table II. For this case we adopted $c = 0.21\ R$ and $d = 0.10\ R$, and the system has been scaled to a 100-ft aperture for a peripheral ϕ of 65°, which yields a peripheral θ of approximately 60° and a value of 93 ft for R.

The spread of the spill light surrounding the target can be reduced still further by blending the outer zones of the

FIG. 5

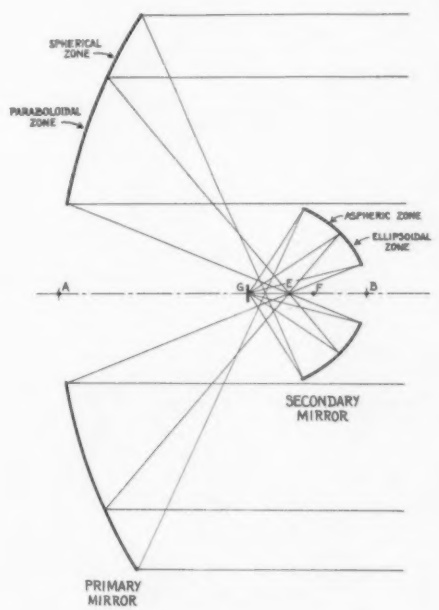

sphere-corrector combination in Fig. 4 with the inner zones of a system consisting of a paraboloidal primary and an ellipsoidal secondary. This blended system is sketched in Fig. 5. The transition was arbitrarily chosen to occur at $\phi = 50°$, and the slope was made continuous across the transition so that neither the primary nor the secondary would have any optical discontinuity. It can be shown that the paraboloidal portion of the primary is

$$Y^2 = 2(R - X_0)\ (X + \Delta)$$

where X_0 is the coordinate of the junction $(0.09369\ R)$ and where $\Delta = 0.00484\ R$. The ellipsoid is given by

$$\frac{(x + 0.08085\ R)^2}{(0.17601\ R)^2} + \frac{y^2}{(0.17357\ R)^2} = 1$$

Its eccentricity is found to be 0.1657. For $\phi < 50°$, all rays from the primary pass through the same axial intercept E, and the magnification of the secondary is found to be

$$m = 1.0564 + 0.3406 \cos \phi$$

The final images formed on a plane normal to the axis at F have sagittal half-widths of

$$b = 0.004654\ (QE)\ m$$

and meridional half-widths of

$$a = b \sec \theta$$

where the angle of convergence θ is given by

$$\theta = \arcsin \left[\frac{1}{m} \sin \phi \right]$$

The distribution of the spill light for this blended optical system of Fig. 5 has been calculated as it was for the paraboloid. Both distributions are plotted in Fig. 6 for comparison.

FIG. 6.

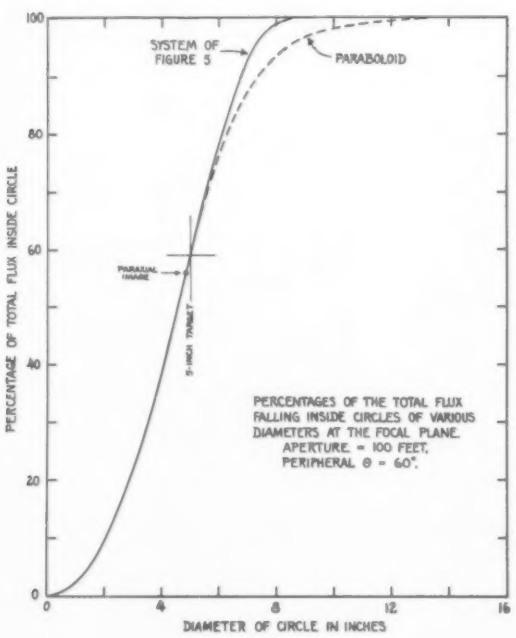

IV. MOUNTING FOR A TWO-MIRROR SYSTEM

Fig. 7 shows how the two-mirror optical system, described above, may be embodied with an altazimuth mounting. Such a mounting has a precedent in large construction — it has been used for the Manchester radio telescope of 250-ft aperture. The separate angular motions of altitude and azimuth may be controlled and coordinated by separate sun trackers with associated servomechanisms or by programmed drives.

This altazimuth mounting has several notable features: (a) Relative immunity to high winds, (b) Protection of optical parts from weather, (c) Facility for optical adjustment, (d) Target plane faces upward, (e) Primary movable to a "horizontal" position for maintenance and repair.

Fig. 7 illustrates the general appearance of the envisioned furnace, while Fig. 8 shows three sectional views of the furnace. The main structure turns in azimuth on a circular track, and this frame supports the furnace proper on trunnions that allow it to rotate in altitude.

This construction provides the observing station that is detailed in Fig. 7 and shown further in Fig. 8. Observation directly into the furnace hot spot is afforded from this station. Observers may work on its cylindrical half-floor when the furnace is tipped, and on the level half-floor when the furnace is pointing vertically. Experience of astronomers with the prime-focus cage of the 200-in. Palomar telescope serves as a precedent to show that such an observing system is practical. Fig. 8 shows how the observer enters the observing station by an elevator to the trunnion level, and thence by steps.

At the hot spot, when a crucible is exposed, it will be inclined upward by at least 30°, and it will be nearly vertical at high noon in early summer. A prearranged set-up for an experiment or for routine exposure may be raised to trunnion level by the elevator indicated. From there it goes horizontally across the cat-walk to a door in the central shaft and thence to the hot spot by a lift. This cat-walk may be turned, during exposure, to a position affording minimum obstruction (as shown in Fig. 8, upper right).

The artist has shown an ensemble of sloped radial vanes to serve (1) as an attenuator, (2) as the slow shutter, and (3) as a protecting roof. The vanes are mounted so that they turn open over the beams that support the observing station, thereby minimizing light obstruction.

A similar but smaller ensemble of vanes (not shown) could conveniently be located radially (to form an inward pointing cone) and reach from the rim of the secondary mirror to the central shaft. Such a secondary set of vanes could serve as the fast shutter.

For adjusting the facets of the primary mirror, and aligning the primary with the secondary, we envision the furnace pointed toward a platform on a nearby tower. By bringing the center of curvature of the spherical part of the primary within surveillance of an observer there, the spherical facets can be adjusted by autocollimation, as remarked in Section III.

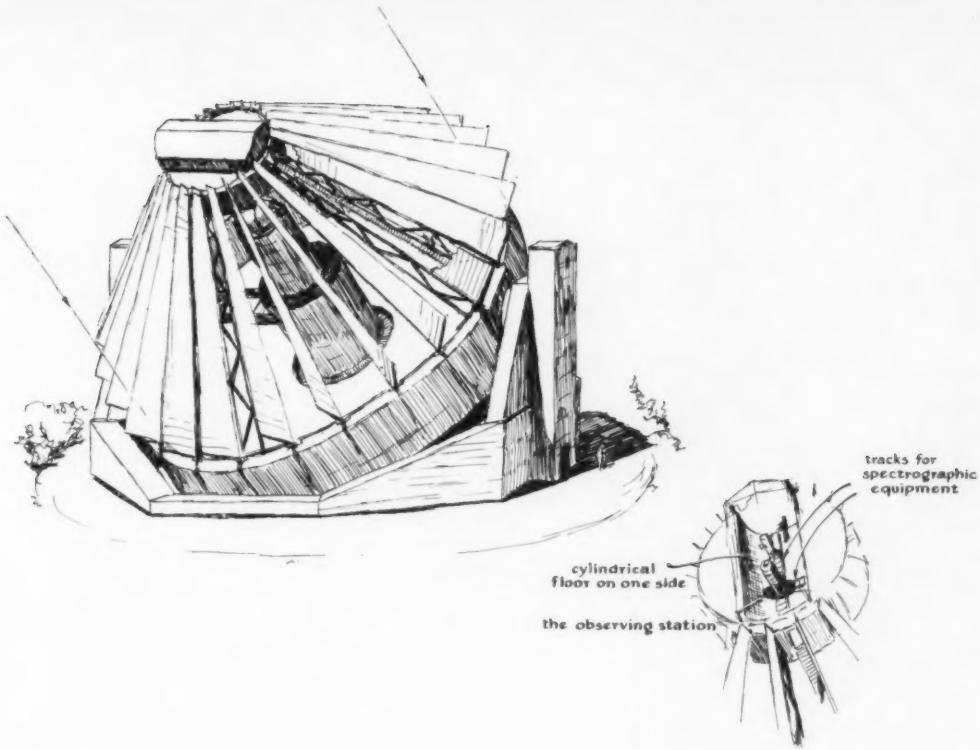
tracks for
spectrographic
equipment
cylindrical
floor on one side
the observing station

FIG. 7.

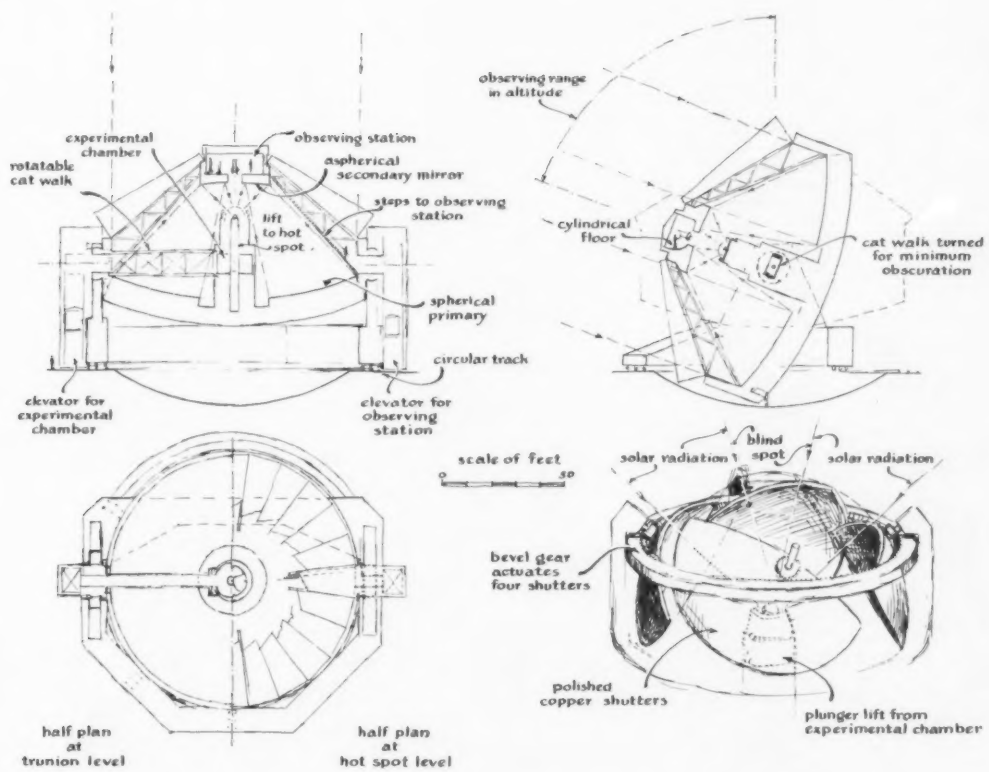
observing range
in altitude
experimental
chamber
observing station
rotatable
cat walk
aspherical
secondary mirror
steps to observing
station
lift
to hot
spot
cylindrical
floor
cat walk turned
for minimum
obscuration
spherical
primary
circular track
elevator for
experimental
chamber
elevator for
observing
station
scale of feet
0
50
blind
spot
solar radiation
solar radiation
bevel gear
actuates
four shutters
polished
copper shutters
plunger lift from
experimental chamber
half plan
at
trunion level
half plan
at
hot spot level

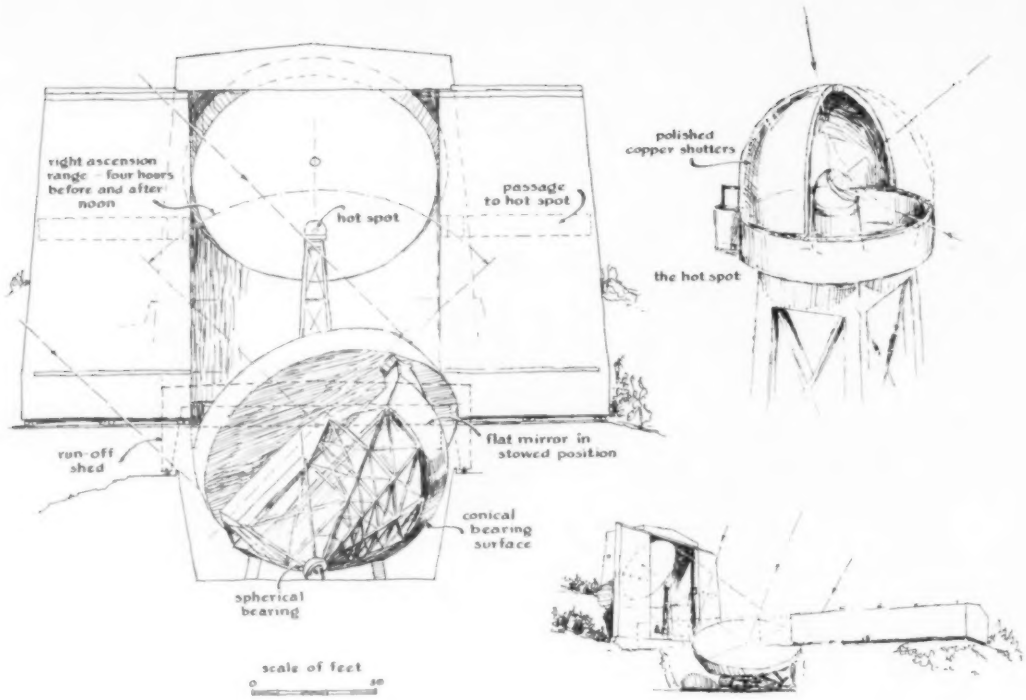

FIG. 9.

FIG. 10.

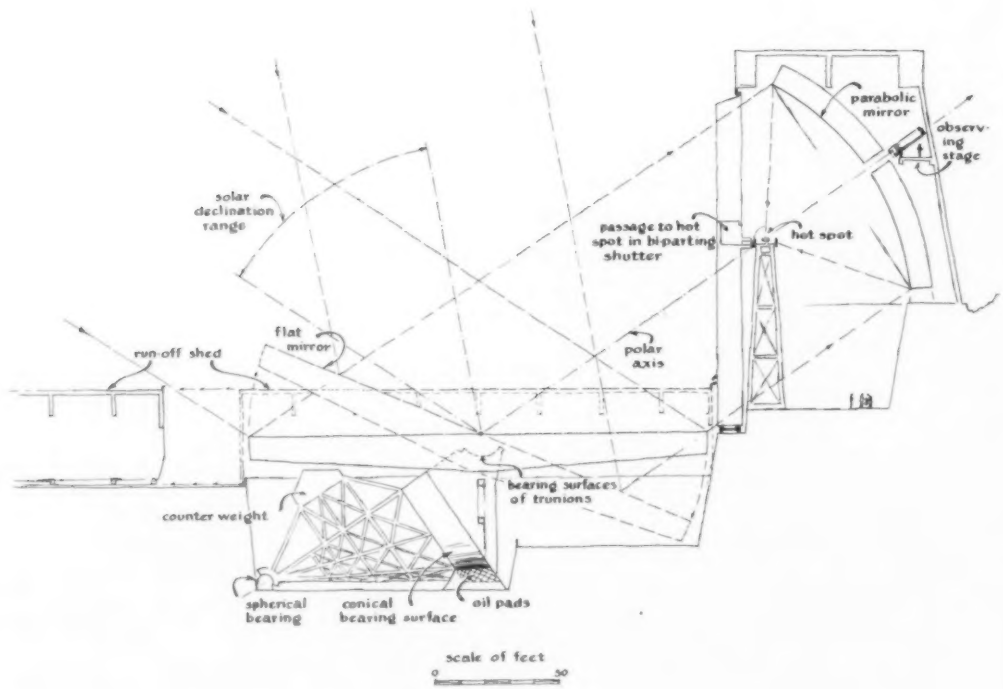

The facets of the aspheric secondary mirror may be adjusted with a radial template arm (not shown) which is perpendicular to the optical axis and rotatable around it.

If the central part of the primary mirror is paraboloidal, as discussed in the latter part of Section III, it may be lined-up simply by putting a point light source at the focus after preliminary adjustment of the secondary mirror. The parabolic facets may be observed by means of penta-prisms mounted, one for each zone of facets, on the template arm mentioned above.

Optical line-up may be carried out during cloudy weather or at night.

Finally, it is to be noted that this furnace construction is compact, and that it may be located in a depression of terrain to further protect it from winds during operation and from damage during storms. This mounting is certainly more immune to wind than one that has separated components separately mounted.

V. ALTERNATIVE SYSTEM USING A PARABOLOIDAL MIRROR

Figs. 9 and 10 show Mr. Hayward's conception of an arrangement using a "horizontal" rather than the previously proposed "vertical" heliostat. This arrangement has the disadvantage of requiring a larger flat mirror; but the following advantages inhere in it:

(a) The working focal plane faces upward.

(b) By means of bi-parting shutters and a retractable shed, all optical parts may be protected from wind and weather.

In this arrangement we propose using the bi-parting shutter as attenuator, with a rotating half-hemisphere for the fast shutter. Access to the hot spot chamber by a passage in one of these bi-parting shutters provides for the safety of personnel.

SUGGESTED METHODS OF ALIGNING THE PLANES OF THE SOLAR FURNACE HELIOSTAT MIRRORS INTO PARALLELISM*

By FRED ALLISON AND GORDON HUGHES

Department of Physics, Alabama Polytechnic Institute, Auburn, Alabama

Three possible methods for measuring the alignment of the planes of the individual mirrors of the heliostat of the proposed Department of Defense solar furnace are described. Two of the methods are optical and one is mechanical. The optical methods require, in one case, a theodolite of high precision and large aperture, and, in the other case, a specially built instrument as shown in Fig. 4. The mechanical method would use high precision spirit levels with the heliostat set in the horizontal plane.

AN OPTICAL METHOD

(By DR. FRED ALLISON)

This method is based on adjustments made possible by means of the Gaussian eyepiece.

The frame holding the heliostat mirrors is brought as nearly as possible into the east-west vertical plane and clamped. †With the heliostat so positioned, the mirrors, one by one, are to be aligned with their planes parallel by means of the adjustment screws.

A theodolite of high precision and large aperture, securely mounted on a "cat walk" in as close proximity as possible to the heliostat mirror, is adjusted so that the azimuth circle and the axis of the telescope lie in horizontal planes.

FIG. 1.

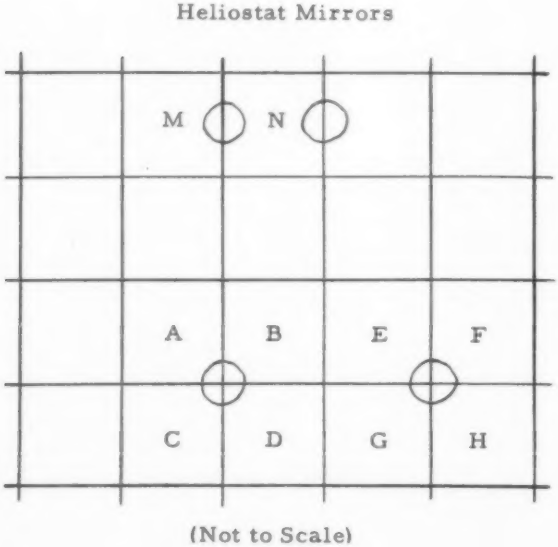

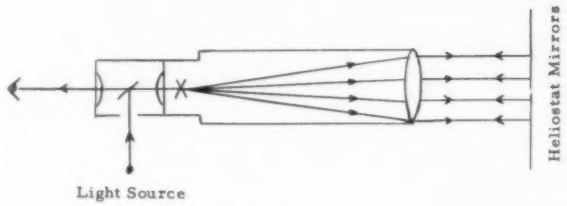

FIG. 2.

In order to expedite the work of alignment, it is suggested that the mirrors in groups of four may be aligned without resetting the theodolite, in the following manner.

The theodolite telescope, its axis set in the *n-s* plane and the cross-hairs of the Gaussian eyepiece properly illuminated, is directed at the contiguous corners of four mirrors, as *A, B, C, D.* (See Figs. 1 and 2.) One of these mirrors, say *A,* is adjusted by the screws until it is autocollimated with the telescope, i.e., until the light reflected from *A* forms an image of the cross-hairs in coincidence with the direct image of the cross-hairs as seen in the eyepiece.

In a precisely similar manner, one proceeds with the adjustment of *B* to obtain coincidence of the cross-hair image with the two already in coincidence. In the same way, the cross-hair image due to light reflected from *C* is brought into coincidence with the other three; and finally, the image due to *D.* Five cross-hair images would thus be in coincidence when the planes of the four mirrors are parallel. If the multiplicity of cross-hair images in the field of view should cause confusion, one could first adjust

*Originally issued as Holloman Air Development Center, *Technical Memorandum* No. HDGR-57-12, September 10, 1957.

†NOTE: The foregoing paper was written early in the summer, when it was understood, according to temporary plans then available, that the heliostat mirror could be set in the vertical plane. Revised plans do not permit vertical setting of the heliostat mirror. For positions of the heliostat mirror other than vertical, the method above suggested, with certain obvious modifications in the adjustment of the theodolite and the constant-deviation prism, should have practically the same applicability.

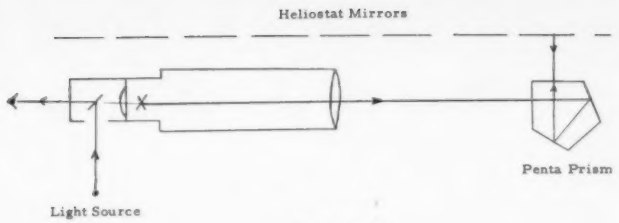

FIG. 3.

mirror *A*, with the corners of *B*, *C*, and *D* covered, then proceed to align each of these three in turn, keeping the corners of the others covered.

The operation described above would be repeated for other groups of four mirrors in the same double row until all mirrors of the heliostat were included.

Some variations in the procedure may be suggested.

(a) Set the telescope on the four contiguous corners of mirrors *B*, *D*, *E*, and *G*. (See Fig. 1.) Instead of readjusting the theodolite by the levels, adjust it until the cross-hair image due to *B* (and *D*) falls on the cross-hairs of the eyepiece. Then adjust *E* and *G* as above described. The next setting would be in the corners of *E*, *F*, *G*, *H*, and so on. This process would align only two mirrors at a setting, and the errors would be accumulative.

(b) Instead of working with the groups of four mirrors, groups of two, as *M*, *N*, etc., using the same method, may be aligned across each horizontal row.

Once the mirrors are adjusted for parallelism, the test for accumulated errors in their over-all alignment throughout the heliostat mosaic is as indicated below.

The telescope is autocollimated on a selected mirror and is then accurately turned in azimuth through 90° looking into a constant-deviation prism which is on an adjustable mounting in front of a second selected mirror in the same horizontal row. (See Fig. 3.) If the planes of the two selected mirrors have been correctly aligned, the light incident on the second selected mirror will retrace its path through the constant-deviation prism, and the cross-hair images due to the returned light will be in coincidence with the cross-hair image of the eyepiece. By proper adjustment of the telescope in altitude, the second mirror may be selected in any horizontal row as well as in any vertical column of mirrors.

Whether the methods above suggested would yield satisfactory results could be determined by preliminary experimentation.

FIG. 4.

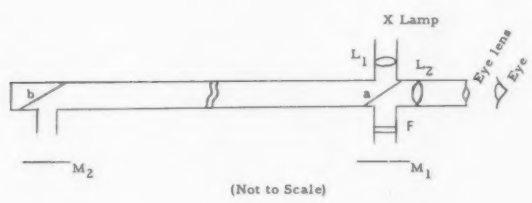

A SECOND OPTICAL METHOD

(By DR. GORDON HUGHES)

The method to be proposed assumes that an observer and a device may be held in a relatively fixed position within some 10 ft of the heliostat mirrors.

Suppose a relatively rigid metal tube, say some 8 to 9 ft long, is provided with side ports as indicated in Fig. 4. Mirror *a* is a half-silvered surface placed at 45° with the axis of the tube. Mirror *b* is full silvered and placed as shown. An electric lamp with its filament in the shape of an x is placed at the focal point of lens L_1 and observed through lens L_2 with an eye lens.

Two dishes of mercury, M_1 and M_2, are observed. Since these two surfaces are parallel, two images of the light source indicate that mirror *b* should be adjusted until the single image of the lamp filament is seen. A color filter at point *F* in the system might be employed to distinguish the light returned from the two floating mirrors.

Now, if the device is placed before two of the heliostat mirrors instead of the two floating mirrors, they may be aligned with an accuracy determined by the sharpness of the lamp filaments and their magnification.

If the alignment procedure starts at one side of the heliostat and progresses across the entire face, an error may accumulate of sufficient magnitude to render the alignment as unsatisfactory. Since the instrument is designed with appreciable length, it should be possible to align alternate mirrors and then check between the alternate pairs.

A pentaprism may be employed to replace mirror *b* if the deformation of the tube under its own weight throws the device out of alignment.

Advantages of this method of alignment:

(a) There is no loading of the glass surface using this technique.

(b) The mirrors may be aligned when the heliostat is in any position.

(c) The reference signal is from the heliostat itself with this device so that random motions of the heliostat from wind gusts will not negate the method.

(d) The device will work even though it may be turned through small angles with reference to the normal to the mirrors.

(e) Cumulative errors in the alignment may be detected and corrected.

A MECHANICAL METHOD

(By DR. FRED ALLISON)

The method is based on the possibilities of achieving horizontal adjustments of plane surfaces by means of high precision spirit levels of the cross-arm type. It is assumed that in the revised design of the heliostat mounting the mosaic mirror may be set in the horizontal plane. With the mirror so positioned and with a movable walk-way immediately above the mirror, the procedure of bringing in turn, by the adjustment screws, each of the component mirrors into the horizontal plane as determined by the

spirit level, could be accomplished with comparative ease and speed. The work could be facilitated by using a number of workers, each provided with a properly designed spirit level.

This method appears to have the following advantages: (a) precision comparable and probably superior to that of optical methods; (b) no accumulative errors; (c) highly trained personnel not required; (d) ease and speed of operation.

A disadvantage as compared with optical methods: the spirit level would make contact with each mirror, adding its weight thereto.

A SOLAR FURNACE USING A HORIZONTAL HELIOSTAT ARRAY*

By GORDON HUGHES

Department of Physics, Alabama Polytechnic Institute, Auburn, Alabama

A two-component solar furnace, condenser-heliostat combination, is described in which the condenser faces downward at 30° towards a heliostat comprised of numerous rows of plane mirrors mounted on a horizontal turntable. It is shown that for a south-facing condenser, with the angle of the final flux beam limited to 30° below the horizontal, the rows of heliostat mirrors may be mounted so they overlap, resulting in a reduction of the edge losses occurring when the heliostat mirrors are all held in a single plane. The over-all size of the heliostat turntable is calculated for a 6-hour workday throughout the year, and a suggestion is made for using the heliostat control mechanism to provide shutter action. The saving in flux possible by the elimination of an independent shutter is estimated at about eight per cent.

INTRODUCTION

The design for a solar furnace presented here has been developed as a study to overcome some of the less desirable features in the present design of the Department of Defense solar furnace to be built near Cloudcroft, New Mexico. Some of these objectionable features are: (a) the required construction of a very large movable structure which must be tilted and rotated with considerable accuracy; (b) the required construction of several additional movable structures; (c) the horizontal direction of the final flux beam, and (d) the lack of protection of the optical elements from the weather.

The first of these objectionable features will make the furnace more difficult and expensive to construct when windy weather is taken into account. The horizontal direction of the flux beam will limit the usefulness of the furnace for metallurgical work. The last of the undesirable features mentioned may limit the use of the furnace after storms of sleet, snow, hail, etc.

THE CONDENSER AND ITS HOUSING

In the production of high temperature alloys and ceramics, heat flux incident from above is a distinct advantage, if not a necessity. If an angle of 30° is sufficient for the purposes anticipated in alloying studies, then this proposed solar furnace may be made in a simple manner.

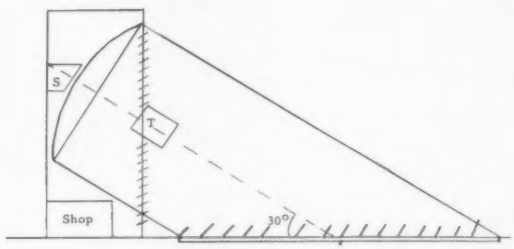

FIG. 1.

If a larger angle of incidence is required, the design becomes more complicated.

Since the design calls for no large movable structures above ground level, wind load problems are reduced to a minimum. One tall stationary building is required, however, to house the condenser mirror with space enough unused to house all the laboratories, shops, offices, etc., that may be required. This single tall building, except for its open front, is in no way unusual and might be constructed in the manner of factory buildings of steel frame and corrugated Transite walls.

The condenser mirror, as previously stated, is housed in the single central building, and thus protected from the weather. Since it faces slightly downward, it is somewhat protected from dust. The heliostat mirrors, as shown later, are mounted in long rows and may be faced downward when not in use so they too are somewhat protected. If facing the heliostat mirrors downward is not sufficient protection, a low metal shed structure might be constructed to roll over the entire heliostat since it will be at ground level.

Fig. 1 indicates the general scheme of the furnace.

The tall building, facing south, carries the condenser just under its roof, facing slightly downward toward the heliostat mirror. The height of the condenser mirror above ground depends on the choice of angle of the final flux beam with the horizontal. For the 30° angle, a building 58 ft by 105 ft by 142 ft high would accommodate not only the mirror but a spectrographic laboratory directly behind the center of the mirror and numerous working spaces below the mirror. In any case, the condenser mir-

*Originally issued as Holloman Air Development Center, *Technical Memorandum* No. HDGR-57-13, September 20, 1957.

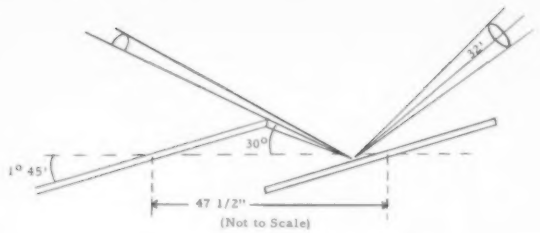

FIG. 2.

ror should be mounted high enough so that the heliostat mirror may be constructed completely outside of the main building.

The target house is a 12-ft diameter cylinder, tilted so that its axis is parallel to the principal axis of the condenser mirror. The floor of this house is made similar to stair steps, their size and shape dependent on the tilt angle.

If a shutter is thought necessary in this design, it should be placed in the plane of the target house as in the Cloudcroft design.

THE HELIOSTAT

The heliostat of this proposed solar furnace consists of a number of parallel rows of flat mirrors, 4 x 4 ft, mounted on a horizontal ground level turntable. The extreme cases of heliostat mirror position may be calculated from the altitude and azimuth data of Table I, which is correct for a location at north latitude 33°.

TABLE I

Date	Hour angle	Azimuth	Altitude
June 21	0h	180°	80° 30′
June 21	−3h	91° 37′	49° 33′
Dec. 21	0h	180°	33° 40′
Dec. 21	−3h	136° 41′	19° 41′

The minimum slope angle of the heliostat mirrors, assuming a 30° angle of incidence of the flux onto the target, is determined from the December 21 altitude of the sun of 33° 30′ at noon. All other hours and days of the year require a larger angle. A choice of 1° and 45′ for the minimum slope angle for the heliostat mirrors for this hour and date will permit a slight spacing between the upper and lower faces of adjacent mirrors if the rows of mirrors slightly overlap, and if they are 48 in. wide and ¼ in. thick. Fig. 2 indicates the angles which occur in the extreme case.

The mirror rows of the heliostat should slightly overlap one another, the one closer to the condenser overlapping the next row farther away in order to minimize the reflection loss due to mirror edges. A suggested spacing is 47½ in. If the mirror edges are sharp, the loss in reflection at the edge is due to the cone of the sun and to the fact that the mirrors are back surface reflecting as shown in Fig. 3.

Comparing the edge loss in overlapping mirrors with that in flush-mounted mirrors, as in the present design for the Cloudcroft furnace, it is seen that the loss due to the cone of the sun is present in both types of mounting.

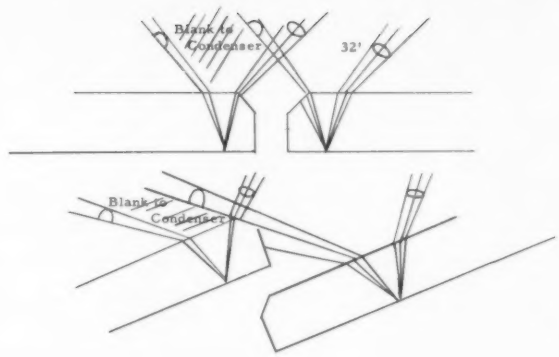

FIG. 3.

Any spacing between flush-mounted adjacent mirrors produces a loss not seen in overlapping mirrors. This applies to the beveled edges of the mirrors as well. The fact of back surfacing produces a loss common to both types of mounting. This back-surface loss increases with increasing angles of incidence on the mirror and therefore would be larger with a south-facing solar furnace than with a north-facing one.

The rotation of each row of heliostat mirrors about its horizontal axis should be controlled by a sun-tracking servo system which might be mounted in the unused center part of the heliostat turntable. It should be possible to introduce an error signal into the sun-tracking servo network in order to defocus the optical system quickly. If such could be accomplished, then the need for an independent shutter might be eliminated completely with a resulting increase in available flux of about 8 per cent above that of the present plan.

THE TURNTABLE

The several rows of heliostat mirrors are mounted as a unit on a large turntable whose axis of rotation may coincide at the ground level with the intersection of the condenser mirror axis and the ground, or it may rotate about any point in the turntable, provided that point is on the center line of the optical system. The turntable is large, but since it may be supported on a number of concentric horizontal tracks its rigidity requirement should not be excessive. If an angle of 30° between the condenser mirror axis and the horizontal will suffice, then the heliostat mirror supports may be mounted in a horizontal plane. If this angle is not sufficient for the furnace user, then the turntable surface must be raised on the side toward the condenser through an angle equal to the difference between the desired angle and 30°

If the turntable surface is to be horizontal, then its shape for a particular instant must be an ellipse, and for a 105-ft condenser at 30° the ellipse will have a minor axis of 105 ft and a major axis of 210 ft. For use from 9 a.m. to 3 p.m. over a period of a year, the extreme rotation of the heliostat turntable will occur on June 21 in the amount of 45° 36′ to the east and west of the noon position.

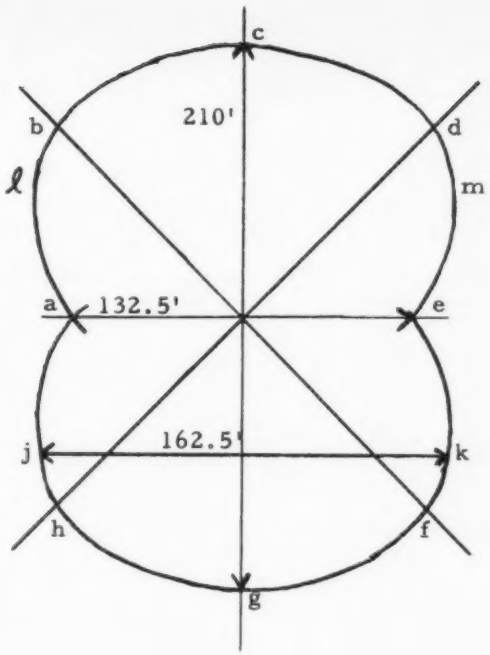

FIG. 4.

As stated above, the rotation of the heliostat turntable may be about a number of points but for the sake of economy should be about that point where the total area of the turntable is a minimum. The shape of the heliostat, as required for center rotation, is shown in Fig. 4. The areas for rotation of the turntable about its center and about one end are approximately as follows:

Rotation about one end .....52,000 sq ft
Rotation about the center .....27,500 sq ft

Since these represent the extreme cases, it is obvious that center rotation is the desirable type.

The areas above and the dimensions of Fig. 4 have been calculated as though the sun were a point source. It can be shown that the dimensions of the surface of the heliostat should be enlarged on each side by an amount al, where a is the mean angular diameter of the sun and l is the distance from a particular point at the edge of the heliostat to the corresponding point on the condenser. These additional widths are given in Table II for the points as indicated in Fig. 4.

TABLE II

Points	Addition to the width
a, e	0.88 ft.
b, c, d	1.25 ft.
f, g, h	0.41 ft.
j, k	0.56 ft.
l, m	0.70 ft.

CONCLUSION

A comparison of the advantages and disadvantages of this proposal and the present design for the Department of Defense solar furnace is presented as a conclusion to this report.

Advantages

(1) One high stationary structure required rather than one high stationary plus one movable and one high accessory structure.

(2) Factory type construction may be used for the main building.

(3) All working spaces will be under one roof.

(4) Radiation flux is incident on sample from above.

(5) Heliostat mirrors may be aligned and cleaned from ground level.

(6) Condenser mirror is protected and should stay clean for long periods.

(7) Condenser mirror may be realigned or repaired in bad weather down-time of the furnace.

(8) Heliostat mirrors may face downward when not in use and, if provided with shed cover, may be cleaned in adverse weather down-time of the furnace or at night.

(9) Eliminates a difficult wind load problem for an extremely large tilting structure.

(10) This proposal brings the target house lower to the ground.

(11) The shutter might be eliminated with a saving in flux.

Disadvantages

(1) The single structure required is some 50 per cent higher.

(2) Target house stands at an angle with some less working space available.

(3) Heliostat turntable is somewhat larger in area in this proposal but will carry some less load.

(4) Shutter, if required, will cause somewhat greater loss in flux and, being larger, will be somewhat more difficult to construct.

SOLAR ABSTRACTS

Beal, George Malcolm, "Natural light and the inside-outside heliodon." *Kansas Univ. Publ., Bull. Eng. & Archit.* No. 38, 1956. 40 p. Illus.

Discusses the development of model sun machines for architectural analysis with special attention to the inside-outside heliodon designed at the University of Kansas for the Dept. of Architecture. The heliodon comprises a movable floodlight mounted on a calibrated arm which is suspended over an architectural model. The system, simulating the motion of the sun, gives patterned sunlight according to the latitude on the inside of the building, at the same time exposing the play of sunlight on outside walls and the surrounding area.

* * *

Birkebak, Richard C. and Hartnett, J. P., "Measurements of the total absorptivity for solar radiation of several engineering materials." *Trans. ASME* 80(2):373-78, Feb. 1958. Illus.

Values are presented of the total solar absorptivity of several porous materials presently being considered for transpiration cooling of high-speed vehicles. To specify these surfaces, photomicrographs and a chemical analysis are presented. Two schemes used in the measurement of the absorptivity values are described in the text, a comparison technique and an integrating radiometer method. (authors' abstract)

* * *

Bonnet, G., "Etude de la radiation solaire à Lwiro en 1953." *Acad. Roy. Sci. Colon. Cl. Sci. Nat. & Méd.* 6(6):1958. 77+ p. Illus. (Study of solar radiation at Lwiro in 1953.)

A survey of the activity of the Solar Radiation Laboratory at Lwiro since its foundation in 1953 and a summary of the solar radiation data obtained in 1952 and 1953. The techniques of observation and analysis used are described in detail. Measurements have been made of the total radiation arriving at the ground and that in certain spectral regions, the duration of insolation, ultraviolet radiation arriving at the ground, various meteorological measurements, wind, rain, barometric pressure, etc. The equipment used for gathering and recording data is described, and methods of reducing the data outlined. Tables give the direct and global radiation in cal per sq cm and the duration of insolation (daily) from October 1952 to December 1953, together with total monthly and average daily values.

* * *

Carlson, Allan; Deshotels, Warren; Jost, Jacob M. and Shiozawa, Lebo R., "Research on methods of treating cadmium sulfide elements." Wright Air Develop. Centre, *Tech. Rept.* 57-749, ASTIA Document No. AD 151024, Nov. 1957. 52 p. Illus. (PB 131847)

This study forms part of a program for the development of a cadmium sulfide single crystal solar battery. Emphasis was placed on a fundamental study of photovoltaic electrodes formed on cadmium sulfide crystals by copper compounds. It was found that the behavior of such junctions as circuit elements was in agreement with published theory. The cells had photoelectric energy conversion efficiencies in sunlight ranking between that of selenium and silicon solar batteries. A number of other ohmic and non-ohmic electrodes on cadmium sulfide crystals were also prepared and studied.

The spectral response of cadmium sulfide photovoltaic cells is not that predicted by analogy with the silicon solar battery. The expected response from photon energies greater than the intrinsic energy gap is replaced by a broad band of photon energies ranging from about one-half to about nine-tenths of the intrinsic band gap energy.

Experiments on impurity doping of crystals by solid-state diffusion resulted in measured diffusion constants for indium and aluminum. Ingots of large undoped cadmium sulfide crystals were grown from the vapor phase. Resistivities within single crystal grains varied from 10^9 ohm-cm to 10 ohm-cm. This was interpreted as being due to small variations in concentrations of copper ions and anion vacancies. (authors' abstract)

* * *

Cunniff, Charles V., "Solar radiation on walls facing east and west." *Air Cond. Heat. Vent.* 55(10):82-88, Oct. 1958. Illus.

A report and analysis of four years of solar radiation measurements at Blue Hill Observatory from September 1952 to August 1956. Average hourly, daily, and monthly values are given for radiation received on a vertical surface facing east and west during cloudless days, and average daily values on horizontal and east and west vertical surfaces with sky covers of 0 to 3/10, 4 to 7/10, and 8 to 9/10, and with an overcast sky of low clouds and of middle clouds.

* * *

Gomella, Cyril, "Solar distillation developments in the eastern Mediterranean." (In: Symposium on Saline Water Conversion, November, 1957, *Proceedings.* Wash., National Academy of Sciences-National Research Council, 1958. *Publication* 568. p. 131-36. Illus.)

The possibilities for solar distillation in North Africa and developments in this field over the past two years are described. Basic research has been carried out by the author, Lejeune and Savornin, and Mediger. On a practical level, a small distillation cell consisting of a molded asbestos-cement shell with a glass cover, set on rock wool insulation, originally built in 1955, has been improved and is in wide use. Some aspects of its performance are described including the daily variation in yield. Tests to obtain additional energy yield, investigations into prevention of scale formation, and the use of plastic materials are described. Future plans include the construction of an experimental area at Touggourt, where various apparatus will be tested under identical conditions.

* * *

Guillemin, J., "L'Hélliodyne de l'Observatoire d'Alger." *Rev. Aluminium* 34(240):171-85, Feb. 1957. (The heliodyne at the Algeria Observatory.)

A description of the solar furnace at the Observatory in Algeria. This 39-ft high furnace was built to study processes, minerals, and chemicals on a semi-industrial basis. The problems which had to be solved in making a parabolic aluminum mirror with a diameter of 27 ft 7 in. and achieving sufficient rigidity of the light metal frame are discussed. (*Elec. Eng. Abst.*)

* * *

Hassler, Gerald L., "An air film osmotic stack for low cost multiple evaporation." (In: Symposuim on Saline Water Conversion, Washington D.C., 1957, *Proceedings.* p. 150-156. Illus.)

Work is reported on a polarised form of air-film osmotic stack for use in multiple evaporation which requires no pressure activation. The design uses air gaps entirely free of any supporting

screen, with hard, rigid, very thin, self-supporting flow doublets which may be produced automatically. The process by which air-film evaporators are utilized in osmotic purification of seawater is described schematically and compared to orthodox 3-stage stills. The theory of heat and mass diffusion exchange in the air-film evaporator is developed. Mention is made of a number of tests carried out in connection with the design of a flow doublet.

* * *

International Association of Meteorology, Radiation Commission, Subcommission for Radiation Instructions, "Radiation instruments and measurements." *Ann. Int. Geophys. Year* 5(6):367-466. *(IGY Instruction Manual* Part 6.) Illus.

This handbook explains the construction and manipulation of every instrument in the field of meteorological radiation and advises on methods for obtaining worldwide comparability of radiation measurements. Ch. 1 presents a discussion of the International Pyrheliometric Scale 1956 with a summary of the basis for its establishment and its relation to the earlier Angström and Smithsonian scales. The next two sections are concerned with solar intensity (i.e., direct solar radiation on a surface at normal incidence to the sun's rays) and total (or global) and diffuse sky radiation received on a horizontal surface. Ch. 4 is devoted to observation of terrestrially originated radiation and the radiation balance. The questions of the evaluation of records and the processing of the derived data are dealt with in Ch. 5, together with information on the publication of IGY radiation measurements. Special tables are provided to facilitate the calculation of indices of atmospheric turbidity.

* * *

Lof, George O. G., "Design and cost factors of large basin-type solar stills." (In: Symposium on Saline Water Conversion, Washington, D. C., 1957, *Proceedings.* p. 157-74. Illus.)

The objects of this paper are (1) to explain the procedure and results of an engineering study culminating in the detailed design of a solar distillation plant large enough to yield performance and cost information representative of large practical plants, and (2) to describe a solar still design believed cheaper, less subject to maintenance problems, and more practical for large installations than other types. A deep-basin solar still design is described and compared with shallow-layer types. The performance of the deep-basin distiller at a hypothetical test site (La Jolla, Calif.) is predicted in calculations based on weather and solar conditions and theoretical and empirical heat transfer rates. Productivity of the deep-basin still was found to be approximately 0.11 gal per sq ft per day from May through August. Annual average production should rate 0.8 gal per sq ft per day. Twelve detailed drawings prepared for contractor bidding and construction of a 5000-sq ft solar distillation pilot plant in Southern California are reproduced. Cost estimates for construction of this still, based on evaluation of the finished design and construction firm bids, indicated a total basin cost of nearly $3.00 per sq ft. Tanks, pumps, piping, and electrical equipment brought the total to nearly $7.00 per sq ft. Developments which may bring the cost of the distillation plant to $1.00 per sq ft are considered.

* * *

L'vova, E. M. and Moroz, G. S., "Integrated coefficient of absorption of solar radiation by some materials and coatings." *Zh. Tekh. Fiz.* 26(4):850-52, 1956. (In Russian.)

Describes a comparator method and gives results for several substances including silver (5 per cent), zinc oxide (9.4 per cent), aluminum foil (12.0 per cent), and copper foil (15.0 per cent). *(Phys. Abst.)*

* * *

Maslakovets, Yu. P.; Poltinnikov, S. A.; Dubrovskii, G. B. and Subashiev, V. K., "Photoelectric converters of solar energy made from *p*-type silicon." *Zh. Tekh. Fiz.* 26 (10):2396-97, 1956. (In Russian.)

Vapour phase diffusion of Sb in *p*-type Si gave *n-p* junctions showing a photovoltaic peak response at 700 mμ. One such element, area 1 sq cm, had the following characteristics in direct sunlight: short circuit current 10 ma, open circuit voltage 450 mv, maximum conversion efficiency 2.8 per cent with 300 mv generated across a 33 ohm load. *(Phys. Abst.)*

* * *

Nebbia, Giorgio, "An experiment with a plastic tubular solar still." (In: Symposium on Saline Water Conversion, Washington, D. C., 1957, *Proceedings.* p. 175-76. Illus.)

Tests to verify the practical efficiency of a rigid tubular solar still with a 3.5-sq. ft blackened aluminum water pan in a Plexiglass case, designed to reduce heat losses through the bottom of the pan, are reported. The amount of solar radiation available and production of water for June and July 1957 are given. Loss of solar energy appears to be 40 per cent; another 30 per cent incident heat is lost from the still itself.

* * *

New Mexico Highlands University, "Literature survey for an investigation of solar energy storage materials." 40 p.

Lists some 500 papers on heat storage chemicals, published during the period 1919-1956.

* * *

Pearson, G. L., "Conversion of solar to electrical energy." *Am. J. Phys.* 25(9):591-98, Dec. 1957. Illus.

A photovoltaic device has been developed which converts solar radiation directly into electrical energy with an over-all efficiency of 11 per cent. This consists of a *p-n* junction formed by gaseous diffusion near the front surface of a silicon plate. In full sunlight a single cell furnishes approximately 30 ma of short circuit current per sq cm of surface, 0.6 v of open circuit voltage, and 12 mw of power into a matched load per sq cm of surface. Like other electric batteries, individual cells may be connected in series or parallel to obtain an increase in terminal voltage or current. The spectral response is a maximum near 0.7 mμ, and the long wavelength cutoff is at approximately 1.1 mμ. The efficiency of this new silicon *p-n* junction photovoltaic cell is greater by a factor of 20 than that previously reported for other types of photocells and makes the conversion of the sun's energy directly into electricity possible for a number of interesting applications. A Bell System field trial at Americus, Georgia, in which solar batteries are used to power a rural carrier telephone communication system is described. A number of other possible applications for this new solar energy converter are discussed. (author's abstract)

* * *

Reynolds, D. C. and Greene, L. C., "Crystal growth mechanism in cadmium sulfide crystals." *J. App. Phys.* 29 (3):559-62, March 1958. Illus.

Large cadmium sulfide crystals have been grown from the vapor phase. The crystal growth was studied by observing growth patterns, chemical etch patterns, and vaporization patterns. The studies reveal a layer or lamellar-type growth, the layers resulting from the coalescence of monatomic steps into ledges of many atomic layers in height. The layers are generated at or near the crystal edge and move across the surface by edge nucleation. The exact mechanism by which the steps are generated is not known; however, it is believed that they result from screw dislocations or surface nucleation. (authors' abstract)

* * *

Sekihara, K. and Kano, M., "On the distribution and variation of solar radiation in Japan." *Papers Meteor. & Geophys.* 8(2):144-49, July 1957. Illus.

Records of daily total of solar radiation measured on a horizontal surface for three to seven consecutive years are available for about forty stations in Japan. Using these data, yearly and seasonal mean isopleths of solar radiation are drawn. In the results, the following features are pointed out: (1) The distributions are affected by the meteorological factors rather than by latitude. (2) The amount of solar radiation is larger in the inland district than near the sea. (3) The minima of solar radiation in the Tokyo and Osaka districts are remarkable. (4) The seasonal variation of the amount of solar radiation is largest in summer and then in spring, autumn, and winter in the order of magnitude. (5) The annual variations of solar radiation are mainly brought about by the conditions in summer. (authors' abstract)

Strobel, J. J., "Summary of solar distillation processes." (In: Symposium on Saline Water Conversion, Washington, D. C., 1957, *Proceedings*. p. 117-22. Illus.)

Recent research in solar distillation carried out under the sponsorship of the Office of Saline Water is briefly described. Several different types of nonfocusing solar stills are discussed, including a simple Telkes-type still, a roof-type still, the Lof deep-basin still, a DuPont plastic still, a Telkes flat tilted still, a frame-supported multiple-effect still, and the Bjorksten suspended-envelope still. The author finds there is a need for two types of stills at the present time, a small simple still and a large-capacity still. Future developments, however, appear to depend on advances in reducing costs.

* * *

Telkes, Maria, "Solar still theory and new research." (In: Symposium on Saline Water Conversion, Washington, D. C., 1957, *Proceedings*. p. 137-49. Illus.)

Basic principles of solar still design theory are outlined, and a flat tilted unit that most successfully embodies these principles, together with a roof-type still, are described. A formula is developed for calculating the net heat available for distillation in a single-effect still, and a sample calculation of heat transfer in a flat tilted still is made. Experimental results agree well with the calculated efficiencies. Water yields of roof-type and flat tilted stills are compared experimentally, and other tests, including seawater operation, reuse of heat carried away by the brine, improvements in controlled feeding, and reuse of the heat of condensation, are described. Experimental work on multiple-effect stills includes the development of suitable materials and forms of construction for the frames of successive stages and for the solar heat collectors which supply heat to the first stage. Performance and efficiency of several electrically-heated models is given. Comparisons were made between solar heating and electrical heating in a 4-effect still with a frame area of 7.9 sq ft, and between the efficiency of a single-effect and 3-effect still of the same area.

Veinberg, V. B. and Mal'tsev, Yu. V., "The conversion of radiation into electricity." *Zh. Tekh. Fiz.* 26(10):2373-77, 1956. (In Russian.)

While there have been many discussions of the thermodynamics of converting solar radiation to heat and thence into electrical energy, the thermodynamics of the processes occurring in the heater where the incident radiation is trapped is not normally considered in detail. This paper, which is theoretical, considers the optimal conversion conditions, taking into account the parameters relative to the heater. The characteristics of various types of solar heaters in optimal working conditions are given in tabular form. For Central Asia summer conditions, the daily power per sq m is 100-150 whr; with reflectors, 2 kwhr can be achieved. Thermoelectric installations may give only a third to a quarter of this energy.

* * *

Wilson, Bruce W., "Solar distillation research and its application in Australia." (In: Symposium on Saline Water Conversion, Washington, D. C., 1957, *Proceedings*. p. 123-30.)

Progress made during the past two years towards the development of solar stills to meet Australian requirements is described. In initial experiments with a tent-shaped, Telkes-type still, water yields up to 1.5 lb per sq ft per day were obtained, and a 40 sq ft commercial unit at Mildura gave yields of 2.0 lb per sq ft per day. A modified Gomella-type solar still was tested, and, although producing less water, proved to be cheaper and simpler to construct. An empirical relation is developed to describe the relation between the instantaneous rate of distillation, the still temperature, and the partial pressure of water vapor in the air in the stills. Current work includes investigation of two new methods of constructing Gomella-type stills, a solar still for the Antarctica, and a 50-gal per day installation in N.W. Victoria.

A SURVEY OF SOLAR FURNACE INSTALLATIONS IN THE UNITED STATES

SUPPLEMENT

Since the publication of the original survey of U.S. solar furnaces by Raymond K. Cohen and Nevin K. Hiester in April-July 1957 issue of the *Journal* and the first Supplement in the October 1957 issue, details of two other furnaces have been received by the editor. These furnaces and their characteristics are listed below.

Organization	Rocketdyne	B. F. Goodrich Co. Research Center
Principal investigators	R. P. Clifford R. C. Speiser	J. E. Jansen, M. Roha R. E. Frost, F. W. Smith
Furnace location	Canoga Park, Calif.	Brecksville, Ohio
Date initiated	May 1957	January 1957
Furnace description, Main mirror:		
Mounting	Altazimuth	Altazimuth
Mirror material	Glass	Copper
Reflecting surface material	———	Rhodium
Reflecting surface	Back	Front
Aperture	60 in.	60 in.
Focal length	26 in.	25.8 in.
Rim angle	———	60°
Theoretical image diam.	9/32 in.	0.24 in.
Auxiliary mirrors & lenses:		
No. of auxiliary mirrors	None	None
No. of auxiliary lenses	None	None
Furnace operation, Guiding:		
Type	Phototubes	Phototubes
Temperature control:		
Type	Manual Shades Cylinder	Manual Cylinder
Sensing device	Radiamatic pyrometer	———
Temperature measurement:		
Sensing device	Optical pyrometer on graphite cavity	Incomplete
Specimen holder:		
Materials of construction	Original searchlight equipment for holding and traversing graphite rods.	Stainless and machine steel
Type of traversing mechanism		3 variable speed motors
Applications & experimental results:		
Use of furnace	Obtaining thermal electric properties of refractory metal thermocouples, fusing kaliophilite 5430°F	High temperature chemistry, chemical and physical properties of materials at high temperature
Max. temperature obtained		To be determined
Reflectivity efficiency factor*	———	85% (est.)
Shadowing loss factor**	———	95% (approx.)

*Takes into account losses by reflectivity and/or absorptivity of all optical parts of furnace. 100% would denote no losses.
**Takes into account losses due to shadowing of mirror by devices for mounting mirrors, targets, etc. 100% would denote no shadowing.

WORLD RESEARCH ACTIVITIES

The following three items arrived too late for inclusion in the comprehensive survey of world activities in the April 1958 issue of **Solar Energy**.

GERMANY

Physikalisch-Chemisches Institut der Universität Marburg. Biegenstrasse 12, Marburg 16.

H. T. Witt.

Investigating fast photochemical reactions and the primary process of photosynthesis, using the method of flash photolysis. Results include the detection of photochemically-produced charged radicals and the observation of chlorophyll reactions (within 10^{-6} to 10^{-5} seconds) in photosynthesis.

JAPAN

Micro-Algae Research Institute of Japan. Kunitachi-machi, Tokyo.

Kiichi Minami; Yuji Nishiyama; Hiroshi Tamiya; Hiroaki Iwamoto.

Began operation of culture ponds of one acre total area at the end of March 1958, with plans to produce 10 tons of dried algae a year for laboratory use. Investigating apparatus, methods of harvesting and extracting chlorophyll and vitamins, and the economics of the mass culture of *Chlorella* and other micro-algae.

NEW ZEALAND

University of Auckland, School of Engineering. Auckland.

C. F. Kettleborough.

Investigating the characteristics and fundamental behaviour of flat-plate collectors and data on solar radiation intensity, as part of design studies leading to a project on space heating by solar energy.

ERRATA AND ADDENDA

Description of cover picture in Vol. II, No. 2, April, 1958, p. 1: Temperatures expected in the proposed Holloman Air Force Base solar furnace will be in the vicinity of 7,000°F, not 7,000°C.